

Characterization of LpxC Inhibitors and Resistant Mutants

by

Daina Zeng

Department of Biochemistry
Duke University

Date: _____

Approved:

Pei Zhou, Supervisor

Michael D. Been

Kenneth N. Kreuzer

Raphael H. Valdivia

Robert A. Nicholas

Dissertation submitted in partial fulfillment of
the requirements for the degree of Doctor
of Philosophy in the Department of
Biochemistry in the Graduate School
of Duke University

2012

Abstract

Characterization of LpxC Inhibitors and Resistant Mutants

by

Daina Zeng

Department of Biochemistry
Duke University

Date: _____

Approved:

Pei Zhou, Supervisor

Michael D. Been

Kenneth N. Kreuzer

Raphael H. Valdivia

Robert A. Nicholas

An abstract of a dissertation submitted in partial
fulfillment of the requirements for the degree
of Doctor of Philosophy in the Department of
Biochemistry in the Graduate School
of Duke University

2012

Copyright by
Daina Zeng
2012

Abstract

LpxC, the deacetylase that catalyzes the second and committed step of lipid A biosynthesis in *E. coli*, is an essential enzyme for virtually all Gram-negative bacteria and one of the most promising novel antibiotic targets for the treatment of multidrug-resistant Gram-negative infections. Here, we report the characterization of two novel LpxC inhibitors that have apparent binding affinities for *E. coli* LpxC in the picomolar range. Furthermore, these compounds display broad spectrum activity against a plethora of Gram-negative pathogens.

In anticipation for the advancement of LpxC inhibitors in clinical trials, we undertook studies to probe potential bacterial resistance mechanisms to these compounds. In this study, we report a two-step isolation of spontaneously resistant *E. coli* mutants that have > 200-fold resistance to LpxC inhibitors. These mutants have two chromosomal point mutations that account for resistance additively and independently: one in *fabZ*, a dehydrase in fatty acid biosynthesis, and the other in *thrS*, the Thr-tRNA ligase.

For both enzymes, the isolated mutations result in reduced enzymatic activities *in vitro*. Most unexpectedly, we observed a decreased level of LpxC in bacterial cells harboring *fabZ* mutations, suggesting that the biosyntheses of fatty acids and lipid A are tightly regulated to maintain balance between phospholipid and lipid A. Additionally, we show that the mutation in *thrS* slows protein production and cellular growth, providing the first example that reduced protein biosynthesis confers a suppressive effect on inhibition of membrane biosynthesis. Altogether, our studies reveal an impressive compensatory ability of bacteria to overcome inhibition of lipid A biosynthesis by

rebalancing cellular homeostasis, a unique mechanism of antibiotic resistance.

Dedication

This dissertation is dedicated to Christian R.H. Raetz (1946 - 2011) – an extraordinary scientist and mentor.

Table of Contents

Abstract.....	iv
List of Tables	xi
List of Figures.....	xii
List of Abbreviations	xv
Acknowledgements.....	xvi
1. Introduction.....	1
1.1 Consequences of antibiotic resistance in Gram-negative bacteria	2
1.2 Lipid A as an antibiotic target	4
1.3 LpxC inhibitors are novel antibiotics	7
1.4 Study of LpxC inhibitors and mechanisms of resistance to these inhibitors.....	9
2. Characterization of LpxC Inhibitors	11
2.1 Introduction.....	12
2.2 Materials and Methods	16
2.2.1 MIC assay	16
2.2.2 LpxC enzymatic inhibition assay.....	16
2.2.3 Creation of “W3110NG,” the <i>Neisseria gonorrhoeae</i> LpxC knock-in strain ..	21
2.3 Results.....	25
2.3.1 Characterization of LPC-009	25
2.3.2 Characterization of LPC-011	29
2.4 Discussion.....	31
3. Isolation and Characterization of Spontaneously Arising Resistant Mutants to CHIR-090	33
3.1 Introduction.....	34

3.2 Materials and Methods	35
3.2.1 General materials and methods.....	35
3.2.2 Isolation of CHIR-090 resistant mutants	36
3.2.3 MIC assay	36
3.2.4 Disc diffusion assay	37
3.2.5 Whole genome sequencing	38
3.2.6 Construction of CRM <i>wtfabZ</i> and CRM <i>wtfabZ</i> , <i>wthrS</i> mutants	36
3.3 Results.....	41
3.3.1 Isolation of spontaneously resistant mutants to CHIR-090	41
3.3.2 Mutants are resistant to a variety of LpxC inhibitors	43
3.3.3 Mutants defective in growth and not resistant to other antibiotics	46
3.3.4 Mutations of <i>fabZ</i> and <i>thrS</i> confer CHIR-090 resistance additively and independently.....	48
3.4 Discussion.....	50
4. Characterization of FabZ Mutants	52
4.1 Introduction.....	53
4.2 Materials and Methods	55
4.2.1 Construction of pBAD33.1(<i>fabZ</i>).....	55
4.2.2 Liquid chromatography coupled with mass spectrometry (LC-MS)	55
4.2.3 FabZ assay	57
4.2.4 LpxC activity assay.....	60
4.2.5 Western blot.....	61
4.2.6 Extraction and visualization of lipid profile	63
4.2.7 Construction of pBAD33.1(<i>lpxC</i>).....	64

4.2.8 Construction of chromosomal <i>fabZ</i> -FLAG tag.....	65
4.2.9 Reverse transcription polymerase chain reaction (RT-PCR).....	67
4.2.10 Supplementation of <i>R</i> -3-hydroxymyristic acid.....	68
4.2.11 Cloning of <i>Vibrio harveyi</i> acyl-ACP synthetase.....	69
4.3 Results.....	69
4.3.1 Point mutations in <i>fabZ</i> are recessive and decrease enzymatic activity	69
4.3.2 FabZ and LpxC are co-regulated	78
4.4 Discussion.....	80
5. Characterization of ThrS Mutants	94
5.1 Introduction.....	95
5.2 Materials and Methods	95
5.2.1 Construction of pWSK29(<i>thrS</i>)	95
5.2.2 Preparation of ThrS constructs	96
5.2.3 Preparation of RNA substrate	98
5.2.4 ThrS assay setup	103
5.2.5 Construction of W3110 <i>muthrS</i>	104
5.2.6 Protein labeling experiments	107
5.2.7 Growth curves.....	107
5.2.8 Isolation and characterization of other resistant mutants.....	108
5.2.9 Slowing cellular growth experiments	111
5.3 Results.....	111
5.4 Discussion.....	118
5.4.1 Reduction of protein synthesis suppresses inhibition of lipid A biosynthesis	118

5.4.2 Point mutation in <i>thrS</i> is not the only mechanism for resistance.....	119
5.4.3 Significance of our study	120
References.....	122
Biography	130

List of Tables

Table 2.1: MIC value comparisons between CHIR-090 and LPC-009	28
Table 3.1: Sequence of indicated primers used	41
Table 3.2: Point mutations and MIC of mutant strains.....	44
Table 3.3: MIC of CRMs to other antibiotics.....	47
Table 3.2: Point mutations and MIC of mutant strains.....	44
Table 4.1: MIC assay show <i>fabZ</i> point mutations are recessive.....	70
Table 4.2: Specific activities of FabZ proteins	75
Table 4.3: MIC of FabZ mutants (CRM1 and CRM5) to aminoglycosides	93
Table 5.1: Table of CHIR-090 mutants	110
Table 5.2: MIC assay show <i>thrS</i> point mutations are recessive	112
Table 5.3: Ser517Ala ThrS has ~ 20-fold less Thr-tRNA charging activity compared to the wild-type enzyme.....	114
Table 5.4: MICs show W3110 <i>muthrS</i> is ~ 2-fold resistant to the fluoroquinolones ciprofloxacin and nalidixic acid relative to the wild-type strains W3110 and W3110 <i>wthrS</i>	117

List of Figures

Figure 1.1: New antibiotic approved by the US Food and Drug Administration, per 5-year period.	3
Figure 1.2: A representation of the <i>E. coli</i> cell envelope	6
Figure 1.3: Biosynthetic Pathway of Kdo ₂ -lipid A in <i>E. coli</i>	8
Figure 2.1: Structures of LpxC inhibitors.....	13
Figure 2.2: NMR structure of <i>A. aeolicus</i> LpxC/CHIR-090 complex.....	14
Figure 2.3: CHIR-090 resistance generated by steric clashes between S214 in RILpxC and the distal ring of CHIR-090	15
Figure 2.4: Chemo-enzymatic synthesis of [α - ³² P]UDP-3- <i>O</i> -[(<i>R</i>)-3-hydroxymyristoyl]- <i>N</i> -acetylglucosamine.....	19
Figure 2.5: LpxC assay setup.....	20
Figure 2.6: Complementation of <i>E. coli</i> <i>lpxC</i> with <i>N. gonorrhoeae</i> <i>lpxC</i>	23
Figure 2.7: LPC-009 overcomes RILpxC CHIR-090 resistance.	27
Figure 2.8: Inhibition curve of LPC-009 against <i>E. coli</i> LpxC	29
Figure 2.9: Inhibition curve of LPC-011 against <i>E. coli</i> LpxC	30
Figure 2.10: Structure of the <i>E. coli</i> LpxC/LPC-011 complex.....	31
Figure 3.1: Resistant mutants were isolated in a two-step process.....	43
Figure 3.2: Disc diffusion assays.....	45
Figure 3.3: Growth curves for CRM mutants	47
Figure 3.4: FabZ and ThrS point mutations confer resistance independently and additively	49
Figure 4.1: FabZ and LpxA share a substrate used in lipid A biosynthesis	54
Figure 4.2: Final FabZ proteins purity as visualized by SDS-PAGE analysis	59
Figure 4.3: FabZ-FLAG primer design	66

Figure 4.4: X-ray structure of PsFabZ.....	71
Figure 4.5: FabZ assay setup.....	73
Figure 4.6: FabZ enzymatic activity assay based on reverse phase LC-MS.....	75
Figure 4.7: LC-MS analyses of FabZ mutants lipid A profile.....	76
Figure 4.8: LC-MS analyses of FabZ mutants fatty acid profile.....	77
Figure 4.9: LpxC activity and level in FabZ mutants.....	79
Figure 4.10: Phospholipid profile in FabZ mutants.....	82
Figure 4.11: TLC analyses of lipid profiles in FabZ mutants.....	85
Figure 4.12: FabZ protein level does not change.....	88
Figure 4.13: RT-PCR shows <i>lpxC</i> and <i>fabZ</i> mRNA levels do not change.....	89
Figure 4.14: Western blot showing down-regulation of LpxC when <i>lpxA</i> is overexpressed on a pBAD33.1 plasmid.....	90
Figure 4.15: MIC of W3110 cells supplemented with 50 µg/mL of <i>R</i> -3-hydroxymyristic acid.....	91
Figure 5.1: ThrS reaction scheme.....	95
Figure 5.2: Final protein purity of ThrS judged by SDS-PAGE analysis.....	98
Figure 5.3: Purity analysis of transcribed RNA constructs on 8% PAGE gel/7M Urea chromatography.....	99
Figure 5.4: Final protein purity of <i>E. coli</i> tRNA nucleotidyltransferase enzyme judged by SDS-PAGE analysis..	101
Figure 5.5: [α - ³² P]-tRNA ^{thr} labeling reaction.....	102
Figure 5.6: tRNA labeling reaction..	103
Figure 5.7: Generation of W3110 <i>muthrS</i>	106
Figure 5.8: X-ray structure of <i>E. coli</i> ThrS.....	113
Figure 5.9: PEI-Cellulose plate shows Ser517Ala ThrS has significantly reduced Thr-tRNA charging activity compared to the wild-type enzyme (wtThrS).....	114

Figure 5.10: Point mutation in *thrS* defects protein synthesis.....116

Figure 5.11: Point mutation in *thrS* defects cellular growth.....117

Figure 5.12: Schematic illustration showing homeostatic responses between lipid A, phospholipid, protein, and DNA biosyntheses to generate resistance to LpxC inhibitors
.....119

List of Abbreviations

ACP – acyl carrier protein

CRM – CHIR-090 resistant mutants

DEAE – diethylaminoethyl

LC-MS – liquid chromatography coupled with mass spectrometry

LPS – lipopolysaccharide

LpxC – UDP-3-*O*-(acyl)-*N*-acetyl glucosamine deacetylase

FabZ – *R*-3-hydroxymyristoyl acyl carrier protein (ACP) dehydrase

MIC – minimum inhibitory concentration

OD₆₀₀ – optical density at wavelength of 600 nm

PBS – phosphate buffered saline

PEI – polyethyleneimine

RT-PCR – reverse transcription polymerase chain reaction

ThrS – threonine-tRNA ligase

Acknowledgements

I would like to thank Dr. Pei Zhou, Dr. Michael Been, Dr. Robert Nicholas, Dr. Kenneth Kreuzer, Dr. Raphael Valdivia, Dr. John Hsieh, Dr. Hak Suk Chung, Mr. Chuljin Lee and all of the members of Raetz laboratory for their contributions to experimental design, data interpretations, and general morale. I am also very grateful to Dr. Xiaofei Liang and Dr. Eric Toone for the generous gifts of LpxC inhibitors used in this study, Mr. Ali Masoudi for help in the preparation of acyl-ACP, Dr. William T. Doerrler for providing the polyclonal LpxC antibody.

Chapter 1

Introduction

1.1: Consequences of antibiotic resistance in Gram-negative bacteria

Antibiotics first became commercially available in the 1940s and have become essential for the treatment of potentially life-threatening bacterial infections. Many antibiotics originated from natural sources that use these compounds against other organisms in nature. In response, bacteria have evolved defenses including resistance to these antibiotics. With few exceptions, each introduction of a new antibiotic has been followed within a few years by the first cases of resistance. In his 1945 Nobel Prize lecture, Alexander Fleming himself warned of the danger of resistance: “It is not difficult to make microbes resistant to penicillin in the laboratory by exposing them to concentrations not sufficient to kill them.”

Over the past decades, due to financial and regulatory disincentives, the number of new antibiotics developed by the pharmaceutical industry has substantially decreased (Spellberg et al, 2008) (Figure 1.1). Regrettably, and perhaps not surprisingly, this decrease corresponds to an increasing prevalence of multidrug-resistant bacteria. Per year in America, there are 2 million hospital acquired infections resulting in 8 million additional hospitalization days with total annual costs between 21 to 34 billion dollars. Of the 2 million cases of hospital acquired infection, 99,000 of these result in death, mainly due of the presence of multidrug resistance (Infectious Society of America). The extent of damage done by multidrug-resistant bacteria is so great that the World Health Organization have identified antimicrobial resistance as one of the three greatest threats to mankind.

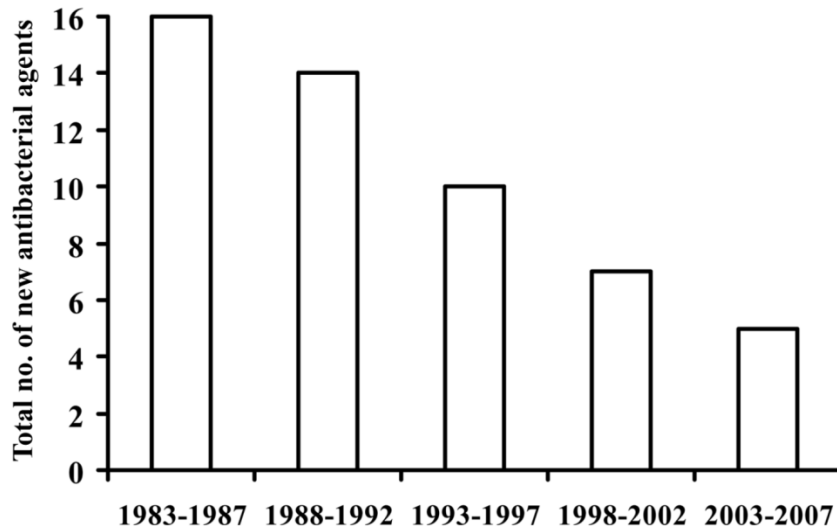


FIGURE 1.1: New antibiotics approved by the US Food and Drug Administration, per 5-year period (Spellberg et al, 2008).

The most problematic multidrug-resistant bacteria that cause infection in hospitals have been identified as the “ESKAPE” pathogens: *Enterococcus faecium*, *Staphylococcus aureus*, *Klebsiella pneumoniae*, *Acinetobacter baumannii*, *Pseudomonas aeruginosa*, and *Enterobacter* species. Unfortunately, this term is particularly appropriate as it emphasizes their detrimental ability to effectively “escape” the effects of antibacterial drugs (Boucher et al, 2009). Though methicillin-resistant *S. aureus* (MRSA) remains a significant problem, killing more Americans annually than HIV/AIDS, Parkinson’s Disease, emphysema, and homicide combined, several highly resistant Gram-negative pathogens—namely *Acinetobacter* species, multidrug-resistant *P. aeruginosa* and carbapenem-resistant *Klebsiella* species, and *Escherichia coli*—are emerging as key pathogens worldwide.

Moreover, our therapeutic options for these Gram-negative pathogens are so limited that clinicians are forced to use older drugs such as colistin, that have been previously discarded due to their association with frequent and serious nephrotoxicity and neurotoxicity (Falagas & Kasiakou, 2005). The growing number of elderly patients and patients undergoing surgery, transplantation, and chemotherapy will produce an even greater number of immunocompromised individuals at risk for these infections (Chopra et al, 2008). A consensus statement from academic and industrial experts who met in London in September 2006 stated “The discovery of new drugs active against hospital-acquired Gram-negative bacteria is essential to prevent a future medical and social catastrophe.”

These studies underscore the limitations of current antibiotics. Indeed, the antibiotics currently used to treat Gram-negative infections are limited to three major classes: inhibitors of cell wall peptidoglycan biosynthesis, protein synthesis, and DNA replication (Walsh, 2000). In the worsening battle against multidrug resistance, novel antibiotics that inhibit previously unexploited targets must be identified (Projan & Youngman, 2002).

1.2: Lipid A as an antibiotic target

Gram-negative bacteria have an outer membrane and an inner membrane. The inner membrane is composed of a symmetric phospholipid bilayer and is surrounded by a thin peptidoglycan layer, consisting of a sugar and amino acid polymer. The inner leaflet of the outer membrane is comprised of phospholipids while the outer leaflet is

made of a hexa-acylated, glucosamine derived disaccharide called lipid A. Lipid A serves as the hydrophobic anchor for lipopolysaccharide (LPS) that surrounds and protects Gram-negative bacteria against external agents such as antibiotics and detergents (Raetz & Whitfield, 2002) and is the major contributing factor for the decreased permeability of Gram-negative bacteria compared to Gram-positive organisms (Figure 1.2).

With a few exceptions, Gram-negative bacteria lacking lipid A are not viable, and the few Gram-negative bacteria that can tolerate loss of lipid A have severely reduced pathogenicity (Moffatt et al, 2010; Nguyen et al, 2011; Peng et al, 2005; Steeghs et al, 1998). In addition to its role as an essential membrane component, lipid A (also known as endotoxin) is a potent activator of the mammalian host Toll-like receptor 4. This activation is capable of eliciting life-threatening septic shock that is lethal in ~ 50% of the cases (Aderem & Ulevitch, 2000; Miller et al, 2005). In fact, septicemia is the tenth leading cause of death in the United States with more than 30,000 deaths annually (Heron, 2007). All these unique properties make lipid A an attractive target for the development of novel therapeutics against Gram-negative pathogens.

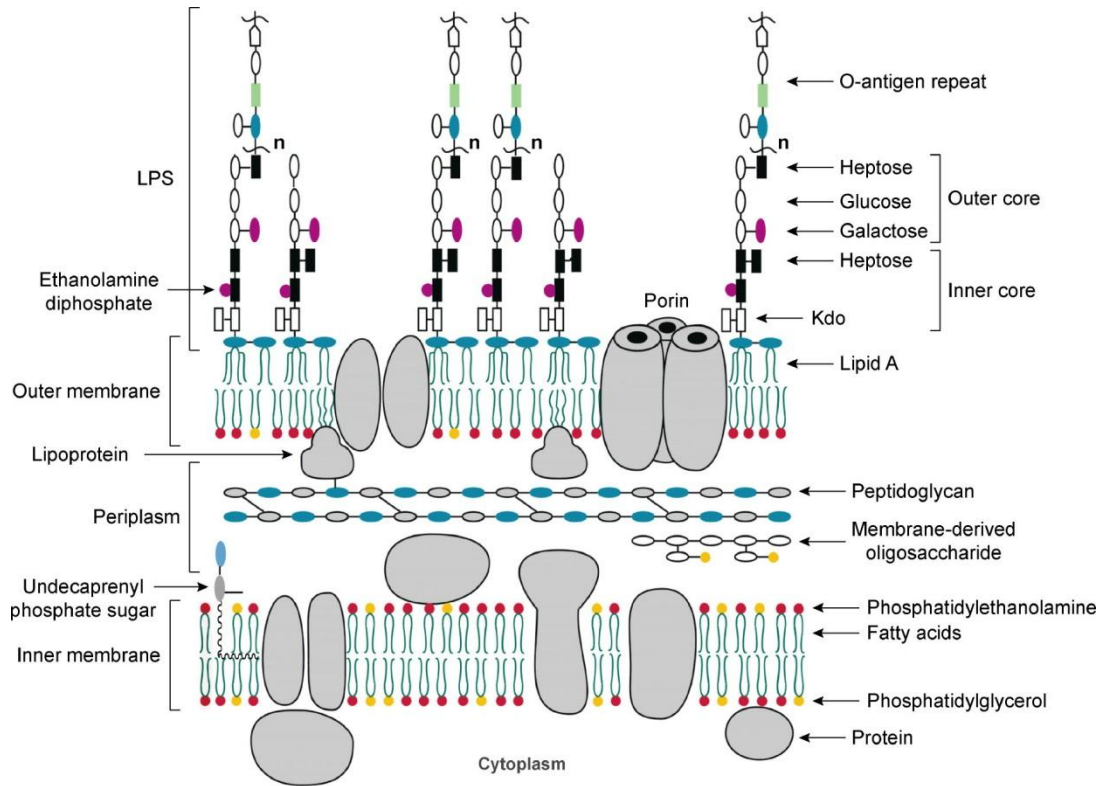


Figure 1.2: A representation of the *E. coli* cell envelope. *E. coli*, a typical Gram-negative bacterium, has two membranes. The inner membrane is composed mainly of a phospholipids bilayer, followed by a thin peptidoglycan layer. The inner surface of the outer membrane is also composed mainly of phospholipids, while the outer membrane is composed mostly of lipopolysaccharide (LPS). Lipid A, a hexa-acylated disaccharide, anchors LPS in the membrane (Raetz et al, 2007b).

Lipid A biosynthesis is an essential pathway conserved in the majority of Gram-negative organisms (Raetz & Whitfield, 2002). Hence, targeting lipid A biosynthesis brings three major benefits. First, disrupting lipid A biosynthesis is bactericidal (Galloway & Raetz, 1990). Second, since LPS is a formidable barrier for many antibiotics, inhibiting lipid A biosynthesis increases outer membrane permeability rendering Gram-negative organisms hypersensitive to other antibiotics and host defense

systems (Normark et al, 1969). Indeed, mutants deficient in lipid A biosynthesis have been shown to be severely hypersensitive to antibiotics that normally cannot permeabilize through the Gram-negative outer membrane including vancomycin, fusidic acid, and rifampicin (Vaara & Nurminen, 1999). Finally, because lipid A is the active component of endotoxin, killing bacteria by reducing their lipid A content may reduce the complications of septic shock during treatment (Wyckoff et al, 1998). As a result of these properties, enzymes involved in lipid A biosynthesis have become attractive targets for novel antibiotic discovery.

1.3: LpxC inhibitors are novel antibiotics

Lipid A biosynthesis is carried out by nine constitutive enzymes conserved in most Gram-negative bacteria (Raetz et al, 2007a; Raetz & Whitfield, 2002). The pathway has been well-characterized in *E. coli*. Although the biosynthesis begins with acylation of UDP-*N*-acetyl-glucosamine (UDP-GlcNAc) by LpxA using *R*-3-hydroxymyristoyl acyl carrier protein (ACP), this reaction is thermodynamically unfavorable (Anderson et al, 1993). Thus, the first committed step of lipid A biosynthesis is the deacetylation reaction catalyzed by UDP-3-*O*-(acyl)-*N*-acetyl glucosamine deacetylase (LpxC). From here, eight additional steps are required to form Kdo₂-Lipid A, which is the minimal structure required to maintain bacterial viability under most growth conditions (Figure 1.3) (Barb et al, 2007a).

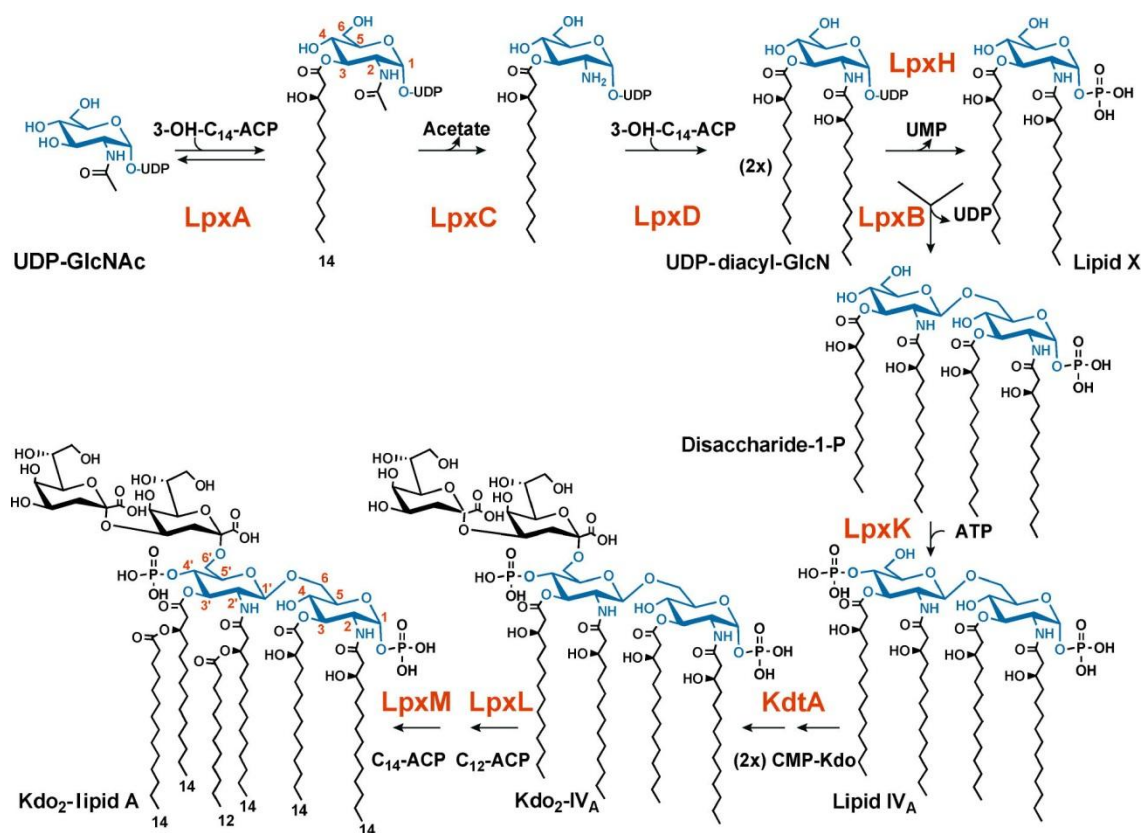


Figure 1.3: Biosynthetic Pathway of Kdo₂-lipid A in *E. coli*, modified from (Raetz et al, 2007b). LpxC catalyzes the committed step of lipid A biosynthesis. Numbers in *red* correspond to the carbons on the glucosamine rings (*blue*); Kdo subunits are in *black*. The numbers at the bottom of acyl chains correspond to the length of the predominant species found in *E. coli*.

Among the enzymes involved in lipid A biosynthesis, LpxC is a particularly attractive target for the design of novel antibiotics. It is an essential enzyme in lipid A biosynthesis and has no mammalian homologues; thus, inhibitors of LpxC are unlikely to cause severe side effects. Additionally, LpxC is a zinc metalloamidase, a class of enzymes known to be inhibited by hydroxamate-containing compounds that bind the catalytic zinc ion.

1.4: Study of LpxC inhibitors and mechanisms of resistance to these inhibitors

The current study focuses on the development of LpxC inhibitors and understanding novel mechanisms of resistance to these inhibitors. Chapter 2 reports the kinetic characterization of novel, potent inhibitors of LpxC inhibitors that display impressive broad-spectrum antibiotic activity against multidrug-resistant Gram-negative pathogens. These studies lay the framework for further development of optimized LpxC inhibitors that target the particularly problematic multidrug-resistant Gram-negative pathogen *Neisseria gonorrhoeae*.

Chapter 3 describes the isolation and characterization of spontaneously resistant *E. coli* mutants that are over > 200-fold more resistant to all LpxC inhibitors. This is the highest level of resistance ever observed for these inhibitors. Using whole genome sequencing, we identified two chromosomal point mutations that account for resistance additively and independently: one in *fabZ*, a dehydrase in fatty acid biosynthesis, and the other in *thrS*, the Thr-tRNA ligase.

Chapters 4 and 5 focus on the elucidation of how the identified point mutations in FabZ and ThrS confer resistance to LpxC inhibitors respectively. Specifically, biochemical characterization shows that for both enzymes, the isolated mutations result in reduced enzymatic activities *in vitro*. In chapter 4, study of the FabZ mutants led to the surprisingly observation of decreased level of LpxC in bacterial cells harboring *fabZ* mutations, suggesting that the biosyntheses of fatty acids and lipid A are regulated to maintain balance between phospholipids and lipid A. In chapter 5, study of the ThrS mutant showed that the mutation in *thrS* slows protein production and cellular growth,

establishing that reduced protein biosynthesis can confer a suppressive effect on inhibition of membrane biosynthesis. Altogether, these studies reveal an impressive compensatory ability of bacteria to overcome inhibition of lipid A biosynthesis by rebalancing cellular homeostasis, a unique mechanism of antibiotic resistance.

In total, the following chapters not only allow for a greater understanding of LpxC inhibition and mechanism of high-level resistance to these inhibitors, they also provide fundamental clues for understanding bacterial cellular regulation and its impact in drug development and antibiotic resistance.

Chapter 2
Characterization of LpxC Inhibitors

Reproduced in part with permission from Lee CJ, Liang X, Chen X, Zeng D, Joo SH, Chung HS, Barb AW, Swanson SM, Nicholas RA, Li Y, Toone EJ, Raetz CRH, and Zhou, P “Species-specific and inhibitor-dependent conformations of LpxC: implications for antibiotic design.” *Chemistry and Biology*

Copyright © 2011 Elsevier Ltd All rights reserved.

AND

Reproduced in part with permission from Liang X, Lee CJ, Chen X, Chung HS, Zeng D, Raetz CRH, Li Y, Zhou, P, and Toone EJ “Syntheses, Structures and Antibiotic Activities of LpxC Inhibitors Based on the Diacetylene Scaffold.” *Bioorganic and Medicinal Chemistry*

Copyright © 2011 Elsevier Ltd All rights reserved.

2.1: Introduction

Over the past 20 years, there has been significant progress on the development of potent, broad-spectrum LpxC inhibitors (Figure 2.1). All of these known inhibitors prevent LpxC enzymatic catalysis by chelating the active site zinc ion through their hydroxamate moiety. The first inhibitor, L-161,240, is a phenyloxazoline hydroxamic acid that is a competitive inhibitor of *E. coli* LpxC ($K_I \sim 50$ nM). Although, L-161,240 displays a minimal inhibitory concentration (MIC) of 6 $\mu\text{g/mL}$ against wild-type *E. coli*, it has no antibiotic activity against the problematic Gram-negative pathogen *P. aeruginosa* (Jackman et al, 2000; Onishi et al, 1996). Subsequently, targeted screening with a metalloenzyme inhibitor library yielded a series of sulfonamide-containing hydroxamate compounds with inhibitory activity against LpxC. The most potent of these species (BB-78485) possesses a slightly broader antibacterial spectrum compared to L-151,240, but it is still inactive against *P. aeruginosa* (Clements et al, 2002).

Over the past decade, the Raetz and Zhou labs at Duke University have characterized a unique compound called CHIR-090 (Anderson, 2004). CHIR-090 is a two-step, slow, tight binding inhibitor of *E. coli* LpxC with an apparent K_I of 4 nM and K_I^* of 0.5 nM (Barb et al, 2007a). Compared to its predecessors, CHIR-090 is the best LpxC inhibitor reported to date and kills both *E. coli* and *P. aeruginosa* in bacterial disc diffusion assays with an efficacy rivaling that of ciprofloxacin (McClerren et al, 2005). Though CHIR-090 exhibits more broad-spectrum antibiotic activity compared to L-161,240 and BB-78485, it is still ineffective against other Gram-negative bacteria; for example, compared to *E. coli* LpxC, CHIR-090 is ~ 600 -fold less effective against

LpxC orthologs from the *Rhizobium* family with an apparent K_I of 340 nM against *Rhizobium leguminosarum* LpxC. Though *Rhizobium leguminosarum* is not a human pathogen, its high level of intrinsic resistance suggests that other pathogenic CHIR-090-sensitive strains, such as *E. coli* and *P. aeruginosa*, may acquire resistance through a similar mechanism.

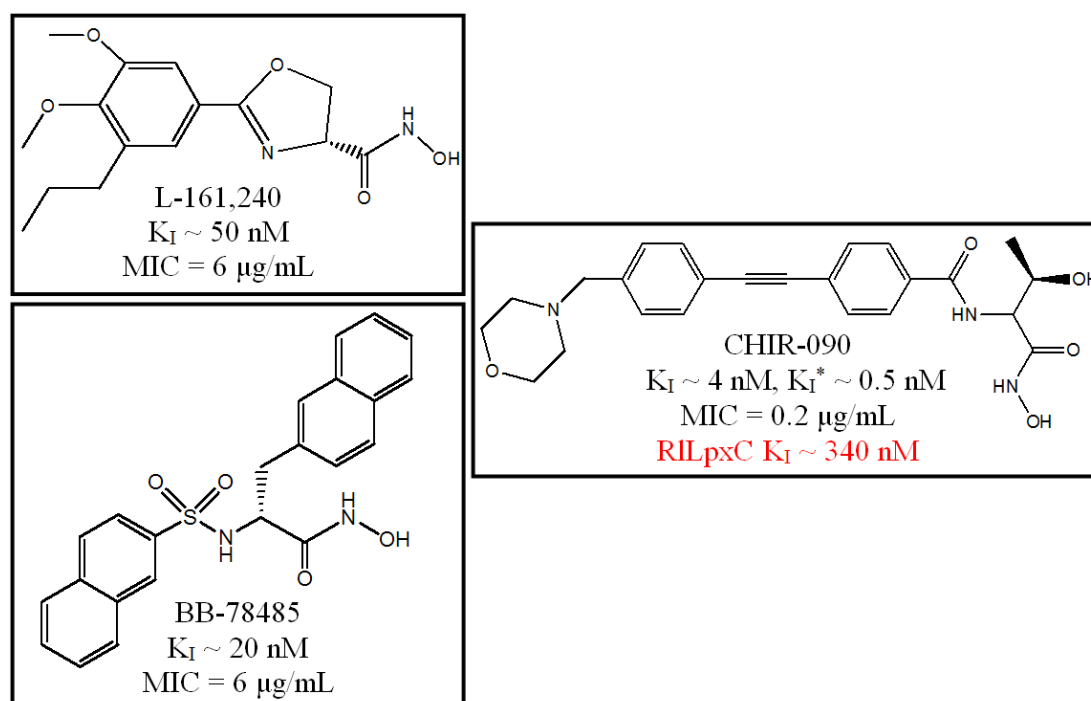


FIGURE 2.1: Structures of LpxC inhibitors. K_I and MIC values are against *E. coli* LpxC and *E. coli* K12 wild-type strain W3110 respectively. The K_I value of CHIR-090 against *Rhizobium leguminosarum* LpxC (RILpxC) is 340 nM.

Structural studies show that CHIR-090 occupies the hydrophobic substrate-binding passage where the acyl chain of the LpxC substrate would reside. The first phenyl group (proximal to the hydroxamate group) is located near the active site and next to the entrance of the hydrophobic passage, the acetylene group lies in the narrowest part of the passage, and the second phenyl ring (distal to the hydroxamate group) emerges from the passage (Figure 2.2) (Barb et al, 2007a).

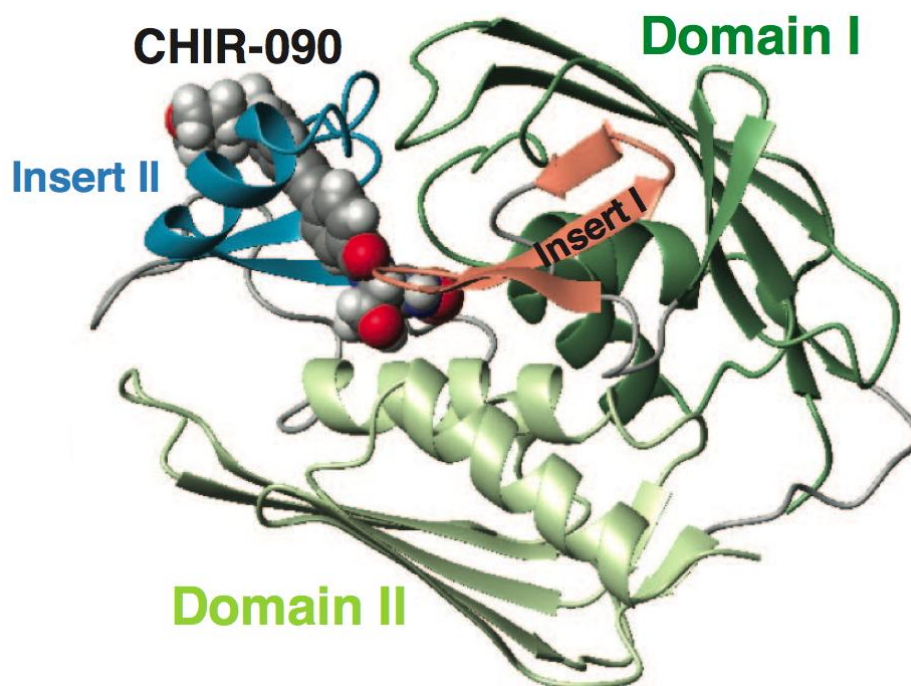


FIGURE 2.2: NMR structure of *A. aeolicus* LpxC/CHIR-090 complex PDB ID: 2JT2 (Barb et al, 2007a). CHIR-090 occupies the hydrophobic substrate-binding passage consisting of the Insert II region of Domain II of LpxC.

The exit of the substrate-binding passage contains a glycine residue that is conserved in LpxC orthologs sensitive to CHIR-090 inhibition. In *Rhizobium* LpxC, this glycine residue is replaced by a serine residue. This replacement narrows the substrate-binding passage and causes a van der Waals steric clash with the distal phenyl ring of CHIR-090 (Figure 2.3). Furthermore, biochemical studies show a Ser-to-Gly RILpxC mutant is 100-fold more sensitive to CHIR-090 inhibition relative to the wild-type enzyme (Barb et al, 2007a). This motivated us to evaluate novel inhibitors with a narrower scaffold to overcome this resistance mechanism.

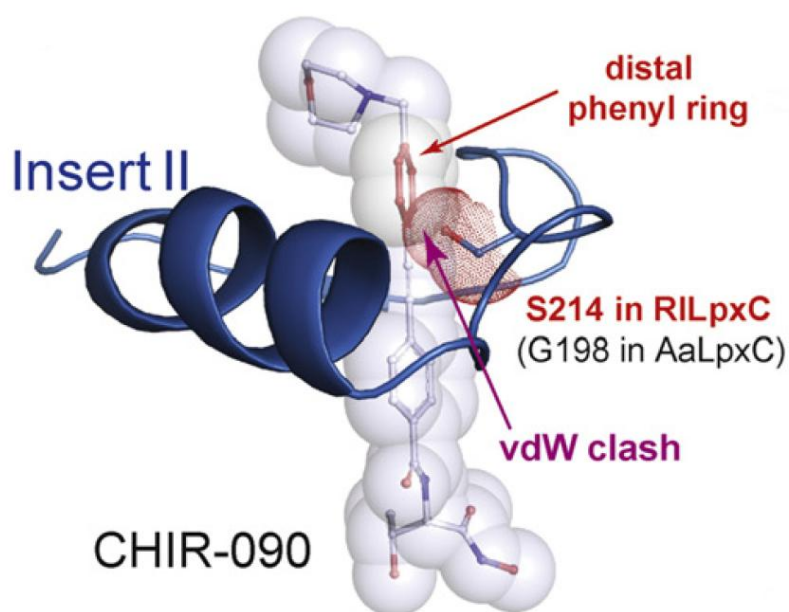


FIGURE 2.3: CHIR-090 resistance generated by steric clashes between S214 in RILpxC and the distal ring of CHIR-090. CHIR-090 and the S214 side chain are shown in stick and transparent-sphere models. The distal phenyl ring of CHIR-090 and the side chain of S214 in RILpxC are highlighted in red. The Insert II conformation was generated using homology modeling based on the structure of the AaLpxC/CHIR-090 complex (PDB entry: 2JT2), which contains a Gly (G198) at the corresponding position of S214 in RILpxC.

In this chapter, we describe the biochemical characterization of two new LpxC inhibitors based on the diacetylene motif that effectively overcome the resistance of RILpxC. Most excitingly, these compounds have enhanced binding against EcLpxC and superior broad spectrum potency against a wide variety of clinically important Gram-negative pathogens, including *E. coli*, *P. aeruginosa*, *Salmonella typhimurium*, *Klebsiella pneumonia*, *Vibrio cholera*, *Bordetella bronchiseptica*, *Burkholderia cepacia*, *Burkholderia cenocepacia*, and *Burkholderia dolosa*.

2.2: Materials and Methods

2.2.1: MIC assay

MICs were determined according to the NCCLS protocol (NCCLS, 1997) adapted to 96-well plates and LB media. Briefly, 1.0×10^5 bacterial cells in LB medium containing 5% DMSO and various concentrations of the compound were incubated at 37 °C for 22 hours. After the incubation, [4,5-dimethylthiazol-2-yl]-2,5-diphenyltetrazolium bromide solution (MTT) was added (0.2 mg/mL final concentration) and incubated at 37 °C for another 3 hours. The MIC was determined as the lowest concentration of an antibiotic that prevented color change (yellow to black).

2.2.2: LpxC enzymatic inhibition assay

UDP-3-*O*-[(*R*)-3-hydroxymyristoyl]-*N*-acetylglucosamine and [α - 32 P]UDP-3-*O*-[(*R*)-3-hydroxymyristoyl]-*N*-acetylglucosamine were prepared and assayed as previously described. Briefly, UTP [α - 32 P]-800Ci/mmol 10mCi/ml, 250 μ Ci

(PerkinElmer, Waltham, MA) was added in a solution (with a final volume of 62.5 μL) containing 0.5 mM Glucosamine 1-Phosphate (Sigma-Aldrich, St. Louis, MO), 1 mM MgCl_2 , 5 mM DTT, 100 mM Tris-HCl pH 8.0, inorganic pyrophosphatase 10U/50 μL (Sigma, St. Louis, MO), and UDP-glucose pyrophosphorylase 100U/200 μL (Sigma St. Louis, MO) for 1 hour at room temperature. Following this addition, 63 μL water, 75 μL methanol, 5 μL saturated sodium carbonate, and 2.0 μL acetic anhydride were added, and the mixture was incubated for another 20 minutes at room temperature, at which time 1 μL of acetic anhydride was spiked into the reaction. To monitor conversion, 1 μL aliquots were taken before reaction 1, before reaction 2, and after the addition of 1 μL of acetic anhydride. These aliquots were diluted 1:100 with water, and 1 μL of these solutions were spotted on a polyethyleneimine (PEI) cellulose plate to check for percent conversion. The plate was dried, washed in methanol for 10 min, dried again, and ran in a solvent system containing 0.2 M guanidine HCl. The developed plate was dried and exposed to a PhosphorImager screen for 30 minutes.

The reaction mixture was diluted with the addition of ~1545 μL of water and loaded on a 1 mL column of diethylaminoethyl (DEAE) Sepharose fast-flow resin (pre-equilibrated by washing with 5-10 mL of water followed by 10-15 mL of 10 mM triethylammonium bicarbonate pH 8.5) for buffer exchange. The column was washed with 10 mL of water, and fractions (1 mL each) were eluted with a total of 8 mL 100 mM triethylammonium bicarbonate pH 8.5. The fractions that contained the most counts per minute (cpm) as determined by a scintillation counter were collected and speed vacuumed to dryness overnight at room temperature.

The mixture was recovered by resuspending in 200 μ L of water. [α - 32 P]UDP-3-*O*-[(*R*)-3-hydroxymyristoyl]-*N*-acetylglucosamine was produced from a reaction mixture containing [α - 32 P]UDP-GlcNAc (100 μ Ci, 0.18 μ M), 18 μ M (*R*)-3-hydroxymyristoyl-ACP, 10 mg/ml fatty acid-free bovine serum albumin, 40 mM Hepes pH 8.0, and purified EcLpxA (0.2 μ M) (generous gift from Dr. Sanghoon Joo) to a final volume of 688 μ L. Low-specific-radioactivity (high mass) [α - 32 P]UDP-3-*O*-[(*R*)-3-hydroxymyristoyl]-*N*-acetylglucosamine was produced from a reaction mixture identical to that above, but containing [α - 32 P]UDP-GlcNAc (1 μ Ci, 480 μ M), R-3-hydroxymyristoyl-ACP (480 μ M). Reactions were initiated by the addition of enzyme and were incubated at 30 $^{\circ}$ C for 1 hour. The entire reaction mixture was loaded onto a 1 mL column of DEAE-Sepharose fast flow resin (prewashed with 5 mL of 1 M bis-Tris, pH 6.0, 3 mL of 50 mM bis-Tris, pH 6.0 + 1 M NaCl, and then 4 mL of 10 mM bis-Tris, pH 6.0) that was connected to a Sep-Pak C₁₈ cartridge (Waters, Milford, MA). The Sep-Pak C₁₈ cartridge had been washed with 10 mL of 100% acetonitrile followed by 20 mL of water. After loading the sample, the combined column and cartridge were washed with 15 mL of 200 mM NaCl. The Sep-Pak, which contained the desired product, was removed and further washed with 30 mL of water. The UDP-3-*O*-[(*R*)-3-hydroxymyristoyl]-*N*-acetylglucosamine was eluted from the cartridge with 50% acetonitrile in 0.5 mL fractions. The fractions that contained the most counts per minute (cpm) as determined by a scintillation counter were collected, lyophilized overnight, and recovered in 10 mM bis-Tris, pH 5.5, to give a final concentration of 0.5-1.0 mM. The product was stored at -20 $^{\circ}$ C (Figure 2.4).

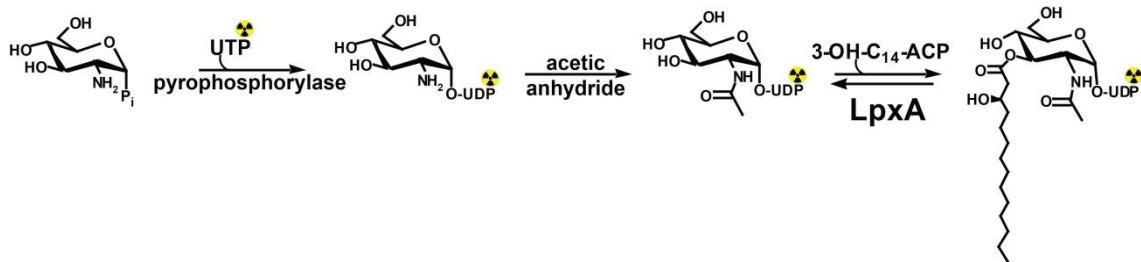


FIGURE 2.4: Chemo-enzymatic synthesis of $[\alpha\text{-}^{32}\text{P}]\text{UDP-3-O-}[(R)\text{-3-hydroxymyristoyl}]\text{-N-acetylglucosamine.}$

Assays of LpxC activity were performed at 30 °C in 25 mM sodium phosphate (pH 7.4), 1 mg/mL bovine serum albumin, 25 mM KCl, and 0.5 mM DTT, in the presence of 5 μM of UDP-3-O-[(R)-3-hydroxymyristoyl]-N-acetylglucosamine, 100,000 cpm/reaction of $[\alpha\text{-}^{32}\text{P}]\text{UDP-3-O-}[(R)\text{-3-hydroxymyristoyl}]\text{-N-acetylglucosamine}$ and 0.2 nM EcLpxC, unless noted otherwise. 10% DMSO was included and held constant in assay mixtures. Reactions were initiated by the addition of enzyme, and time points were taken over the course of 30 minutes by removing 1 μL aliquots and mixing with 2 μL of 1.25 M sodium hydroxide in a second microcentrifuge tube to stop the reaction. The tubes were then incubated at 30 °C for 10 min to remove ester-linked fatty acids (Figure 2.5A). These samples were neutralized with 1 μL of 1.25 M acetic acid and 1 μL of 5% trichloroacetic acid. The tubes were placed on ice for 5 min and then centrifuged for 2 min. A 2 μL portion of the supernatant was spotted onto a PEI cellulose plate. The plate was dried, washed in methanol for 10 min, dried again, and developed in 0.2 M guanidine HCl. The developed plate was dried and exposed to a PhosphorImager screen overnight. The percent deacetylation was calculated from the

relative amounts of $[\alpha\text{-}^{32}\text{P}]\text{UDP-GlcNAc}$ and $[\alpha\text{-}^{32}\text{P}]\text{UDP-GlcN}$, as detected by a PhosphorImager (Molecular Dynamics, Inc.) (Figure 2.5B).

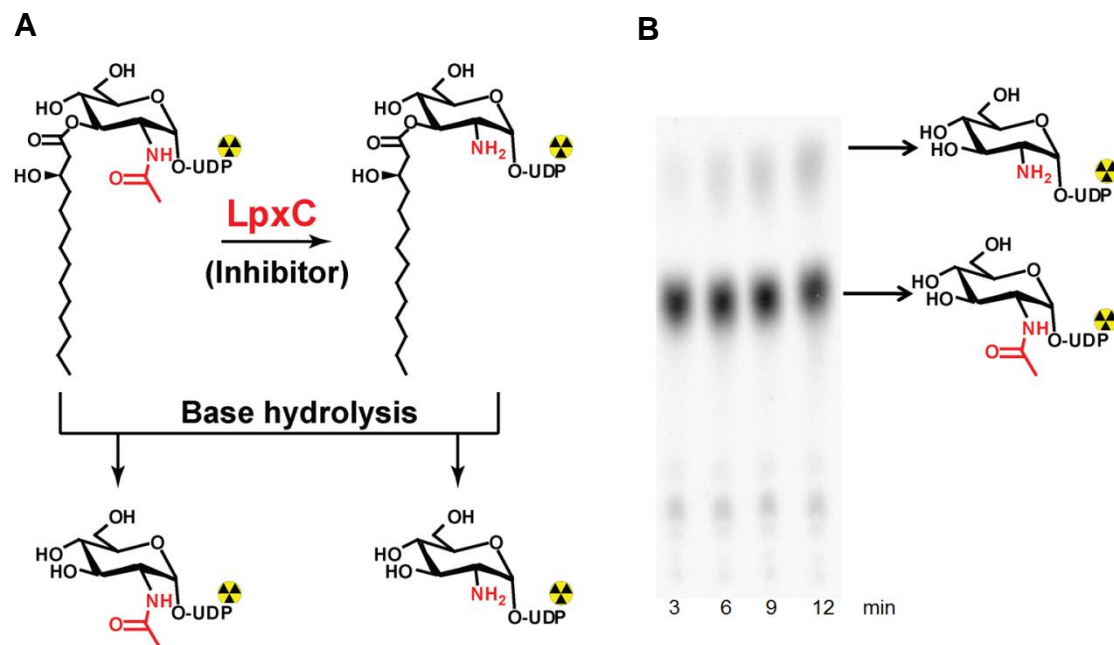


FIGURE 2.5: LpxC assay setup. (A) LpxC assay reaction. (B) Resolution and visualization of product conversion as a function of time.

Initial velocities were calculated from the linear portion of reaction progress curves (<10% conversion of substrate to product). K_M and V_{max} values were determined by varying the substrate concentration from 0.5 to 50 μM . Data were analyzed using an Eadie-Hofstee plot (Dowd & Riggs, 1965) and by a nonlinear curve-fitting program (KaleidaGraph, Synergy Software); the resultant values were nearly identical within experimental errors.

To determine a K_I value, LPC-009 concentrations were varied from 12.5 pM to 15 nM. Fractional activity (v_i/v_0) versus LPC-009 concentration was plotted and fitted to calculate a K_I^{app} value using the Morrison equation (Copeland, 2005):

$$\frac{v_i}{v_0} = 1 - \frac{([E]_T + [I]_T + K_I^{app}) - \sqrt{([E]_T + [I]_T + K_I^{app})^2 - 4[E]_T[I]_T}}{2[E]_T}$$

where v_i is the initial velocity of the reaction in the presence of the inhibitor, v_0 is the initial velocity of the reaction in the absence of the inhibitor, $[E]_T$ is the total enzyme concentration, and $[I]_T$ is the total inhibitor concentration. A K_I value was calculated using the following equation:

$$K_I = \frac{K_I^{app}}{1 + [S]/K_M}$$

where $[S]$ is the substrate concentration. All measurements were done in triplicates.

2.2.3: Creation of "W3110NG," the *Neisseria gonorrhoeae* *LpxC* knock-in strain

To determine if *Neisseria gonorrhoeae* (*N. gonorrhoeae*) *lpxC* complements *E. coli lpxC*, *N. Gonorrhoeae lpxC* was cloned into a pBAD33.1 (Chung & Raetz, 2010) plasmid and the chromosomal EcLpxC was knocked-out. *N. gonorrhoeae lpxC* was amplified from genomic *Neisseria gonorrhoeae* strain FA19 chromosomal DNA (generous gift from Dr. Robert Nicholas) using primers 5' GGCGCAGCATATG CTGCAAAGAACTTTGGCGAAATCC 3' and 5' 5' GCAGAAGCTTTTATCCGC AATTTCTGATGTTTCAGCTCGT 3'. The PCR fragment was gel extracted and purified using QIAquick Gel Extraction Kit (Qiagen, Valencia, CA). A pBAD33.1 plasmid

(Chung & Raetz, 2010) was miniprep using QIAprep Miniprep Kit (Qiagen, Valencia, CA). Both the vector and PCR fragment was digested using restriction enzymes *NdeI* and *HindIII* (NEB, Ipswich, MA). The vector was treated with calf intestinal alkaline phosphatase (NEB, Ipswich, MA) for 1 hour. After PCR purification, the vector and DNA fragment were ligated using T4 DNA ligase (Invitrogen, Carlsbad, CA), transformed into XL1-Blue Competent cells (Stratagene, Santa Clara, CA), and grown on LB agar containing 25 µg/mL of chloramphenicol (Sigma, St. Louis, MO). Correct constructs were confirmed using primers 5' GTCACACTTTGCTATGCCAT 3' and 5' AATTCTGTTTTATCAGACCGCTT 3' for DNA fragment amplification and sequencing. Confirmed constructs were transformed into chemically competent W3110 as previously described (Wang & Kushner, 1991).

A confirmed colony was infected with P1*vir* lysate containing *E. coli* DNA that has a kanamycin cassette (Baba et al, 2006) in the place of *lpxC* on the chromosome. For P1*vir* transduction, a liquid culture of the confirmed colony was grown from a single colony in LB media + 25 µg/mL of chloramphenicol at 37 °C to OD₆₀₀ ~ 0.6. 1 mL of this culture was collected per reaction and centrifuged at 13,000 rpm for 1 minute to pellet the cells. After the supernatant was discarded, the cell pellet was resuspended in 100 µL (0.1 x volume) of P1 salts solution (10mM CaCl₂ and 5 mM MgSO₄). Each reaction was mixed with 10, 30, or 100 µL of P1*vir* lysate. A negative control reaction with no phage lysate reaction was included. Reactions were incubated at 37 °C for 25 minutes at which time 200 µL of 1M sodium citrate (Na₃C₆H₅O₇) was added followed by 1 mL of LB media containing 25 µg/mL of chloramphenicol and a

varying amount of L-arabinose (0, 0.02%, and 0.2%). Cells were grown at 37 °C for ~ 1 hour and centrifuged at 13,000 rpm for 1 minute to pellet the cells. The supernatant was discarded and cells were resuspended in 50 µL of 1M sodium citrate and spread onto plates containing 25 µg/mL of chloramphenicol, 50 µL/mL kanamycin, 5mM sodium citrate and a varying amount of L-arabinose (0, 0.02%, and 0.2%). Colonies were purified three times by sequential restreaking of individual colonies upon plates containing the same medium. Genomic DNA was isolated from colonies and the region around *lpxC* was amplified and sequenced using primers 5' ACAACGTCCTGAAATCACTCTGGTGA 3' and 5' TCCCTAATAAGAG ATGCGGCCAGAAGTA 3'. Colonies with *N. gonorrhoeae lpxC* on a pBAD33.1 plasmid only grew in the presence of 0.02% or 0.2% L-arabinose (Figure 2.6).

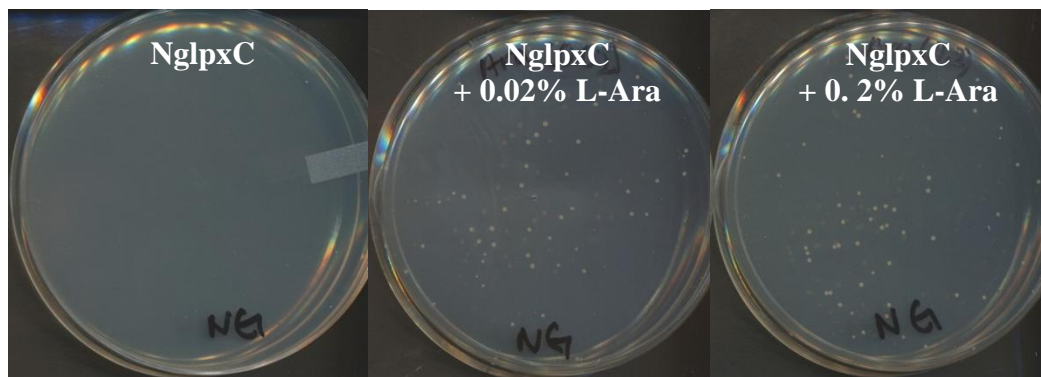


FIGURE 2.6: Complementation of *E. coli lpxC* with *N. gonorrhoeae lpxC*. Cells with *N. gonorrhoeae lpxC* (*NglpxC*) on a pBAD33.1 plasmid only grow in the presence of L-arabinose (L-Ara) to induce expression of *NglpxC* in W3110 *E. coli lpxC* knock-out cells

After establishing that *N. gonorrhoeae lpxC* can indeed complement *E. coli lpxC*, linear PCR product containing the *N. gonorrhoeae lpxC* was used to replace *E. coli* chromosomal *lpxC*. A linear PCR product containing the *N. gonorrhoeae lpxC* with flanking sequences complementary to the upstream 5' region of *E. coli lpxC* and to the downstream 3' region of *E. coli lpxC* was amplified from *Neisseria gonorrhoeae* strain FA19 chromosomal DNA using primers 5' CGAATGTATAG TACTTTCGGTTGGATAGGTAATTTGGCGAGATAATACGATGCTGCAAAGA ACTTTGGCGAAATCC 3' and 5' AGAGAGTGCCAGATTTGCCAGTCGAAT TTTATACGACAGTATAAATGTCGTTATCCGCAATTTCTGATGTTTCAGCTCGT 3'. The PCR product was gel purified and electroporated into *E. coli* DY330 cells, an *E. coli* host containing λ -Red recombinase to promote homologous recombination, using previously established protocols (Yu et al, 2000). While DY330 cannot survive on the LB/agar plate supplemented with 30 μ g/mL of L-161,240, cells wherein *E. coli lpxC* replaced with *N. gonorrhoeae lpxC* can survive on this media. Transformants were therefore selected directly using L-161,240. Genomic DNA from resistant colonies was isolated, and the region around *lpxC* was amplified and sequence with primers 5' ACAAACGTCCTGAAATCACTCTGGTGA 3' and 5' TCCCTAATAAGAG ATGCGGCCAGAAGTA 3'.

One clone in which *N. gonorrhoeae lpxC* had replaced chromosomal *E. coli lpxC* was selected and grown at 30 °C. This strain was used to generate P1_{vir} lysate, which was used to transduce chromosomal *N. gonorrhoeae lpxC* into the chromosome of *E. coli* W3110. Transduced cells were plated on LB/agar containing 30 μ g/mL of L-

161,240 and 5 mM sodium citrate. The resulting colonies were purified three times on this media. Genomic DNA from resistant colonies was isolated, and the region around *lpxC* was amplified and sequenced using primers 5' ACAAACGTCCTGAA ATCACTCTGGTGA 3' and 5' TCCCTAATAAGAG ATGCGGCCAGAAGTA 3'. The colony that harbored the *N. gonorrhoeae lpxC* knock-in was named as "W3110NG."

2.3: Results

2.3.1: Characterization of LPC-009

Since point mutations that narrow the LpxC substrate binding passage can confer resistance to CHIR-090, we reasoned that compounds with a narrower, diacetylene chemical scaffold would be able to overcome the CHIR-090 resistance represented by RILpxC. The diacetylene scaffold was among the many chemical structures initially discussed in the international patent WO 2004/062601 A2 (Anderson, 2004), but its effect on the antibiotic profile was not quantified.

To normalize for differences between membrane permeability and efflux between *E. coli* and *Rhizobium leguminosarum*, we used an RILpxC *E. coli* knock-in strain (W3110RL). In this strain, the chromosomal *E. coli lpxC* gene is replaced with *R. leguminosarum lpxC* (Barb et al, 2007a) (Figure 2.7). Hence, since W3110RL is identical to the wild-type *E. coli* strain W3110 except for the *lpxC* gene, any difference in the MIC value should directly reflect the difference in the binding affinity values of the compound against the two different LpxC enzymes.

As expected, the MIC values of CHIR-090 are vastly different for these two bacterial strains, and the ~ 600-fold variation in MIC values correlates with the ~ 150-fold differences in the K_I values (Barb et al, 2007a). Further evaluation of a modified compound, LPC-004, which lacks the morpholine moiety, showed a similar reduced efficacy (~ 800 fold) for W3110RL than for W3110 (Figure 2.7), confirming that the bulky distal phenyl group, but not the morpholine group, is responsible for decreased activity against RILpxC. Replacing the phenyl-acetylene group with a (N,N-dimethylamino)methyl-diacetylene group generated a weaker inhibitor (LPC-007), but the ratio of the MIC values for W3110 and W3110RL started to diminish (~ 160-fold). Finally, addition of a phenyl ring to the diacetylene group (LPC-009) reduced the MIC values of W3110RL to 6.3 $\mu\text{g}/\text{mL}$ (Figure 2.7). Excitingly, LPC-009 also appears to be 4-fold more potent than CHIR-090 for inhibiting the growth of *E. coli* in MIC assays (Figure 2.7) (Lee et al, 2011).

To establish that the diacetylene-based compound LPC-009 indeed displays a superior antibiotic profile over CHIR-090, we measured the MICs of LPC-009 and CHIR-090 against a panel of Gram-negative human pathogens, including *P. aeruginosa*, *S. typhimurium*, *K. pneumonia*, *V. cholera*, *B. bronchiseptica*, *B. cepacia*, *B. cenocepacia*, and *B. dolosa*. Consistently, LPC-009 showed a 2 to 64-fold enhancement of antibiotic activity over CHIR-090 (Lee et al, 2011) (Table 2.1).

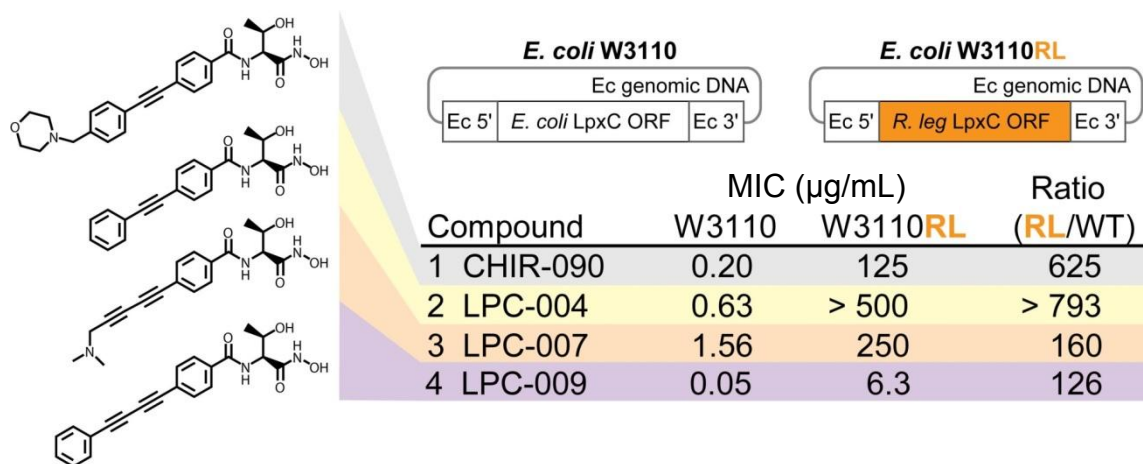


FIGURE 2.7: LPC-009 overcomes RILpxC CHIR-090 resistance. MICs of each compound against strains of wild-type *E. coli* (W3110) and *E. coli* with its genomic lpxC gene replaced by that of *R. leguminosarum* (W3110RL). The narrow diacetylene scaffold not only overcomes the CHIR-090 resistance of RILpxC, but also displays enhanced antibiotic activity against *E. coli* (Lee et al, 2011).

Table 2.1: MIC value comparisons between CHIR-090 and LPC-009 (Lee et al, 2011).

Pathogen	CHIR-090 ($\mu\text{g/mL}$)	LPC-009 ($\mu\text{g/mL}$)
<i>Pseudomonas aeruginosa</i> PAO1	1.6	0.74
<i>Salmonella typhimurium</i> LT2	0.16	0.024
<i>Klebsiella pneumonia</i> 43816	0.64	0.10
<i>Vibrio cholera</i> P4 (P27459 Δ ctxAB::Km ^R , Sm ^R)	0.16	0.010
<i>Bordetella bronchiseptica</i> RB50	16	2
<i>Burkholderia cepacia</i> ATCC 25146	> 32	12
<i>Burkholderia cenocepacia</i> GIIIa J2315 lineage ET12	> 32	32
<i>Burkholderia dolosa</i> AU0158 lineage 5LC6	8	0.125

To further evaluate the inhibition of EcLpxC by LPC-009, we performed detailed enzymatic assays. A K_I^{app} of 0.55 ± 0.09 nM (Figure 2.8) and a corresponding K_I value of 0.18 ± 0.03 nM were calculated according to the assumption of competitive inhibition and a measured K_M of 2.5 ± 0.2 mM for EcLpxC. Interestingly, we observed a similar fractional inhibition of product accumulation with or without inhibitor preincubation (1 hour) with enzyme prior to initiating the reaction, suggesting that unlike the slow tight-binding inhibitor CHIR-090, LPC-009 does not appear to inhibit EcLpxC in a time-dependent fashion.

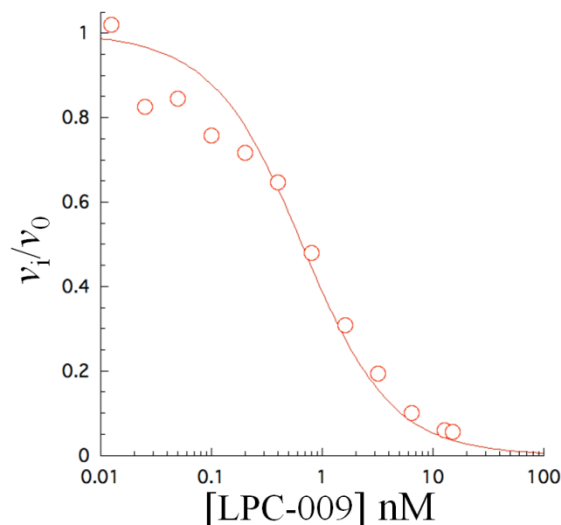


FIGURE 2.8: Inhibition curve of LPC-009 against *E. coli* LpxC.

2.3.2: Characterization of LPC-011

To improve the solubility of LPC-009 in aqueous solution, we have evaluated three amino substituents of the distal phenyl ring. The para-amino substituent, LPC-011, not only improved solubility but also slightly enhanced the antibiotic activity of the parent compound LPC-009 (MIC value of 0.03 $\mu\text{g/mL}$ against *E. coli* W3110). To obtain a more quantitative measure of the inhibitory effect of LPC-011, we performed detailed enzyme kinetic studies. Analogous to LPC-009 but unlike the slow tight-binding inhibitor CHIR-090, we observed a similar fractional inhibition of product accumulation with or without LPC-011 pre incubation (1 to 3 hour) with enzyme, suggesting that LPC-011 does not inhibit *E. coli* LpxC in a time-dependent fashion. A K_I^{app} value of 0.20 ± 0.02 nM and a corresponding K_I value of 0.067 ± 0.007 nM were calculated for LPC-011, resulting in a ~ 2.7 -fold reduction in the K_I^{app} and K_I values of

LPC-011 in comparison with LPC-009 ($K_I^{\text{app}} = 0.55 \pm 0.09$ nM and $K_I = 0.18 \pm 0.03$ nM) (Figure 2.9).

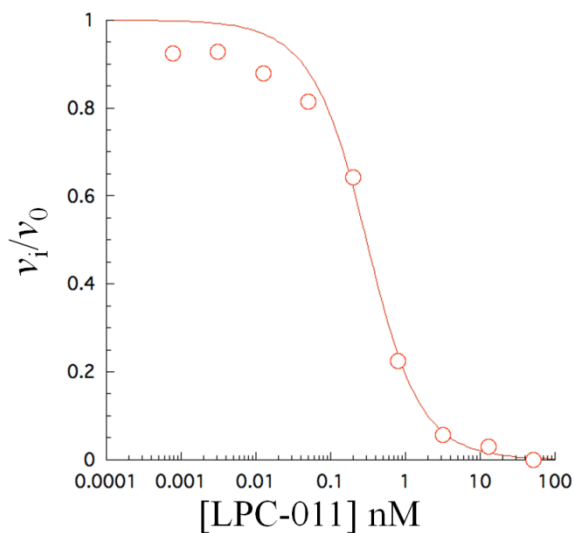


FIGURE 2.9: Inhibition curve of LPC-011 against *E. coli* LpxC.

Structural studies show the para-amino substitution of the distal phenyl group, due to its proximity to Phe212 of *E. coli* LpxC, likely enhances the edge-to-face p-p interaction between the distal phenyl ring of LPC-011 and Phe212 of *E. coli* LpxC, modestly increasing the activity of the para-amino compound LPC-011 relative to LPC-009 for *E. coli* LpxC (Liang et al, 2011) (Figure 2.10).

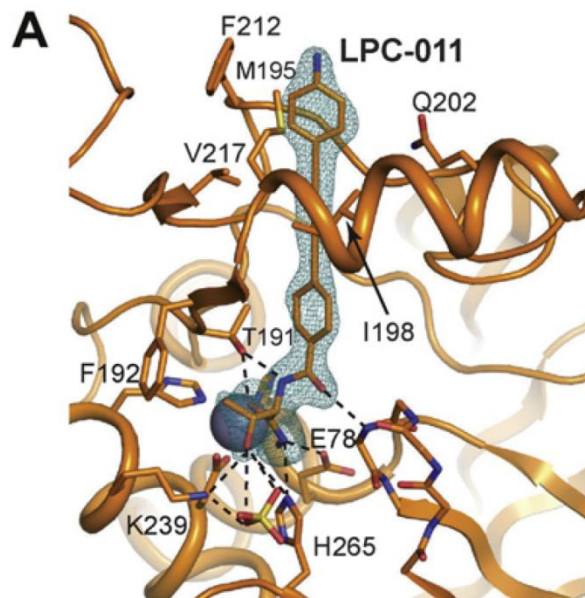


FIGURE 2.10: Structure of the *E. coli* LpxC/LPC-011 complex shows favorable energetic interaction between the para-amino substituted distal phenyl ring with F212 of *E. coli* LpxC (Liang et al, 2011).

2.4: Discussion

The rise of multidrug-resistant microbes and their dire impact on human health highlight the pressing need for novel antibiotics with a distinct mode of action to combat Gram-negative infections. Although LpxC is an attractive and validated novel drug target for these efforts, development of lead compounds has been hampered by a lack of broad-spectrum antibiotic activity against a wide range of Gram-negative bacteria. Here, we detail a successful strategy for designing a broad-spectrum LpxC inhibitor: identifying key residues that confer inhibitor resistance in representative LpxC orthologs and searching for compounds to circumvent these stumbling blocks. The diacetylene-based LPC-009 inhibitor presents an important first step in this process,

as our combined kinetic and structural studies show that LPC-009 inhibits a wide range of orthologs with promising efficacy. Likewise, we have shown that the addition of a para-amino group to LPC-009 results in a compound, LPC-011, that has enhanced binding affinity and potency against *E. coli* LpxC.

Future directions include optimizing derivative compounds to target other Gram-negative pathogens, particularly the superbug *Neisseria gonorrhoeae*. Not only does *Neisseria gonorrhoeae* cause the second most prevalent bacterial sexually transmitted infection globally, leading to high morbidity and socioeconomic consequences, it is also rapidly developing multidrug resistance (Ohnishi et al, 2011). We have already created a *Neisseria gonorrhoeae lpxC* knock-in strain (W3110NG) that is analogous to W3110RL except this knock-in strain has *N. gonorrhoeae lpxC* directly replacing the endogenous *E. coli lpxC* on the chromosome. This knock-in strain will greatly facilitate our studies on identifying and characterizing novel LpxC inhibitors that have potent antibiotic activities against *Neisseria gonorrhoeae*.

Given the attractive properties of LpxC inhibitors outlined in this chapter (low K_I and MIC values and broad-spectrum antibiotic activities), these compounds are excellent candidates for use as future antibiotics against multidrug-resistant Gram-negative bacteria. However before clinical use, it is critical to study mechanisms of resistance to these novel inhibitors that would severely limit their clinical efficacy and life span.

Chapter 3
Isolation and Characterization of Spontaneously Arising Resistant Mutants
to CHIR-090

3.1: Introduction

In anticipation of the progression of LpxC inhibitors into clinical use, it is imperative to study and characterize mechanisms of resistance to LpxC inhibitors described in the previous chapter. This is particularly important since these compounds will be used against multidrug-resistant Gram-negative pathogenic strains, which are not only extremely resilient, but also very resourceful in developing mechanisms of resistance (Livermore, 2012).

Bacteria have three major mechanisms to overcome the toxicity of antibiotic compounds to achieve high-level drug resistance: modification of the target protein, modification of the compound, and altered flux of the compound (Walsh, 2000). For example, one major mechanism of penicillin resistance is through alteration of the protein target site whereby the presence of point mutations in the penicillin-binding proteins significantly decreases the binding affinity of penicillin to bind and inhibit enzymatic catalysis (Smith & Klugman, 1998). Another mechanism of penicillin resistance is caused by the production of beta-lactamases, which are enzymes that deactivate penicillin G and other beta-lactams (Bradford, 2001). Finally, bacteria also employ efflux pumps and/or modifications to porins to decrease the cellular concentration of the compound as a method to reduce the effectiveness of antibiotics.

Indeed resistance to LpxC inhibitors can be acquired through these mechanisms. In *Pseudomonas aeruginosa*, up-regulation of the efflux pumps MexAB-OprM, MexCD-OprJ, or MexEF-OprN confers ~ 8 to 32-fold resistance to CHIR-090, indicating that enhanced efflux can be a mechanism of resistance against LpxC

inhibitors. Furthermore, resistance can also be acquired as a result of point mutations in the target gene LpxC, as a PaLpxC L18V mutant is 16-fold more resistant relative to wild-type. This point mutation does not change enzymatic activity relative to wild-type LpxC but does lead to a decrease in CHIR-090 binding affinity *in vitro* (Caughlan et al, 2011).

Although spontaneously resistant *E. coli* and *Pseudomonas aeruginosa* (*P. aeruginosa*) mutants have been previously reported (Caughlan et al, 2011; Clements et al, 2002), these mutants only displayed moderate resistance, with an average of 4 to 32-fold increased MIC values relative to wild-type, and their biochemical consequences remain largely uncharacterized. In this chapter, we report the two-step isolation and characterization of spontaneously resistant *E. coli* mutants that are > 200-fold resistant to all known LpxC inhibitors. Our studies of resistance in a laboratory setting may ultimately aid in the intervention of these same mechanisms of resistance from arising in a clinical setting.

3.2: Materials and Methods

3.2.1 General materials and methods

All bacteria were grown in LB (Anderson, 2004) liquid or agar medium at 37 °C unless otherwise indicated. DNA primers were purchased from IDT, Inc. (Coralville, IA). Commercial enzymes, reagents, kits, and cells were used according to manufacturer's instructions unless otherwise noted. DNA sequencing was done at Eton Bioscience, Inc. (Research Triangle Park, NC) unless otherwise noted.

3.2.2 Isolation of CHIR-090 resistant mutants

10^9 cells of W3110 (*E. coli* Genetic Stock center, Yale University) diluted from overnight cultures were plated on LB agar containing 1 $\mu\text{g}/\text{mL}$ CHIR-090. After 24 hours of growth, visible colonies were restreaked on the same medium and then purified three times on LB agar. Two colonies were isolated and designated “CRM1” and “CRM5.” 10^8 cells of CRM1 and CRM5, diluted from overnight cultures, were plated on LB agar containing 10 $\mu\text{g}/\text{mL}$ CHIR-090. After 24 hours of growth, visible colonies were isolated, restreaked, and purified using the same process described above. Two colonies, one descended from CRM1 and the other from CRM5, were designated “CRM1B” and “CRM5B” respectively. Among all the mutants isolated in the second step, colonies of CRM1B and CRM5B grew most robustly and were visible after ~ 24 hours whereas other mutant colonies were visible only after > 36 hours of growth.

3.2.3 MIC assay

MICs were determined according to the NCCLS protocol (NCCLS, 1997) with minor modifications and adapted to 96-well plates. Briefly, 96-well plates were prepared < 3 hours in advance to minimize potential degradation of the compound prior to starting the experiment. Using an automatic multi-channel pipette (VWR International, Radnor, Pennsylvania), each well was filled with 100 μL of LB media while wells in the first column were filled with 200 μL of LB media. A specified amount of each compound was added to corresponding wells in the first column of each plate. Solutions were mixed by pipetting 100 μL up and down six times. Then 100 μL

from each well was transferred to the next sequential well in the row. This process was repeated for each well of the row. For the last well of each row, 100 μ L of solution was taken out and discarded. This method results in 2-fold serial dilutions of compounds across each row.

Liquid cultures of each strain were grown from single colonies in LB media at 37 °C to log phase $OD_{600} \sim 0.2 - 0.6$. Cultures were then diluted to $\sim 10^6$ bacterial cells in LB media, and 100 μ L of this solution was added to each well containing various concentrations of the designated compound. Plates were then incubated at 37 °C for ~ 22 hours. After the incubation, [4,5-dimethylthiazol-2-yl]-2,5-diphenyltetrazolium bromide solution (Sigma-Aldrich, St. Louis, MO) was added (0.2 mg/mL final concentration) and incubated at 37 °C for $\sim 12-16$ hours. The MIC was defined as the lowest concentration of compound that prevented color change (yellow to purple). To enhance inhibitor solubility, 10% DMSO was added to the growth media when assaying L-161,240, BB-78485, LPC-009 and LPC-011.

3.2.4 Disc diffusion assay

Assays were done as previously described (McClerren et al, 2005). Briefly, liquid cultures of each strain (W3110, CRM1, CRM5, CRM1B, CRM5B) were grown from single colonies in LB media at 37 °C to $OD_{600} \sim 0.2$. A lawn of cells of each strain was spread onto LB agar plates with sterile cotton swabs. Sterile filter-paper discs (Whatman # 42) were placed on top of the bacterial lawn, and then a specified amount of each compound was spotted onto each disk (10 μ g of CHIR-090, 40 μ g of L-161,240,

and 40 µg of BB-78485). DMSO (100%) was also spotted onto a separate disk as a control. Plates were then incubated overnight at 37 °C. A halo of suspended growth was clearly visible on the next day around disks that had been spotted with active compounds. The diameter of each halo was measured for each compound and strain and compared to W3110.

3.2.5 Whole genome sequencing

Genomic DNA was extracted using Easy-DNA kit (Invitrogen, Carlsbad, CA) from W3110 and CRM mutants and sent off to Ambry Genetics (Aliso Viejo, CA) for Singleton DNA Library Preparation and 50-HiSeq sequencing services. Resulting fastq files were analyzed using program Maq-0.7.1 (SourceForge.net) and aligned to *E. coli* K-12 W3110 (AC_000091.1). Additional point mutations present in CRM strains, but not in the parental strain W3110, with quality scores > 100 are shown in Table 3.2. These point mutations were also independently verified with PCR amplification of designated genes from genomic DNA and sequencing at Eton Bioscience, Inc. (Research Triangle Park, NC) using primers 1-6 (Table 3.1).

3.2.6 Constructions of CRM *wtfabZ* and CRM *wtfabZ*, *wthrS* mutants

To create CRM strains with wild-type *fabZ*, P1*vir* lysate was generated from the Keio mutant JW0195 (*E. coli* Genetic Stock center, Yale University) that has a kanamycin cassette 20 kbps downstream of *fabZ* (Baba et al, 2006) and used to transfect CRM1B and CRM5B. Colonies were plated and purified three times on LB agar

containing 50 $\mu\text{g}/\text{mL}$ kanamycin and 5 mM sodium citrate following established protocols (Wang & Kushner, 1991).

Briefly, to create P1*vir* lysate, liquid cultures of JW0195 were grown from single colonies in LB media supplemented with 0.2% glucose at 37 °C to $\text{OD}_{600} \sim 0.05 - 0.1$. At that time, 5mM CaCl_2 (final concentration) and 0.0005 – 0.002 x volume of P1*vir* lysate was added to each culture. A negative control culture without any phage addition was also done for growth comparison. Cultures were grown for another 2 - 4 hours until phage cultures became clear with visible dead cell debris while the no phage negative control culture remained turbid. Phage cultures were then transferred to glass tubes with solvent resistant caps. Ten drops of chloroform were added to each tube and the solution was vortexed vigorously to kill all remaining bacterial cells. Pellets were centrifuged at 13,000 rpm for ~ 20 minutes. The supernatant was transferred to another glass tube and stored at 4 °C. P1*vir* lysate is stable at 4 °C for several years. To regenerate P1*vir* lysate for infection, W3110, a wildtype strain that does not have any selective markers or antibiotic resistance, was used.

For P1*vir* transduction, liquid cultures of the recipient strains, CRM1B and CRM5B, were grown from single colonies in LB media at 37 °C to $\text{OD}_{600} \sim 0.6$. 1 mL of this culture was collected per reaction and centrifuged at 13,000 rpm for 1 minute to pellet the cells. After the supernatant was discarded, the cell pellet was resuspended in 100 μL (0.1 x volume) of P1 salts solution (10mM CaCl_2 and 5 mM MgSO_4). Each reaction was mixed with 10, 30, or 100 μL of P1*vir* lysate. A negative control reaction with no phage lysate reaction was included. Reactions were incubated at 37 °C for 25

minutes at which time 200 μ L of 1M sodium citrate ($\text{Na}_3\text{C}_6\text{H}_5\text{O}_7$) was added followed by 1 mL of LB media. Cells were grown at 37 °C for ~ 2 hours and centrifuged at 13,000 rpm for 1 minute to pellet the cells. The supernatant was discarded and cells were resuspended in 50 μ L of 1M sodium citrate and spread onto plates containing 50 μ L/mL kanamycin and 5mM sodium citrate. Colonies were purified three times by sequential restreaking of individual colonies. Genomic DNA was isolated from colonies and the region around *fabZ* was amplified and sequenced using primers 1-2. Colonies that harbored wild-type *fabZ* were designated “CRM1B *wtfabZ*” and “CRM5B *wtfabZ*” with respect to their parental strains.

To create CRM5B *wtfabZ*, *wtthrS*, the kanamycin cassette in CRM5B was excised using pCP20 as previously described (Lu et al, 2011). Briefly, the plasmid pCP20 encodes for the FLP recombinase of which mediates recombination between the two FLP sites causing removal of the kanamycin cassette and leaving only a scar of one FLP sequence on the chromosome (Datsenko & Wanner, 2000; Doublet et al, 2008). The pCP20 transformants were selected for ampicillin resistance at 30 °C, followed by purifying single colonies twice at 42 °C by restreaking on LB agar plates in the absence of antibiotic; the 42 °C incubation was necessary for expression of the FLP recombinase and for diluting out the temperature-sensitive replicon of pCP20. The desired strain was then obtained by replica plating for ampicillin and kanamycin sensitivity at 30 °C and designated “CRM5B *wtfabZ*, Δ *metN*.”

P1*vir* lysate was generated from the Keio mutant JW1696 (*E. coli* Genetic Stock center, Yale University) that has a kanamycin cassette 10 kbps upstream of *thrS* (Baba

et al, 2006) and used to transfect CRM5B *wtfabZ*, $\Delta metN$. Colonies were selected and purified as described above. The area around *thrS* was amplified using primers 3-4 and sequenced using primers 3-6. A colony that harbored wild-type *thrS* was designated “CRM5B *wtfabZ*, *wtthrS*” (Table 3.2).

Table 3.1: Sequence of indicated primers used.

Primer Designation	Sequence (5' to 3')
1	CAAGCGTCTGAAATCGCTTGAGCG
2	GACAACGTGAGATTTTCAGTACGGTACCC
3	AACCTTTCAGACGCACCGTGATG
4	ACGGAATTTAATTTTCCTTAACCTGGATAACTTTTT GC
5	GTCTGGAGATCATTCGTCACCTCCTGT
6	ATTTCTCAAGTCTGCTTTAACACGAATGCC

3.2.7: Growth curves

Bacterial cultures were diluted 1:100 from overnight cultures and grown till log phase ($OD_{600} \sim 0.5$). At which point, cells were diluted 10-fold into unused LB media and OD_{600} was measured over the course of ~ 12 generations. To ensure continuous log phase growth, once bacterial cultures reached $OD_{600} \sim 0.5$, cells were continuously diluted 10-fold into unused media.

3.3: Results

3.3.1 Isolation of spontaneously resistant mutants to CHIR-090

CHIR-090 is one of the most thoroughly characterized LpxC-targeting antibiotics discovered to date. It is a slow, tight binding inhibitor for *E. coli* LpxC, and it displays potent antibiotic activity for a wide range of Gram-negative human pathogens (Barb et al, 2007a; Barb et al, 2007b; Barb & Zhou, 2008; Bodewits et al, 2010; Caughlan et al, 2011; Cole et al, 2010; McClerren et al, 2005). It also elicits a very low rate of spontaneous resistance in *E. coli* ($< 10^{-9}$). Accordingly, efforts to isolate and characterize spontaneous mutants with high levels of CHIR-090 resistance in one step have not been successful.

In order to overcome this limitation and isolate spontaneously arising CHIR-090-resistant mutants with a clean background, we employed a two-step approach, starting from the genetically well-characterized *E. coli* strain W3110. First, medium-level resistant mutants were generated by exposing wild-type W3110 cells in the presence of a low concentration of CHIR-090 (1 $\mu\text{g}/\text{mL}$, 5x MIC). Surviving CHIR-090 resistant mutants (CRMs) were isolated at a frequency of $\sim 10^{-9}$. These isolates were used as the starting cells for a second round of selection in the presence of a high concentration of CHIR-090 (10 $\mu\text{g}/\text{mL}$, 50x MIC). Surviving mutants in the second step were isolated at a frequency of $\sim 10^{-7}$. Among these isolates, the two fastest growing resistant mutants (CRM1B and CRM5B) together with their parental strains, (CRM1 and CRM5), were chosen for further characterization (Figure 3.1).

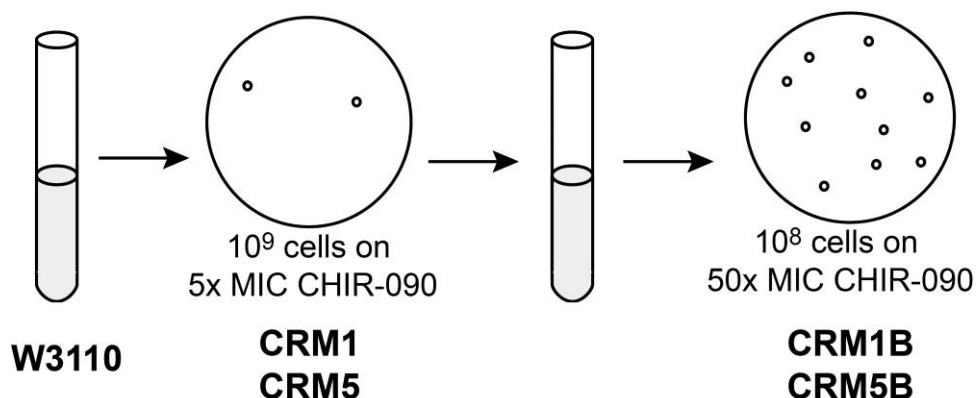


Figure 3.1: Resistant mutants were isolated in a two-step process. W3110 were plated on 5x MIC CHIR-090 (1 $\mu\text{g}/\text{mL}$) plates, surviving colonies, CRM1 and CRM5, were isolated at a frequency of $\sim 10^{-9}$. These mutants were further plated on 50x MIC (10 $\mu\text{g}/\text{mL}$) CHIR-090 plates, surviving colonies able to grow in this higher concentration, CRM1B and CRM5B, were isolated at a frequency of $\sim 10^{-7}$.

3.3.2 Mutants are resistant to a variety of LpxC inhibitors

We first evaluated the four isolated mutants for their resistance to well-characterized LpxC inhibitors, including CHIR-090, the diacetylene-based compounds, LPC-009 (Lee et al, 2011) and LPC-011 (Liang et al, 2011), and the earlier generation of LpxC inhibitors, L-161,240 (Onishi et al, 1996) and BB-78485 (Clements et al, 2002). The CRM1 and CRM5 mutants, isolated after exposure to 1 $\mu\text{g}/\text{mL}$ of CHIR-090, show ~ 50 -fold higher MICs to LpxC inhibitors CHIR-090, LPC-009, and LPC-011, whereas the two mutants CRM1B and CRM5B, isolated after exposure to 10 $\mu\text{g}/\text{mL}$ CHIR-090, showed a remarkable > 200 -fold higher MIC relative to the parental strain W3110 (Table 3.2).

Table 3.2: Point mutations and MIC of mutant strains

Strain	Chromosomal mutations	Protein	CHIR-090 (µg/mL)	LPC-009 (µg/mL)	LPC-011 (µg/mL)
W3110	None	None	0.2	0.04	0.02
CRM1	<i>fabZ</i> : T(50) to A	FabZ: Leu(17) to Gln	12.3	3.13	0.78
CRM1B	<i>fabZ</i> : T(50) to A <i>thrS</i> : T(1549) to G	FabZ: Leu(17) to Gln ThrS: Ser(517) to Ala	56.3	N/D	N/D
CRM5	<i>fabZ</i> : C(212) to T	FabZ: Ala(71) to Val	12.3	6.25	1.56
CRM5B	<i>fabZ</i> : C(212) to T <i>thrS</i> : T(1549) to G	FabZ: Ala(71) to Val ThrS: Ser(517) to Ala	56.3	N/D	N/D
CRM1B <i>wtfabZ</i>	<i>thrS</i> : T(1549) to G <i>metN::kan</i>	ThrS: Ser(517) to Ala	1.25	0.625	0.313
CRM5B <i>wtfabZ</i>	<i>thrS</i> : T(1549) to G <i>metN::kan</i>	ThrS: Ser(517) to Ala	1.25	0.625	0.313
CRM5B <i>wtfabZ</i> , <i>wthrsS</i>	Δ <i>metN</i> <i>ydiU::kan</i>	None	0.2	0.04	0.02

wtfabZ: wild-type *fabZ*, *wthrsS*: wild-type *thrS*, and *muthrsS*: mutant *thrS*, N/D: not determined due to solubility limit of compound

Likewise, our disc diffusion assays show that all of these mutants are highly resistant to the earlier generation of LpxC inhibitors L-161,240 and BB-78585 (Figure 3.2). However, due to the high level of resistance and limitations in compound solubility of LPC-009, LPC-011, L-161,240 and BB-78485, the exact MICs cannot be determined for these compounds. It is important to note that these LpxC inhibitors are based on a variety of chemical scaffolds. The observation that our isolated mutants are universally resistant to these compounds, regardless of their differing chemical structures, suggests that the mutants' resistance mechanisms are unlikely to be caused

by specific mutations in the target enzyme that reduces the potency of LpxC inhibitors, but rather caused by more general resistance mechanisms that counter the suppression of lipid A biosynthesis.

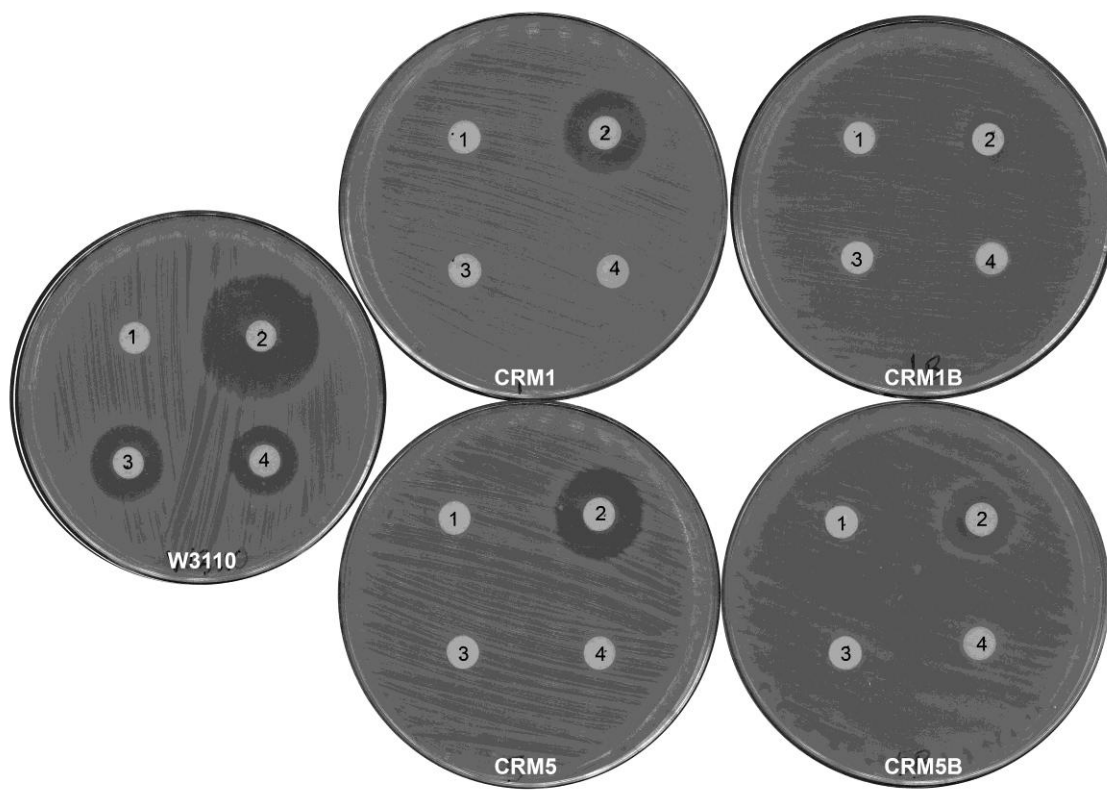


Figure 3.2: Disc diffusions assays. Spot 1 is 100% DMSO (2 μ L), spot 2 is CHIR-090 (10 μ g), spot 3 is L-161,240 (40 μ g), spot 4 is BB-78485 (40 μ g). Compared to W3110 (far left), all mutants are fully resistant to LpxC inhibitors L-161,240 and BB-78485.

3.3.3 Mutants defective in growth and not resistant to other antibiotics

Interestingly these CRM mutants appear to have slower growth compared to wild-type (Figure 3.3). Particularly, the double mutants CRM1B and CRM5B grow significantly slower compared to W3110 suggesting that the point mutation(s) in the second step markedly affects cellular growth. Furthermore, these mutants do not appear to have high-level resistance to other commonly used antibiotics including ampicillin, chloramphenicol, tetracycline, and polymyxin B (Table 3.3), suggesting that their mechanism(s) of resistance is quite specific to inhibition of lipid A biosynthesis.

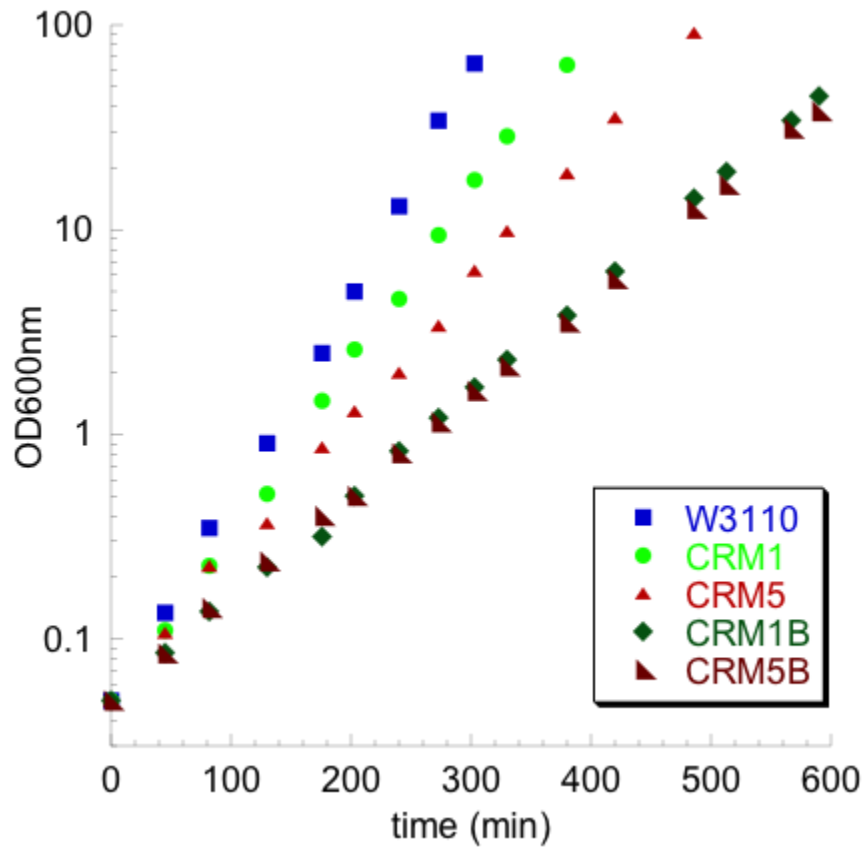


Figure 3.3: Growth curves for CRM mutants. Compared to W3110, CRM1 and CRM5 grow slightly slower while the double mutants CRM1B and CRM5B growth significantly slower.

Table 3.3: MIC of CRMs to other antibiotics

Strain	Ampicillin ($\mu\text{g}/\text{mL}$)	Chloramphenicol ($\mu\text{g}/\text{mL}$)	Tetracycline ($\mu\text{g}/\text{mL}$)	Polymyxin B ($\mu\text{g}/\text{mL}$)
W3110	3.1	12.5	3.1	1.6
CRM1	3.1	12.5	3.1	1.6
CRM5	3.1	12.5	3.1	1.6
CRM1B	3.1	12.5	3.1	1.6
CRM5B	3.1	12.5	3.1	1.6

3.3.4 Mutations of *fabZ* and *thrS* confer CHIR-090 resistance additively and independently

To pinpoint the specific mutations that confer resistance, we obtained whole genome sequencing data for our four mutant strains and compared them with the parental strain W3110. Our results show that CRM1 and CRM5 each have a single point mutation, T50A and C212T respectively, in *fabZ*, a dehydrase of fatty acid biosynthesis, respectively; whereas, both CRM1B and CRM5B have an additional point mutation, T1569G, in *thrS*, the threonine--tRNA ligase, compared to their parental strains (Table 3.2).

In order to determine if point mutations in *fabZ* and *thrS* cause CHIR-090 resistance in a synergistic manner, we replaced the mutated *fabZs* with wild-type *fabZ* on the chromosome of the double mutants CRM1B and CRM5B. The resulting strains, CRM1B *wtfabZ* and CRM5B *wtfabZ*, which contain the single point mutation in *thrS*, show 6-fold higher MIC to CHIR-090 (1.25 µg/mL) compared to the wild-type strain W3110 (0.2 µg/mL). Further loss of the remaining point mutation in *thrS* resulted in a strain (CRM5 *wtfabZ*, *wtthrS*) with an MIC identical to wild-type (Table 3.2, Figure 3.4). These results show that the point mutations in *fabZ* and in *thrS* confer ~ 50-fold and ~ 4 to 8-fold resistance respectively, and that *fabZ* and *thrS* mutations account for > 200-fold resistance in an additive and independent manner.

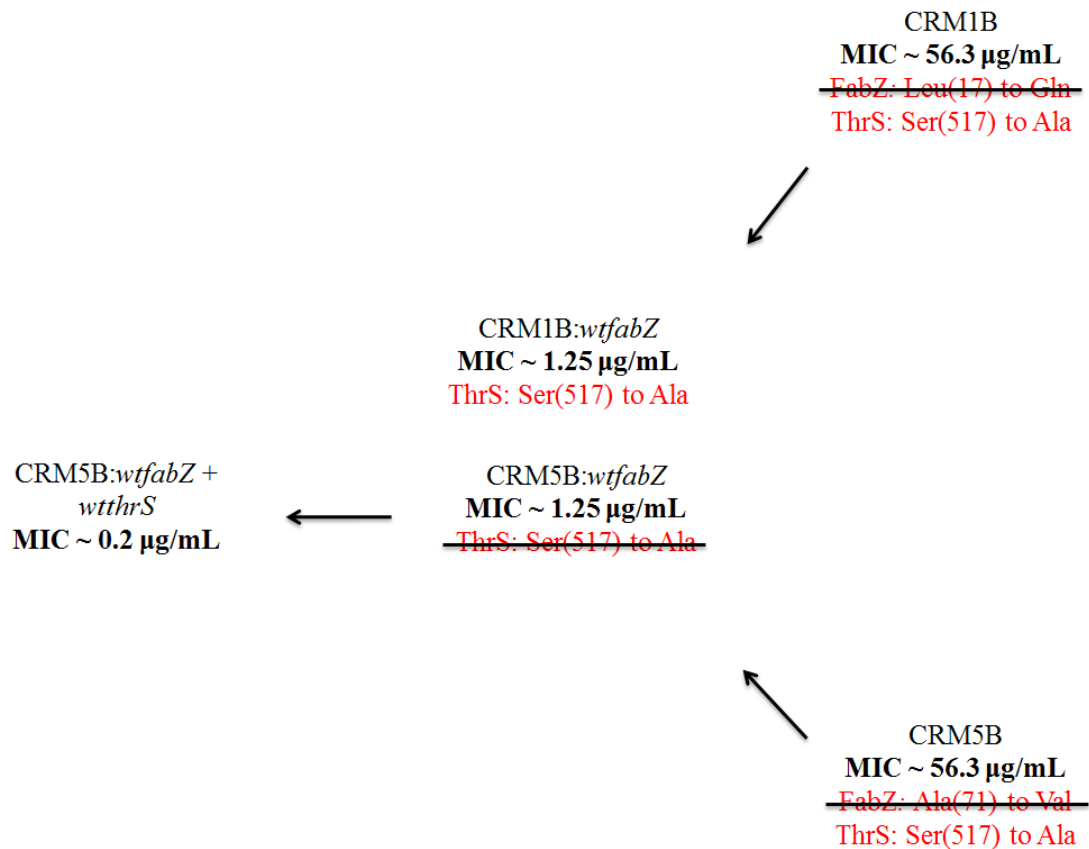


Figure 3.4: FabZ and ThrS point mutations confer resistance independently and additively. Loss of the point mutation in *fabZ* resulted in strains (CRM1B *wtfabZ* and CRM5B *wtfabZ*) that are 6-fold more resistant to CHIR-090 (MIC of 1.25 µg/mL) relative to the wild-type strain W3110 (MIC of 0.2 µg/mL). Further loss of the remaining point mutation in *thrS* resulted in a strain (CRM5 *wtfabZ*, *wtthrS*) with wild-type MIC.

3.4: Discussion

Through a two-step gradual exposure method, we have isolated spontaneously arising resistant mutants that display > 200-fold resistance to CHIR-090 and other LpxC inhibitors. This is the highest level of resistance observed against LpxC inhibitors to date. Indeed, these mutants are so resistant that among all of the LpxC inhibitors we have studied, only the MIC value for CHIR-090 could be determined for the double mutants (CRM1B and CRM5B) since their MIC values for the less potent LpxC inhibitors, L-161,240 and BB-78485 and even for the more potent diacetylene compounds, LPC-009 and LPC-011, are past the limits of compound solubility. This foreshadows that if these same resistant mutant strains develop in a clinical setting, they would be completely untreatable.

It is interesting to note that although the diacetylene compounds have several fold enhanced binding affinity for EcLpxC and MIC values relative to CHIR-090, they are less effective against these CRM mutants due to their lower solubility properties, suggesting that these diacetylene compounds may have limited clinical applications. The isolation and characterization of these mutants underscore the need to develop even more potent inhibitors of LpxC with enhanced solubility to combat these resistant mutants.

These spontaneously highly resistant mutants cannot be isolated in a single step, suggesting that they can arise as a result of cumulative mutations in multiple gene products, such as *fabZ* and *thrS*, which by themselves confer only moderate resistance (~ 6 to 50-fold). Thus in a clinical setting, it may be possible to delay the development

of high-level resistance (> 200-fold) from arising by initially using a high enough concentration of LpxC inhibitor to kill off any moderately resistant mutants.

Most interestingly, these resistant mutants do not appear to display any classical mechanisms of resistance. In contrast to the RILpxC CHIR-090-specific resistance described in the previous chapter, these CRMs appear to be universally resistant to all LpxC inhibitors regardless of their varying structural scaffolds. Also, these mutants do not have any point mutations in LpxC or even any other enzymes involved in lipid A biosynthesis. Furthermore, *fabZ* and *thrS* are essential genes of known functions and are not involved in any efflux pump or porin formation or function. It is also unlikely that *fabZ*, a fatty acid dehydrase, or *thrS*, a tRNA-synthetase, can be secondary targets of LpxC inhibitors, though those exact studies will be addressed in the upcoming chapters. Instead, all of these data suggest that these point mutations in *fabZ* and *thrS* causes global phenomena that can universally counter the suppression of lipid A.

Chapter 4
Characterization of FabZ Mutants

4.1: Introduction

FabZ is an intermediate enzyme of fatty acid biosynthesis catalyzing the dehydration of *R*-3-hydroxymyristoyl-acyl carrier protein (ACP) (Mohan et al, 1994) in fatty acid elongation and shares a common substrate with LpxA, the enzyme that precedes LpxC in lipid A biosynthesis. The end products of fatty acid biosynthesis are used in phospholipid biosynthesis; because *R*-3-hydroxymyristoyl-ACP is used in the biosynthesis of both fatty acids and lipid A, reactions catalyzed by FabZ and LpxC are considered the branch points between phospholipid and lipid A biosynthesis (Figure 4.1).

Spontaneously resistant mutants with 4 to 64-fold resistance to BB-78484 were reported previously (Clements et al, 2002). The majority of these mutants had point mutations in *fabZ*. It was hypothesized that these point mutations likely lead to a reduction in dehydrase activity and confer resistance by increasing the pool of *R*-3-hydroxymyristoyl-ACP, which in turn would increase the concentration of the LpxC substrate and thus suppress the inhibition of LpxC through mass action (Clements et al, 2002). However, the specific effects of these FabZ point mutations both on FabZ activity and its cellular consequences remain to be characterized.

This chapter focuses on the characterization of the FabZ mutants (CRM1 and CRM5) described in the previous chapter. We show these point mutations decrease FabZ enzymatic activity. Most unexpectedly, we observed a decreased level of LpxC in bacterial cells harboring *fabZ* mutations, suggesting that the biosyntheses of fatty acids and lipid A are tightly regulated to maintain balance between phospholipids and lipid A.

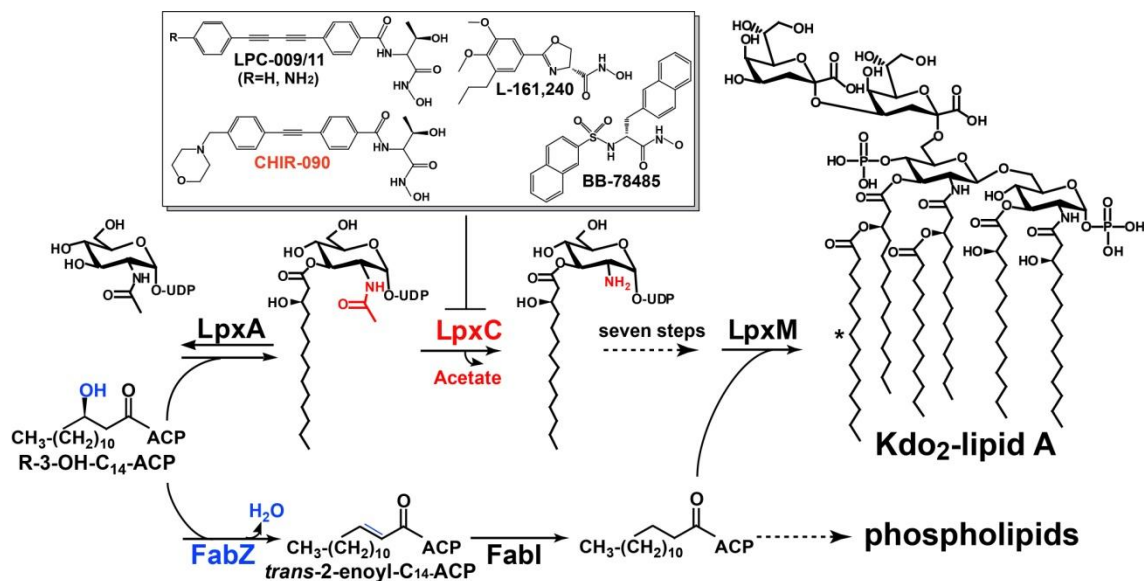


FIGURE 4.1: FabZ and LpxA share a substrate used in lipid A biosynthesis. LpxC (labeled in red) catalyzes the committed step of lipid A biosynthesis in *E. coli* that leads to the formation of Kdo₂-lipid A. The addition of the final myristoyl chain by LpxM is indicated by an asterisk (*). Inhibitors of LpxC include CHIR-090, L-161,240, BB-78485, LPC-009 (R = H), and LPC-011 (R = NH₂). FabZ (labeled in blue) is a dehydratase in fatty acid biosynthesis and shares a substrate with LpxA. Point mutations that decrease FabZ activity have been proposed to increase the flux of R-3-hydroxymyristoyl-ACP towards lipid A biosynthesis.

4.2: Materials and Methods

4.2.1: Construction of pBAD33.1(*fabZ*)

Genomic DNA extracted from W3110 was used to amplify wild-type *fabZ* using primers 5' GGCGCAGCATATGTTGACTACTAACACTCATACTCTGCAGATT GAAGAG 3' and 5' GCAGAAGCTTTCAGGCCTCCCGGCTAC 3'. The PCR fragment was gel extracted and purified using QIAquick Gel Extraction Kit (Qiagen, Valencia, CA). A pBAD33.1 plasmid (Chung & Raetz, 2010) was miniprep using QIAprep Miniprep Kit (Qiagen, Valencia, CA). Both the vector and PCR fragment were digested with the restriction enzymes *NdeI* and *HindIII* (NEB, Ipswich, MA). The vector was treated with calf intestinal alkaline phosphatase (NEB, Ipswich, MA) for 1 hour. After PCR purification, the vector and DNA fragment were ligated using T4 DNA ligase (Invitrogen, Carlsbad, CA), transformed into XL1-Blue Competent cells (Stratagene, Santa Clara, CA), and grown on LB agar containing 25 µg/mL of chloramphenicol (Sigma, St. Louis, MO). Correct constructs were confirmed using primers 5' GTCACACTTTGCTATGCCAT 3' and 5' AATTCTGTT TTATCAGACCGCTT 3' for DNA fragment amplification and sequencing. Confirmed constructs were transformed into chemically competent W3110 as previously described (Wang & Kushner, 1991).

4.2.2: *Liquid chromatography coupled with mass spectrometry (LC-MS)*

The method of normal phase LC-MS was previously described (Guan & Eichler, 2011). Briefly, normal phase LC- MS of lipids was performed using an Agilent 1200

Quaternary LC system coupled to a QSTAR XL quadrupole time-of-flight tandem mass spectrometer (Applied Biosystems, Foster City, CA). An Ascentis Si HPLC column (5 μm , 25 cm \times 2.1 mm) was used for liquid chromatography. Mobile phase A consisted of chloroform/methanol/aqueous ammonium hydroxide (800:195:5, v/v/v), mobile phase B consisted of chloroform/methanol/water/ aqueous ammonium hydroxide (600:340:50:5, v/v/v/v) and mobile phase C consisted of chloroform/methanol/water/aqueous ammonium hydroxide (450:450:95:5, v/v/v/v). The elution program comprised of the following: 100% mobile phase A was held isocratically for 2 minutes and then linearly increased to 100% mobile phase B over the duration of 14 minutes and held at 100% B for 11 minutes. The LC gradient was then changed to 100% mobile phase C over the duration of 3 minutes and held at 100% C for 3 minutes, and finally returned to 100% A over 0.5 minutes and held at 100% A for 5 minutes. The total LC flow rate was 300 $\mu\text{l}/\text{min}$. The post-column splitter diverted \sim 10% of the LC flow to the ESI source of the Q-Star XL mass spectrometer, with MS settings as follows: Ion spray voltage (IS) = $-$ 4500 V; Curtain gas (CUR) = 20 psi; Ion source gas 1 (GS1) = 20 psi; De-clustering potential (DP) = $-$ 55 V; Focusing potential (FP) = $-$ 150 V. For MS/MS, collision-induced dissociation was performed with collision energy ranging from 40 V to 70 V (laboratory frame of energy) and with nitrogen as the collision gas.

Reverse phase LC-MS was performed using a Shimadzu LC system (comprising of a solvent degasser, two LC-10A pumps and a SCL-10A system controller) coupled to a QSTAR XL quadrupole time-of-flight tandem mass spectrometer. LC was operated at

a flow rate of 200 $\mu\text{L}/\text{min}$ with a linear gradient as follows: 100% of mobile phase A was held isocratically for 2 minutes and then linearly increased to 100% mobile phase B over the duration of 14 minutes and held at 100% B for 4 minutes. Mobile phase A consisted of methanol/acetonitrile/aqueous 1 mM ammonium acetate (60/20/20, v/v/v). Mobile phase B consisted of 100% ethanol containing 1 mM ammonium acetate. A Zorbax SB-C8 reversed-phase column (5 μm , 2.1 x 50 mm) was obtained from Agilent (Palo Alto, CA). The post-column splitter diverted $\sim 10\%$ of the LC flow to the ESI source of the mass spectrometer. All data acquisition and analysis were performed using the instrument's Analyst QS software.

4.2.3: *FabZ* assay

Genomic DNA extracted from W3110, CRM1, and CRM5 were used as the templates to amplify wild-type *fabZ*, *fabZ* T50A, and *fabZ* C212T respectively using primers 5' GGCGCAGCATATGTTGACTACTAACACTCATACTCTGCAGATTGAAGAG 3' and 5' GCAGAAGCTTGGCCTCCCGGCTACGAG 3'. Each plasmid containing C-terminally histidine-tagged wild-type *fabZ*, *fabZ* T50A, or *fabZ* C212T was constructed in pET21b(+) (EMD Biosciences, San Diego, CA) vector as described above and cells were grown on LB agar containing 100 $\mu\text{g}/\text{mL}$ ampicillin (Sigma, St. Louis, MO). Correct constructs were confirmed using primers 5' TAATACGACTCACTATAGGG 3' and 5' CTAGTTATTGCTCAGCGGTG 3' for DNA fragment amplification and sequencing and transformed into C41(DE3) (Miroux & Walker, 1996) competent cells prepared as previously described (Inoue et al, 1990).

FabZ tagged with C-terminal histidines was expressed and purified to > 90% homogeneity as determined from SDS-PAGE analysis as previously described (Heath & Rock, 1996). Briefly, one verified colony from each construct (wild-type FabZ, L17Q FabZ and A71V FabZ) was chosen and grown in M9 media (Miller, 1992) supplemented with 1% casein amino acids, 0.4% glucose, 1 mM MgCl₂, and 100 µg/mL ampicillin to OD_{600nm} ~ 0.5 at 37 °C. Isopropyl-1-thio-D-galactopyranoside (Sigma, St. Louis, MO) was then added to a final concentration of 1 mM, and the cells were grown for an additional 3 hours. Cells were then harvested and centrifuged at 8,000 rpm for 10 minutes at 4 °C. The supernatant was discarded and the cell pellets were washed with phosphate-buffered saline (PBS) (Dulbecco & Vogt, 1954) and centrifuged again. The cell pellets was stored at -80 °C overnight.

The cell pellets were resuspended in 8 mL of 20 mM Tris-HCl pH 7.4, 0.5 M NaCl, and 1 mM beta-mercaptoethanol. Cells were lysed using a French Pressure cell at 17000 psi and centrifuged at 45,000 rpm (~140,000 × g) in a Beckman type 70.1 Ti rotor for 1 hour at 4 °C to prepare membrane-free lysate. The supernatant, which contained the soluble proteins, was applied to a Ni-NTA column and washed with 20 column volumes of solution containing 40 mM imidazole, 20 mM Tris-HCl pH 7.4, 0.5 M NaCl, and 1 mM beta-mercaptoethanol. His-tagged proteins were eluted using 20 column volumes of 200 mM imidazole in the same buffer. SDS-PAGE analysis was done on each fraction to determine protein purity. The purest fractions were collected and concentrated to 2 mg/mL final concentration using Amicon Ultra Centrifugal Filters Regenerated Cellulose 10,000 MWCO (EMD Millipore, Billerica, MA). Final protein

purity was > 90% homogeneous as determined by SDS-PAGE analysis (Figure 4.2). Final protein concentrations were determined using the Bradford Reagent (Sigma, St. Louis, MO) and previously described protocols (Bradford, 1976). Purified proteins were stored at -80 °C.

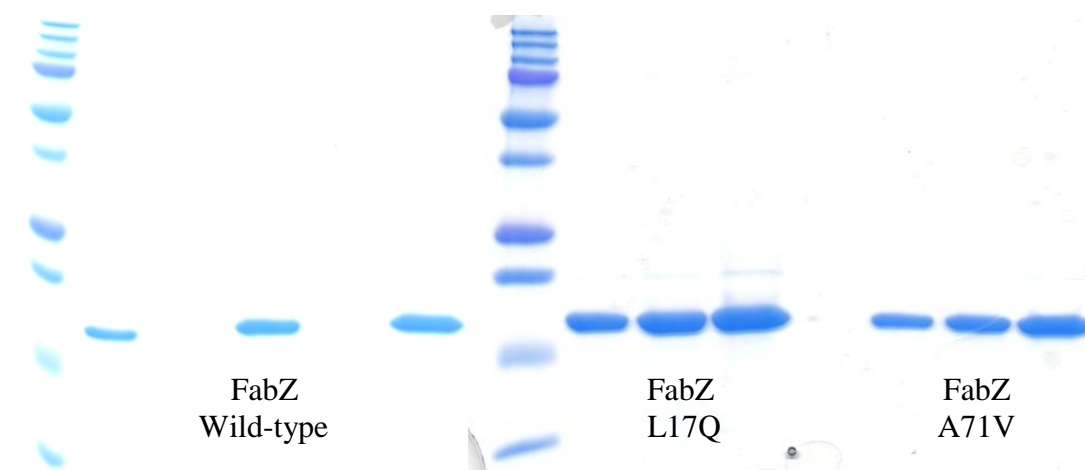


FIGURE 4.2: Final FabZ proteins purity as visualized by SDS-PAGE analysis.

R,S-3-hydromyristoyl-ACP was prepared as previously described (Sorensen et al, 1996). Each 40 μ L assay reaction mixture included 100 mM sodium phosphate pH = 7, 1 mM 2-beta-mercaptoethanol, and 50 μ M *R,S*-3-hydromyristoyl-ACP. Reactions were initiated with the addition of 12.75 - 25.5 nM of wild-type enzyme or 12.75 - 100 nM of mutant enzymes and time points were taken over the course of 20 minutes at 37 °C. Reactions were quenched by the addition of 1x volume of 1.25M sodium hydroxide

and placed on ice. After 10 minutes, an additional 1x volume of 1.25M acetic acid was added. After 10 minutes, 2.2x final volume of methanol and 2.2x final volume of chloroform was added to the mixture for conversion into a 2-phase Bligh/Dyer mixture at room temperature (Bligh & Dyer, 1959). This mixture was vortexed vigorously, centrifuged at 13,000 rpm for 5 minutes, and the lower phase was collected. The sample was then dried under nitrogen and resuspended in 2:1 ratio of chloroform to methanol. Samples were injected on C8 reverse phase column and run on LC-MS as described above. Both *R*-3-hydroxymyristate and *trans*-2-enoyl-myristate eluted at 3 - 3.5 minutes on the column. Peaks were quantified using Analyst QS Software (Applied Biosystems, Carlsbad, CA) and product conversion was determined as $[P]/([S]+[P])$. All quantifications were subtracted from the no enzyme control. Product conversion was linear with respect to both time and enzyme concentrations used.

4.2.4: *LpxC* activity assay

Preparation of cell free extracts and *LpxC* activity assays were performed as previously described (Sorensen et al, 1996). Briefly, single colonies of each strain (W3110, CRM1, and CRM5) were grown in LB broth until $OD_{600nm} \sim 0.8$. Cells were then harvested and centrifuged at 8,000 rpm for 10 minutes at 4 °C. The supernatant was discarded and the cell pellets were washed with PBS and centrifuged again. The cell pellets were stored at -80 °C overnight.

The cell pellets were resuspended in 2 mL of 10 mM HEPES pH 7.5. Cells were lysed using a French Pressure cell at 17000 psi and centrifuged at 45,000 rpm

(~140,000 × g) in a Beckman type 70.1 Ti rotor for 1 hour at 4 °C to prepare membrane-free lysate. Aliquots of the supernatant were stored at -80 °C and were used in LpxC activity assays as well as corresponding Western blots.

4.2.5: Western blots

The LpxC antibody used was previously characterized (Sorensen et al, 1996). Preparations of cell extracts for Western blotting were performed as previously described (Sorensen et al, 1996). Purified LpxC, prepared as previously described (Jackman et al, 1999), was used as a positive control.

W3110 cells harboring pBAD33.1 constructs (vector control or harboring wild-type *fabZ* or *lpxC*) were grown to an optical density at 600 nm (OD₆₀₀) of ~ 0.2 in LB media containing 25 µg/mL chloramphenicol, at which time 0.2% L-Arabinose (Sigma, St. Louis, MO) was added to the LB media in indicated samples only (Fig. 4C). Cells were harvested ~ 50 minutes later, collected by centrifugation, and resuspended in Laemmli sample buffer (Bio-Rad, Hercules, CA) normalized to OD₆₀₀ = 1 per 100 µL of buffer. Samples were then heated to > 95 °C for 10 minutes and loaded on 15% Tris-HCl precast gels (Bio-Rad, Hercules, CA). Overexpression of each protein (FabZ or LpxC) was confirmed by the appearance of a band corresponding to the molecular weight of each protein (~ 17,000 Daltons for FabZ and ~ 34,000 for LpxC) that only appeared in cells harboring the wild-type gene (*fabZ* or *lpxC*) on the plasmid and grown in the presence of 0.2% L-Arabinose as visualized by SDS-PAGE.

For LpxC Western blotting, protein gels were equilibrated in 1x transfer buffer (25mM Tris and 0.2M Glycine) with 20% methanol and then the proteins were transferred to a nitrocellulose membrane using a Transblot Semi-Dry Transfer Cell (Bio-Rad) at 20 V for 40 min. The membrane was incubated in 40 ml of blocking buffer (Sigma, St. Louis, MO) overnight with gentle shaking at room temperature. The membrane was rinsed three times with washing buffer (PBS + 0.2% Tween-20) and incubated with blocking buffer containing a 1:5000-fold dilution of LpxC primary antibody for one hour with gentle shaking at room temperature. The primary antibody used in the Western blots was a polyclonal rabbit antibody generated from purified deacetylase protein and consists of rabbit serum (40 mg/ml) that had been filtered through a total *E. coli* protein column (Pierce, Rockford, IL). The antiserum was produced at Hazelton Research Products Inc. (Denver, PA). The membrane was then rinsed for 1 hour with four changes of washing buffer and incubated with blocking buffer containing 1:1000-fold dilution of anti-rabbit immunoglobulin conjugated with horseradish peroxidase secondary antibody (Pierce, Rockford, IL) for 1 hour with gentle shaking at room temperature. The membrane was washed in the same way as described above and developed using ECL Western Blotting Substrate (Pierce, Rockford, IL).

For FabZ Western blots, a 1:500 dilution of the primary anti-flag immunoglobulin conjugated with horseradish peroxidase antibody (Sigma, St. Louis, MO) was used and the membrane was developed using SuperSignal West Pico Chemiluminescent Substrate (Pierce, Rockford, IL) for enhanced sensitivity.

4.2.6: Extraction and visualization of lipid profile

Phospholipids and lipid A were extracted as previously described (Chung & Raetz, 2010). Briefly, strains (W3110, CRM1, and CRM5) were grown from overnight cultures, diluted 1:100 into 250 mL of LB broth and grown at 37 °C until $OD_{600nm} \sim 1$. Cells were harvested by centrifugation at 4000g for 20 min, washed once with PBS and resuspended in 16mL of PBS, and transferred to glass tubes, or to solvent resistant bottles. Chloroform (20 mL) and methanol (40 mL) were added to make a one-phase Bligh-Dyer system (Bligh & Dyer, 1959). The mixture was incubated at room temperature for 1 hour with occasional shaking and then centrifuged at 2500g for 30 minutes. The supernatant contained phospholipids and fatty acids and the pellet contained the intact LPS and other insoluble debris.

To harvest the fatty acid and phospholipids, the supernatant was converted to a two-phase Bligh-Dyer system (Bligh & Dyer, 1959) by the addition of chloroform (20 mL) and 0.1 N hydrochloric acid (20 mL), followed by thorough mixing and centrifugation at 2500g for 20min. The organic phase was removed, and the aqueous phase was extracted a second time by the addition of the pre-equilibrated organic phase. The organic phases were pooled, neutralized with a few drops of pyridine, and dried by rotary evaporation. Lipids were dissolved in 5 mL of a chloroform/methanol mixture (4:1, v/v) and subjected to sonication in a water solution. The lipids were transferred to fresh glass tubes, dried under nitrogen gas at room temperature, and stored at -20 °C.

To harvest lipid A species, the cell pellet was washed three times with 25 mL of a single-phase Bligh-Dyer mixture. Afterwards, the pellet was suspended in 8 mL of 50

mM sodium acetate (pH 4.5) and was homogenized using a Branson probe sonicator. The suspension was boiled for 30 minutes by submerging in a boiling water bath and then cooled to room temperature. The mixture was adjusted to pH ~ 1.5 using aqueous HCl and converted into a two-phase Bligh-Dyer mixture by the addition of chloroform (20 mL), methanol (20 mL), and 0.1 N hydrochloric acid (10 mL). The aqueous phase which contains the lipids were recovered and dried as described above.

For mass spectrometry analysis, lipid samples were analyzed using LC-MS normal phase as described above (4.2.3: *Liquid chromatography coupled with mass spectrometry*). For TLC analysis, 1/5 of the total phospholipid fraction and 1/2 of lipid A from a 250 mL culture were dissolved in 100 μ L of a chloroform/methanol mixture (4:1, v/v). Next, 5-10 μ L portions were spotted onto 10 cm x 10 cm HPTLC plates (Merck, Darmstadt, Germany). Phospholipids were separated in solvent system consisting of chloroform/methanol/acetic acid (65:25:10 v/v/v) while the lipid A species were separated using chloroform/pyridine/formic acid/water (50:50:16:5). Plates were sprayed with 10% sulfuric acid in ethanol and then charred.

4.2.7: Construction of *pBAD33.1(lpxC)*

Wild-type *lpxC* was amplified using genomic DNA from W3110 and primers 5' GGCGCAGTCTAGATTAACCTTTAAGAAGGAGATATACATATGATCAAACAAA GGACACTTAAACGTATCGTTCAG 3' and 5' GCAGAAGCTTTTATGCCAGTAC AGCTGAAGGCG 3'. Cloning was done as described above (4.2.1: *Construction of pBAD33.1(fabZ)*) using *Xba*I and *Hind*III (NEB, Ipswich MA).

4.2.8: Construction of chromosomal *fabZ*-FLAG tag

Wild-type *fabZ* was amplified using genomic DNA from W3110 and primers 5' CGCCGTTGCTTACAACAGCAG 3', 5' TTATTTGTCATCGTCATCTTTATAATCG GCCTCCCGGCTACGAGCACACATCATCG 3', 5' GGA GGCCGATTATAAAGAT GACGATGACAAATAATTA ACTTTAAGAAGGAGATATACATTACGTGATTGA TAAATCCGCCTTTGTGCA 3', and 5' CTATTTTGAAAACACGTTTCTGTCGCCA CG 3'. A second round of PCR was performed using 1 µL of the previous PCR products as template DNA and primers 5' ACCCAAATACCGTGAGCATTTAGGC 3' and 5' CCGAGCACTTCAACAATGCCCAT 3'. A final round of PCR was performed using 1 µL of the previous PCR product as template DNA and primers 5' GGCGCAGAAGCTTGAATCCCTACCTGACTTACGCGC 3' and 5' GGCGCAGT CTAGAGCACATGTTCTTTCAGAGCGCG 3'. The final PCR product contains wild-type *fabZ* with a ribosome binding site sequence (copied from *pet21b*) and a C-terminal FLAG tag sequence (Figure 4.3).

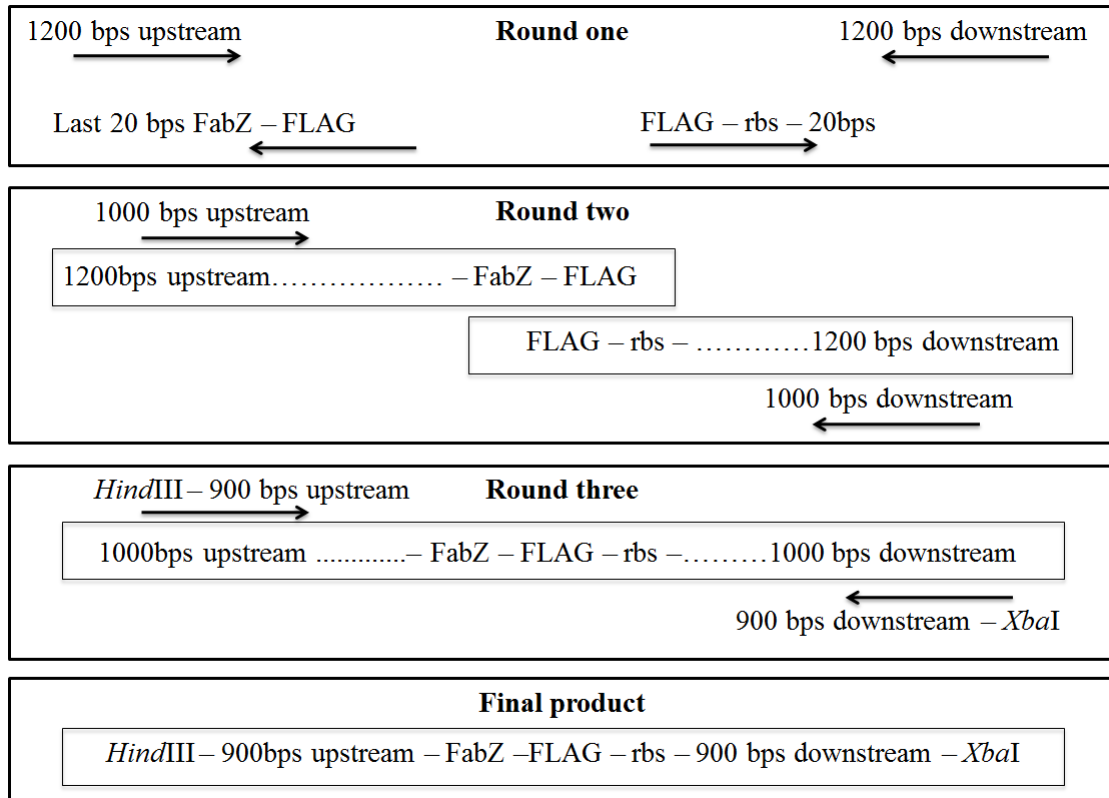


FIGURE 4.3: FabZ-FLAG primer design. The first round of PCR amplified two fragments that incorporated the FLAG sequence at the C-terminus of FabZ. The endogenous stop codon of *fabZ* was removed and added to the end of the FLAG tag to stop translation. Since insertion of the FLAG tag removes the endogenous ribosome binding site (rbs) of *lpxA*, which is only three base pairs (bps) downstream of *fabZ*, the rbs sequence used in pet21b plasmid was copied over and added to the end of the FLAG tag to ensure translation of *lpxA*. These two PCR products were annealed and used as template for a second round of PCR. The resulting product was used as a template in the third round of PCR to amplify the desired final product which consists of *fabZ* with a C-terminus FLAG tag and the restriction sequences for *Hind*III and *Xba*I.

This final PCR product was gel purified and ligated into a pMAK705 plasmid (Brown et al, 2012) using restriction enzymes *Hind*III and *Xba*I (NEB, Ipswich, MA). Cloning was done as described above (4.2.1: Construction of *pBAD33.1(fabZ)*) and the verified construct was transformed into W3110 competent cells. Cells were grown on

LB agar containing 25 µg/mL chloramphenicol at 42 °C. In these conditions, the pMAK705 plasmid replicon cannot replicate (Brown et al, 2012) and surviving cells must have incorporated the plasmid into the chromosome through homologous recombination with the chromosomal copy of wild-type *fabZ*. Purified colonies were then grown at 30 °C in same medium. At this permissive temperature, the pMAK705 plasmid replicon can replicate and surviving cells must have excised the plasmid leaving the original chromosomal wild-type copy of *fabZ* or the original plasmid-borne copy of *fabZ*-FLAG remaining on the chromosome. Single cells were then purified three times at 42 °C in the absence of antibiotic to dilute out the plasmid. Complete loss of the plasmid was confirmed by resulting cells' inability to grow on LB agar containing 25 µg/mL chloramphenicol at 30 °C. PCR analysis and DNA sequencing were employed to confirm the genotypes using primers 5' CGCCGTTGCTTACAACAGCAG 3' and 5' CTATTTTGAAA ACACGTTTCTGTCGCCACG 3' for PCR amplification and primers 5' CAAGCGTCTGAAATCGCTTGAGCG 3' and 5'GACAACGTGAGATTTTCAGTAC GGTAC 3' for DNA sequencing.

4.2.9: *Reverse transcription polymerase chain reaction (RT-PCR)*

Cells were grown as described above. RNA was extracted using the RNeasy mini kit (Qiagen, Valencia, CA) and RNAprotect Bacteria Reagent (Qiagen, Valencia, CA) according to manufacturer's instructions. Reverse transcription was carried out using SuperScript® II Reverse Transcriptase (Invitrogen, Carlsbad, CA) with 2.5 µg of

total RNA and the gene specific primers: 5' TTATTTGGAGATGTGAGCGATCAGG 3' for the housekeeping gene *gapA*, which encodes glyceraldehyde 3-P dehydrogenase A; 5' TTATGCCAGTACAGCTGAAGG 3' for *lpxC*, 5' TCA GGC CTC CCG GCT A 3' for *fabZ*. All reactions were carried out using RNase-free certified reagents, tubes, and tips. The cDNA was diluted 1:10 fold in RNase-free certified water and 1 μ L was used as the template in PCR.

The gene products *gapA*, *lpxC*, and *fabZ* were amplified using primers: 5' ATG ACT ATC AAA GTA GGT ATC AAC GGTTTT 3' and 5' ACT TTG TTG GAGTAA CCG GTT TC 3' for *gapA*; 5' ATG ATC AAA CAA AGG ACA CTT AAA CGT ATC 3' and 5' TTT GAA GGC CAA CGG CA 3' for *lpxC*; 5' TTG ACT ACT AAC ACT CAT ACT CTG CAG ATT 3' and 5' CAC ACATCA TCG TTG CTT CGC 3' for *fabZ*. Amplification of *gapA* and *fabZ* was done in 18-21 PCR cycles while amplification of *lpxC* was done in 36-38 cycles. PCR products were resolved on a 1% agarose gel containing SYBR®-Safe DNA Gel Stain (Life Technologies, Carlsbad, CA). The light intensity of each band was qualified using Quantity One (Bio-Rad, Hercules, CA).

4.2.10: Supplementation of *R*-3-hydroxymyristic acid

MIC assays were performed as described in chapter 3. Briefly, liquid cultures of W3110 were grown from single colonies in LB media at 37 °C to log phase $OD_{600} \sim 0.2 - 0.6$. Cultures were then diluted to $\sim 10^6$ bacterial cells in LB media with 10% DMSO in the presence and absence of 0.5 mg/mL of *R*-3-hydroxymyristic acid (Santa Cruz Biotechnology, Inc, Santa Cruz, CA). The addition of *R*-3-hydroxymyristic acid caused

significant precipitation in solution; however, decreasing the concentration of *R*-3-hydroxymyristic acid did not increase solubility. Furthermore, the additional of ethanol or varying the pH of the solution (from pH 6 to pH 8 by pH 0.5 increments) did not enhance compound solubility.

4.2.11: Cloning of *Vibrio harveyi* acyl-ACP synthetase

Vibrio harveyi acyl-ACP synthetase (*HvaaS*) was synthesized by GenScript USA, Inc. (Piscataway, NJ) and amplified using primers 5' GGCGCAGCATATGAACCAGTATGTAAATGATCCATCCAATTATCAGTTACT 3' and 5' GCAGAAGCTTTTACAGATGAAGTTTACGCAGTTCTTTCTTATCCAC TTT 3' and cloned into a pBAD33.1 (Chung & Raetz, 2010) vector using the restriction enzymes *NdeI* and *HindIII* (NEB, Ipswich, MA) as described above (4.2.1: Construction of pBAD33.1(*fabZ*)). Single colonies of W3110 containing either *HvaaS* or vector control were grown in LB media supplemented with 0.2% L-arabinose and 25 µg/mL chloramphenicol until OD_{600nm} ~ 0.6. Cells were diluted into LB media supplemented with 0.2% L-arabinose, 25 µg/mL chloramphenicol, and 0.5 mg/mL *R*-3-hydroxymyristic acid. MICs were performed as previously described.

4.3: Results

4.3.1: Point mutations in *fabZ* are recessive and decrease enzymatic activity

To verify that the FabZ point mutations indeed confer resistance, we complemented the *fabZ* mutants (CRM1 and CRM5) with the wild-type *fabZ* gene on a

plasmid. The resulting mutants not only completely lost resistance but were also hypersensitive to CHIR-090 (Table 4.1) suggesting the *fabZ* point mutations are recessive and likely cause a decrease of function phenotype.

Table 4.1: MIC assay show *fabZ* point mutations are recessive.

Mutant (pBAD33.1)	CHIR-090 ($\mu\text{g/mL}$)
W3110 (v/c)	0.2
W3110 (<i>fabZ</i>)	0.03
CRM1 (v/c)	6.3 - 12.5
CRM1 (<i>fabZ</i>)	0.03 - 0.065
CRM5 (v/c)	6.3 - 12.5
CRM5 (<i>fabZ</i>)	0.03

v/c: vector control

In our isolated CRM strains, a nucleotide change of T50A or C212T in *fabZ* results in altered FabZ protein with either Leu17 replaced by Gln or Ala71 replaced by Val respectively. In the crystal structure of *P. aeruginosa* FabZ (PDB ID: 1U1Z), which shares 54% sequence identity with *E. coli* FabZ (Kimber et al, 2004), both of these corresponding residues form the lining of the proposed substrate binding site and likely contribute to fatty acid binding (Figure 4.4).

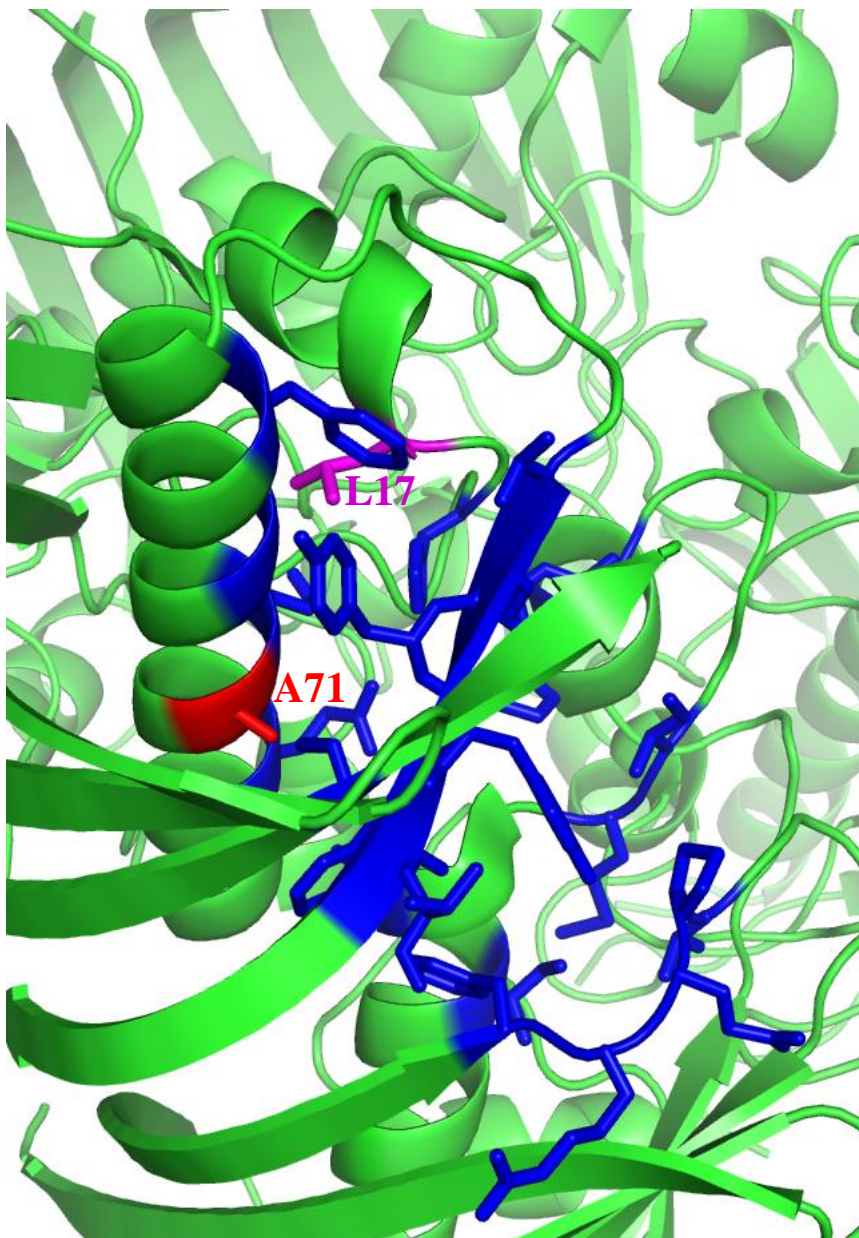


FIGURE 4.4: X-ray structure of PsFabZ (PDB ID: 1U1Z). Residues that form the proposed substrate binding passage are illustrated in blue, leucine 17 is illustrated in magenta and alanine 71 is illustrated in red. Both these corresponding residues form the lining of the proposed substrate binding site.

To examine the effects of the isolated *E. coli* FabZ point mutations on enzymatic activity, we purified wild-type and mutant FabZs to homogeneity and developed a liquid chromatography-mass spectrometry (LC-MS) based assay to determine their specific activities. In this assay, hydroxymyristoyl-ACP was incubated with purified wild-type FabZ or its mutants. Reaction samples were then quenched with base to cleave off the ACP portion (Figure 4.5). The liberated fatty acids were extracted using two-phase Bligh-Dyer and injected on a reverse phase column in the negative ion mode. The ion intensities of the substrate hydroxymyristate (observed as the $[M-H]^-$ ion at m/z 243.18) and product *trans*-2-enoyl-myristate (observed as the $[M-H]^-$ ion at m/z 225.17) in each sample reaction were quantified to calculate product conversion. Under the conditions of our assay, both mutants had reduced specific activities (Figure 4.6): the Leu17Gln mutant is ~ 2.5-fold and the Ala71Val is ~ 8-fold less active compared to wild-type (Table 4.2).

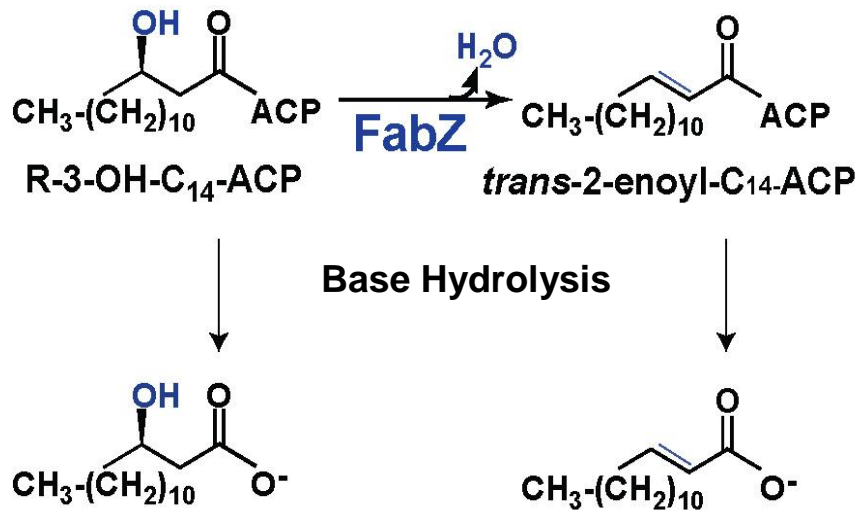


FIGURE 4.5: FabZ assay setup. Hydroxymyristoyl-ACP was incubated with purified wild-type FabZ or its mutants. Each reaction was quenched with base to cleave off the bond between ACP and the fatty acid. Fatty acids were extracted and subjected to LC-MS analyses.

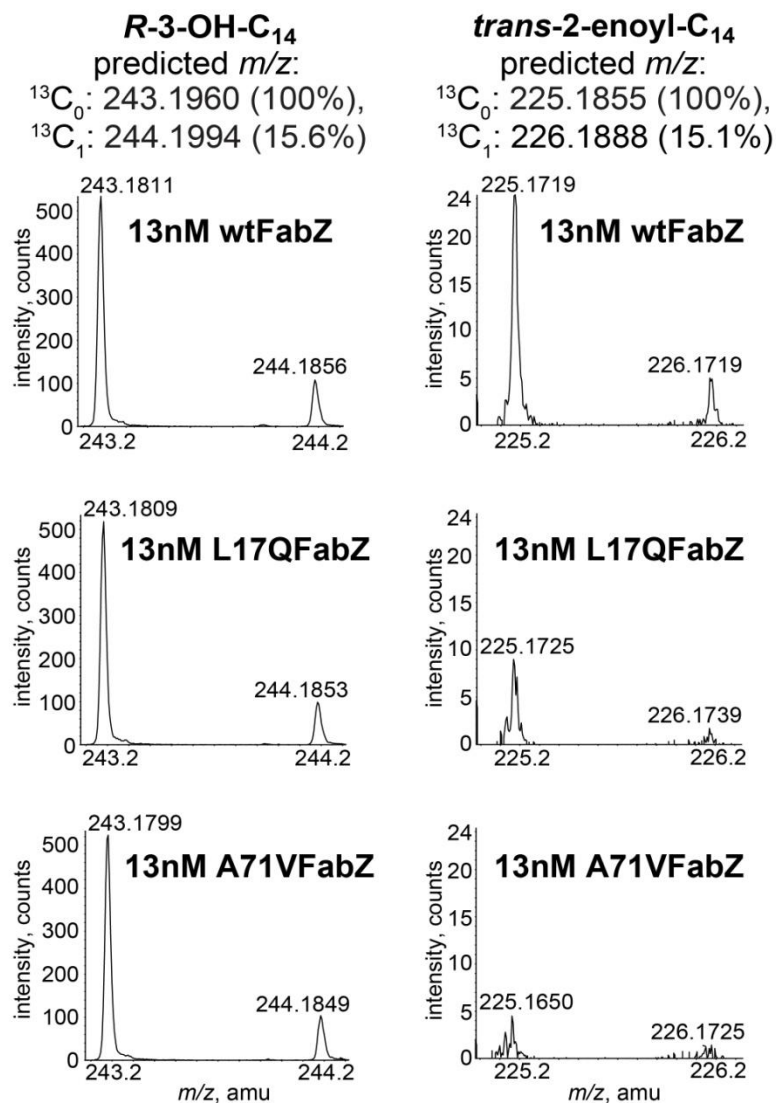


FIGURE 4.6: FabZ enzymatic activity assay based on reverse phase LC-MS. Mass spectra (after blank buffer subtraction) averaged from those acquired during 3 – 3.5 minutes show reduced product conversion (decreased counts of *trans*-2-enoyl-myristate) in the samples with Leu17Gln FabZ (L17QFabZ) or Ala71Val FabZ (A71VFabZ) compared to the wild-type enzyme (wtFabZ) at 10 minutes.

TABLE 4.2. Specific activities of FabZ proteins

FabZ protein	Specific Activity ($\mu\text{mol}/\text{min}/\text{mg}$)
Wild-type	1.87 ± 0.346
Leu17Gln	0.74 ± 0.063
Ala71Val	0.23 ± 0.015

We next assessed whether reduced FabZ activities result in detectable changes *in vivo*. Because FabZ is an important enzyme in fatty acid biosynthesis, decreased FabZ activity is expected to reduce cellular concentrations of myristoyl-ACP, the end product of that fatty acid elongation cycle (Heath & Rock, 1996). Since myristoyl-ACP is also used by LpxM in the last step of lipid A biosynthesis to generate the hexa-acylated lipid A structure (Clementz et al, 1997; Vorachek-Warren et al, 2002) (Figure 4.1), we probed for differences in levels of minor lipid species in the mutant cells. LC-MS analysis of the lipid A species extracted from CRM1 and CRM5 showed enhanced levels of penta-acylated lipid A (observed as the $[\text{M}-2\text{H}]^{2-}$ ion at m/z 792.5) as well as hexa-acylated lipid A decorated with lauroyl (observed as the $[\text{M}-2\text{H}]^{2-}$ ion at m/z 792.5) instead of a myristoyl chain relative to wild-type (Figure 4.7). Although these results do not provide a direct measurement of the myristoyl-ACP concentration in bacterial cells, the observation of altered lipid A profiles is consistent with the notion of reduced cellular concentrations of myristoyl-ACP in CRM1 and CRM5.

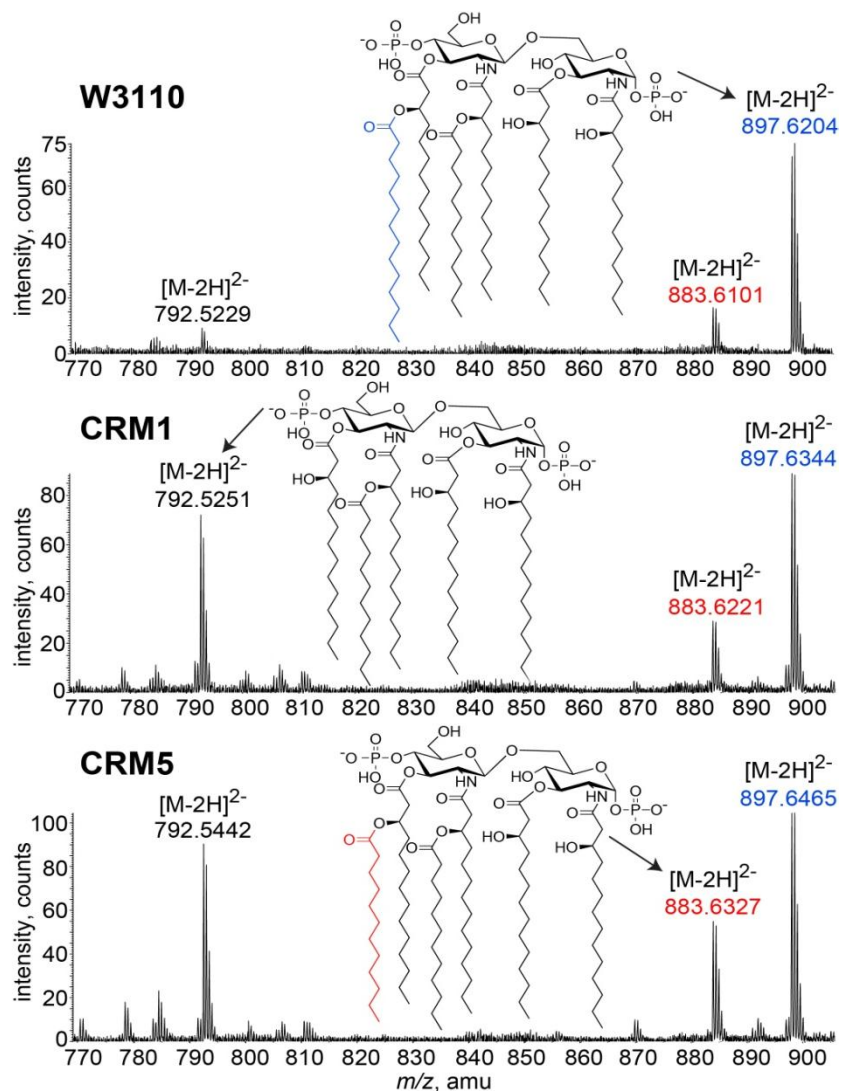


FIGURE 4.7: LC-MS analyses of FabZ mutants lipid A profile. Mass spectra (after background subtraction) of lipid A species eluted during 36 – 38 minutes on normal phase LC-MS show increased amounts of penta-acylated lipid A as well as lipid A with a lauroyl instead of a myristoyl chain in FabZ mutant strains. Lipid A species are detected by ESI/MS in the negative ion mode as the doubly charged $[M-2H]^{2-}$ ions.

In addition, analysis of the global fatty acid composition using LC-MS showed that the FabZ mutants CRM1 and CRM5 have slightly higher levels of unsaturated fatty acids (~ 15%) relative to wild-type (Figure 4.8). This suggests that in these cells, reduced FabZ activity is compensated by FabA, the other dehydrase in fatty acid biosynthesis that also isomerizes *E*-2-decenoyl-ACP to *Z*-3-decenoyl-ACP for the biosynthesis of unsaturated fatty acids (Magnuson et al, 1993).

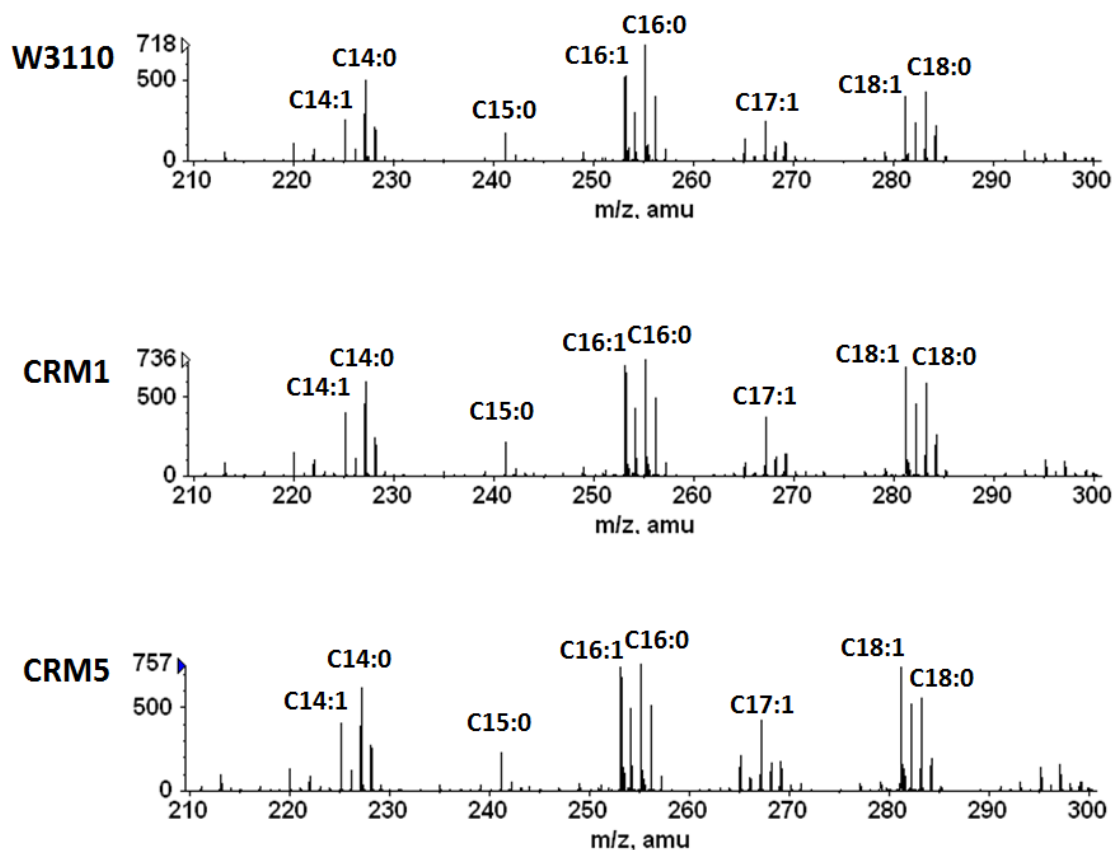


FIGURE 4.8: LC-MS analyses of FabZ mutants fatty acid profile. LC-MS analyses of fatty acid profiles show slightly higher levels of unsaturated fatty acid species (C14:1, C16:1, C18:1) for FabZ mutants relative to W3110.

4.3.2: *FabZ* and *LpxC* are co-regulated

Previously, it has been reported that in cells grown in the presence of *LpxC* inhibitors, the specific activity of *LpxC* is increased by 5- to 10-fold. Since there is no change in the K_M of *LpxC*, such an increase in *LpxC* activity is likely caused by an increase in overall *LpxC* protein amount detected in cell extracts (Sorensen et al, 1996). To examine if the *FabZ* mutants also have elevated *LpxC* activities, which might confer the observed resistance to *LpxC* inhibitors, we measured the *LpxC* specific activities in membrane-free lysates of CRM1 and CRM5. Much to our surprise, we instead observed a significant drop in *LpxC* specific activities (Figure 4.9A) in the CRM mutants. Western blotting using an *LpxC* antibody reveals a corresponding drop in *LpxC* protein concentrations (Figure 4.9B), suggesting that the reduced activities are due to a decrease of cellular protein concentrations. Thus impairment of *FabZ* activity causes a reduction of *LpxC* protein amount and activity.

To further probe the functional connection between *FabZ* and *LpxC*, we overexpressed *FabZ* on a plasmid in W3110 and again measured the level of *LpxC* protein. In this case, we detect an increase of *LpxC* protein concentration in extracts of cells overexpressing *FabZ* (Figure 4.9C). Taken together, these experimental observations strongly suggest that the levels of *FabZ* and *LpxC* are correlated *in vivo*.

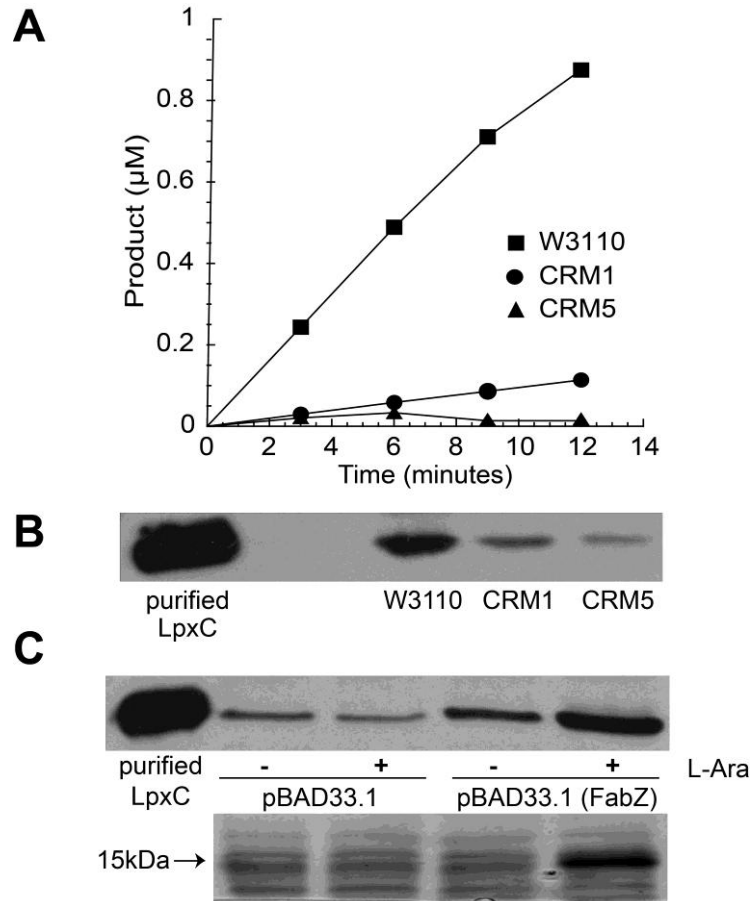


FIGURE 4.9: LpxC activity and level in FabZ mutants. (A) Enzymatic LpxC activity assays show significantly less product (UDP-3-O-(*R*-3-hydroxymyristoyl)-glucosamine) conversion in CRM1 and CRM5 relative to W3110. Each spot was connected for better visualization. (B) Western blot using an LpxC antibody shows that CRM1 and CRM5 express less LpxC protein relative to W3110. (C) Western blot showing increased LpxC protein when FabZ is overexpressed in the presence of 0.2% L-Arabinose (L-Ara) on a pBAD33.1 plasmid in W3110 (top). SDS-PAGE analysis of the protein gel shows overexpression of FabZ (~ 17,000 Daltons) only in the presence of 0.2% L-Arabinose (bottom).

4.4: Discussion

Mutations in *fabZ* appear to be a major contributor of resistance, accounting for as much as 50-fold enhanced resistance to inhibition of lipid A biosynthesis. Although mutations in *fabZ* have been previously implicated in the resistance of a weaker LpxC inhibitor (BB-78485), none of the isolated FabZ mutants were biochemically characterized (Clements et al, 2002).

Here, we used an LC-MS based assay to quantify the effects of our distinct set of FabZ point mutations on the enzymatic activity of FabZ *in vitro*. We show that Leu17Gln and Ala71Val mutations decrease enzymatic activity ~ 2.5-fold or ~ 8-fold respectively. Further supporting this hypothesis, we observe that overexpression of *fabZ* on a pBAD(33.1) plasmid causes hypersensitivity to CHIR-090. This can be rationalized since overexpression of *fabZ* would decrease the flux of *R*-3-hydroxymyristoyl-ACP, leading to a decrease in LpxC substrate. Additionally, we were able to detect accumulation of partially-acylated and lauroyl-acylated lipid A in our FabZ mutant cells, which is consistent with decreased cellular levels of myristoyl-ACP, the downstream product of FabZ.

Since FabZ shares a common substrate with LpxA, it was speculated that decreased FabZ enzymatic activity would increase the concentrations of the LpxA substrate and thus lead to increased levels of LpxC substrate. Accumulation of this substrate would enhance the overall efficiency of catalysis and directly compete with LpxC inhibitor, countering its suppressive effect of lipid A biosynthesis (Clements et al, 2002). However this proposal presents a problem for the cell, since in the absence of

LpxC inhibitors, these FabZ mutant cells would have increased lipid A biosynthesis at the expense of decreased fatty acid biosynthesis. Our results highlight a previously unreported regulation between fatty acid and lipid A biosynthesis that allows cells to maintain overall membrane integrity.

First, we observed a significant decrease of LpxC specific activity and protein amount in our FabZ mutant cells in the absence of LpxC inhibitors, suggesting that these mutant cells down-regulate. Likewise, when FabZ is overexpressed, we detected an increase in LpxC protein level. These data suggest that altered fatty acid synthesis is matched by a proportional alteration of lipid A biosynthesis.

Second, other than the accumulation of partially-acylated and lauroyl-acylated lipid A, LC-MS analysis of the phospholipid and lipid A species did not show other abnormal lipid species in the mutants relative to wild-type cells (Figure 4.10A-C). In particular, TLC analysis shows these mutants have comparable amounts of major species of phospholipids and lipid A relative to wild-type (Figure 4.11A-B).

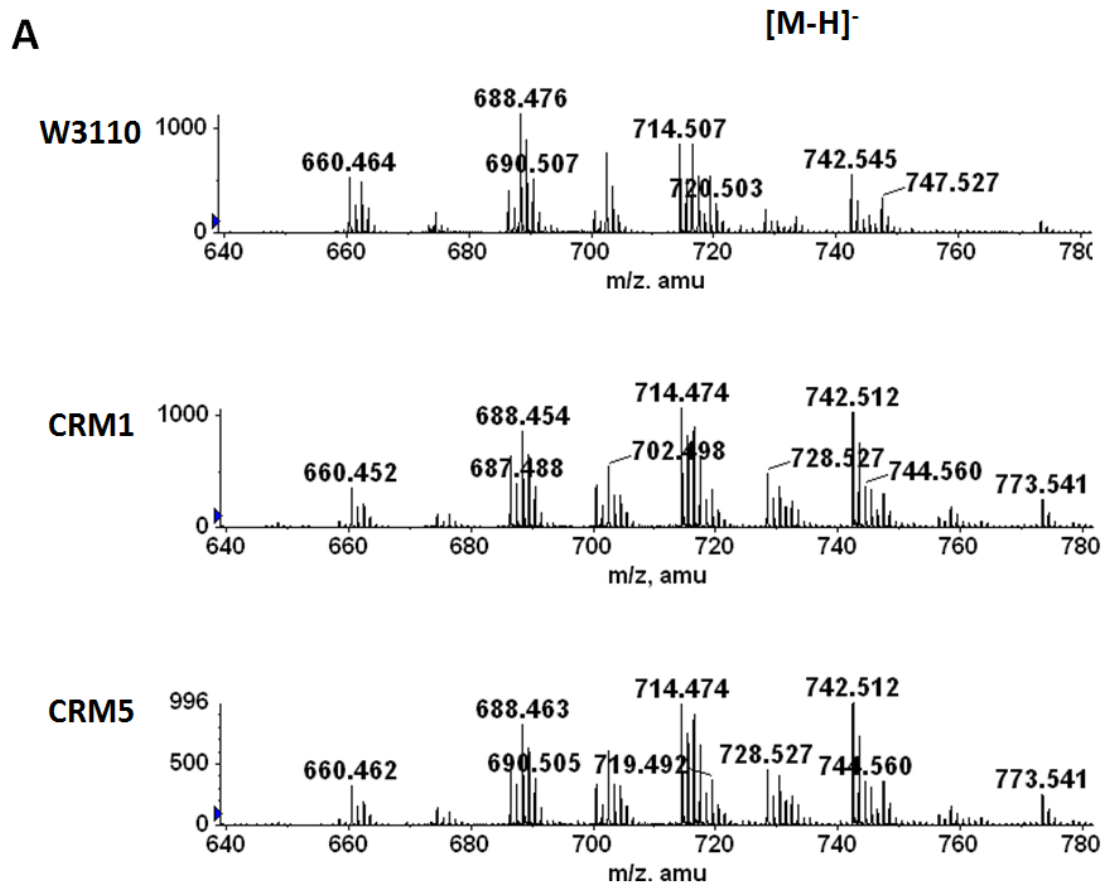


FIGURE 4.10A: LC-MS profile of phosphoethanolamine species shows CRM mutants have comparable species and peaks of phosphoethanolamine lipids relative to W3110.

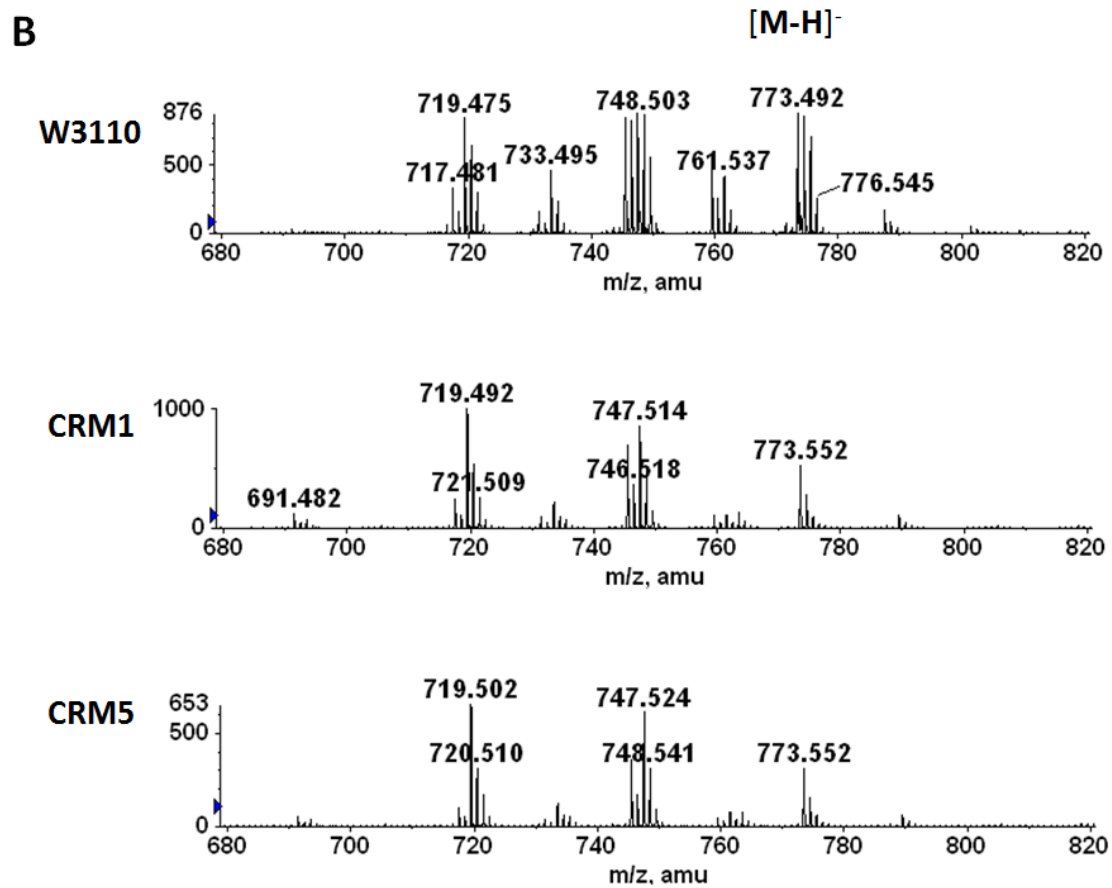


FIGURE 4.10B: LC-MS profile of phosphoglycerol species shows CRM mutants have comparable species and peaks of phosphoglycerol lipids relative to W3110.

C

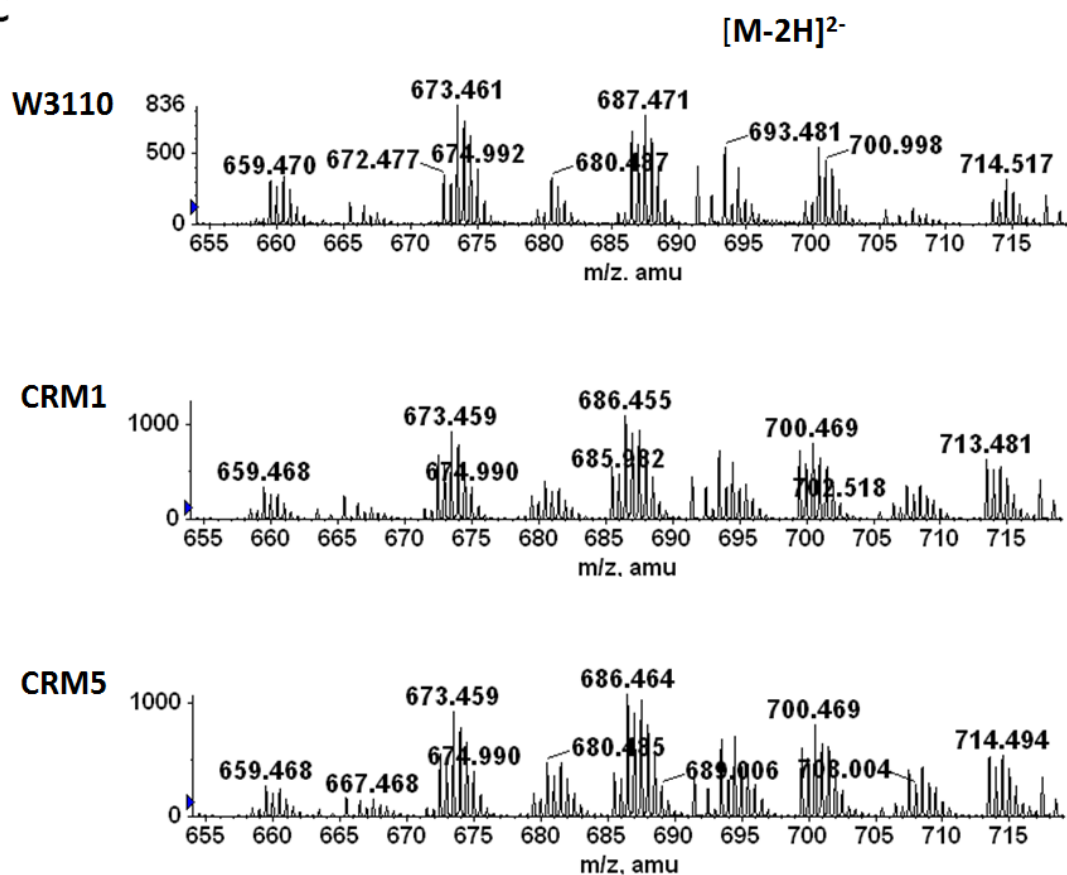


FIGURE 4.10C: LC-MS profile of cardiolipin species shows CRM mutants have comparable species and peaks of cardiolipin lipids relative to W3110.

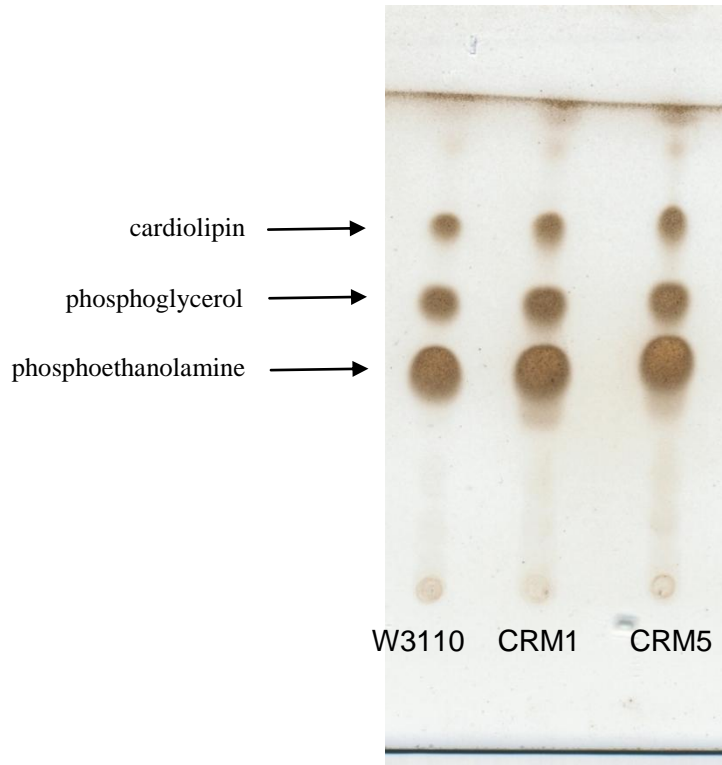


FIGURE 4.11A: TLC analysis of the phospholipid profiles show CRM mutants have comparable major species of phospholipids relative to W3110.

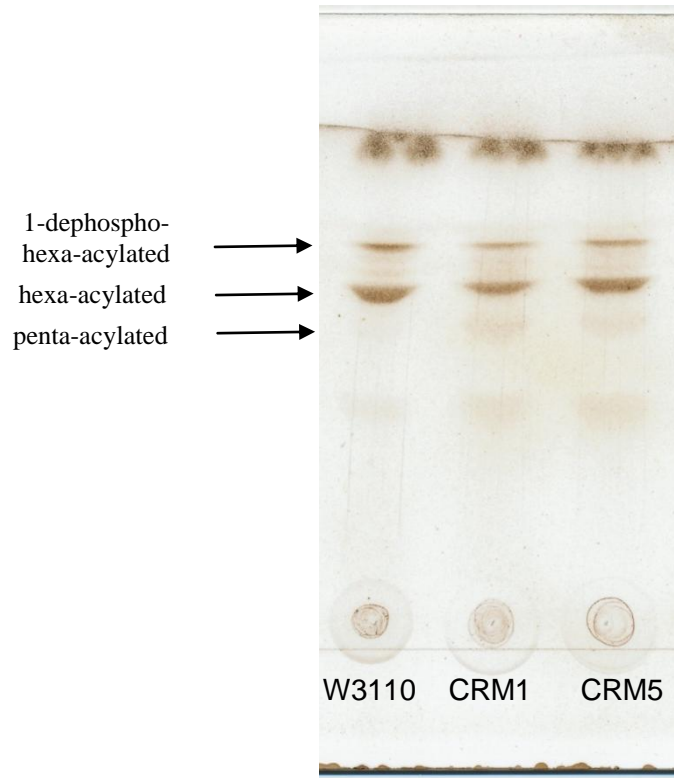


FIGURE 4.11B: TLC analysis of the lipid A profiles show CRM mutants have comparable major species of lipid A relative to W3110. The CRM mutants appear to have slightly more penta-acylated lipid A.

Furthermore these mutants have wild-type MICs to polymyxin B, an antibiotic that specifically targets LPS, and remain resistant to vancomycin (MIC of 250 $\mu\text{g}/\text{mL}$), a glycopeptide that is impermeable through an intact enterobacterial outer membrane. These data suggest that these FabZ mutants do not have an altered LPS structure or any changes in outer membrane permeability relative to wild-type cells. While mutants defective in lipid A biosynthesis or LPS transportation show severe hypersensitivity to polymyxin B (Tran et al, 2005) and vancomycin (Eggert et al, 2001; Vaara & Nurminen, 1999), our FabZ mutants maintain outer membrane integrity.

These results show evidence of a previously unrecognized regulatory mechanism between fatty acid biosynthesis and lipid A biosynthesis that maintains a proper ratio of phospholipids and lipid A, two essential components of Gram-negative bacteria membranes.

In *E. coli* and the vast majority of Gram-negative bacteria, the first step of the lipid A biosynthesis, acylation of UDP-GlcNAc with *R*-3-hydroxyacyl-ACP catalyzed by LpxA, is reversible and thermodynamically unfavorable. Therefore, LpxC, the zinc-dependent deacetylase that catalyzes the second step of the lipid A biosynthesis, is generally regarded as the regulator that commits resources to lipid A biosynthesis (Mohan et al, 1994). The fact that multiple mutations in *fabZ* have been isolated that affect lipid A biosynthesis (Mohan et al, 1994) and cause resistance to LpxC inhibitors (Clements et al, 2002) suggests an important regulatory role for FabZ in fatty acid synthesis in response to changes in lipid A biosynthesis.

How bacterial cells achieve this balance is unclear at this point. However, it is likely such a regulation minimally involves LpxC, as none of the other enzymes in lipid A biosynthesis appear to be regulated. Likewise, FabZ does not also appear to be regulated. To measure chromosomal FabZ protein levels, we incorporated a FLAG-tag on the C-terminus of *fabZ* on the chromosome of W3110 and used a monoclonal anti-FLAG antibody to measure FabZ protein amount. Western blot analysis did not show any difference in FabZ protein levels in W3110 cells overexpressing LpxC on a plasmid compared to vector control (Figure 4.12). This suggests that FabZ is not up-regulated as a response to LpxC overexpression.

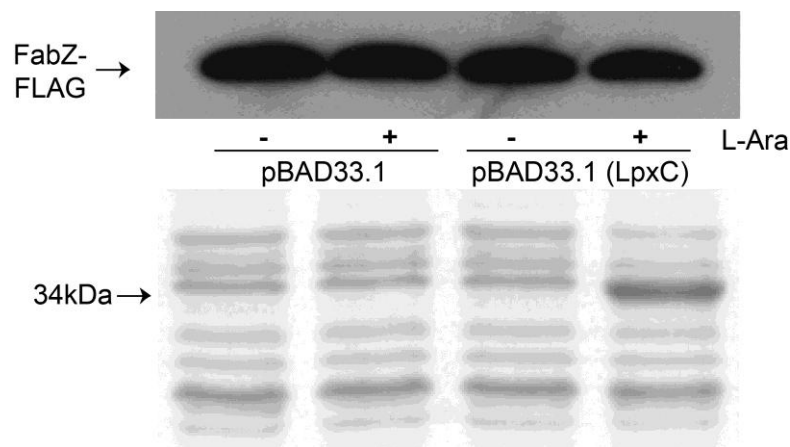


FIGURE 4.12: FabZ protein level does not change. Western blot show comparable FabZ protein amount when LpxC is overexpressed in the presence of 0.2% L-Arabinose (L-Ara) on a pBAD33.1 plasmid in W3110 (top). SDS-PAGE analysis of the protein gel shows overexpression of LpxC (~ 34,000 Daltons) only in the presence of 0.2% L-Arabinose (bottom).

In addition, RT-PCR studies show that under conditions when LpxC is up-regulated as a response to FabZ overexpression, mRNA levels for LpxC and FabZ do not change (Figure 4.13), suggesting that the regulatory mechanism for LpxC is not achieved through transcription and that FabZ does not appear to be regulated. Hence regulation of LpxC is most likely achieved through changes in mRNA translation or protein turnover (Eggert et al, 2001; Sorensen et al, 1996).

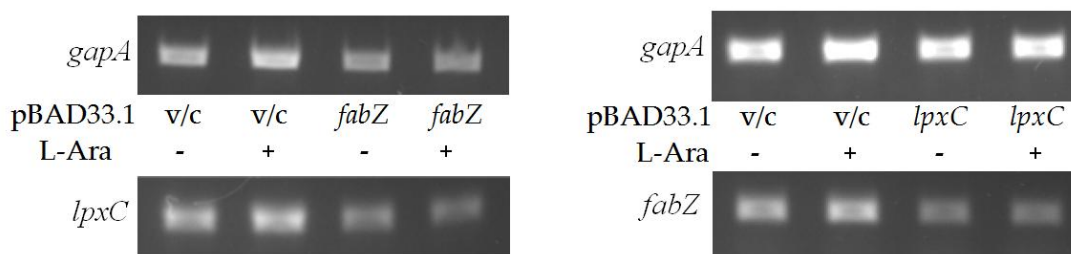


FIGURE 4.13: RT-PCR shows *lpxC* and *fabZ* mRNA levels do not change. Cells that up-regulate LpxC (when *fabZ* is overexpressed in the presence of 0.2% L-arabinose) do not have higher levels of LpxC mRNA. Likewise, mRNA levels of FabZ remain unchanged even in cells that overexpress *lpxC* in the presence of 0.2% L-arabinose. The gene *gapA* was used as the housekeeping gene for normalization of samples.

The protease for LpxC in *E. coli* is FtsH (Fuhrer et al, 2006). It is an essential gene that can only support a loss of function mutation in a strain (*ftsH* null mutant *tolZ21*) that has a dominant point mutation in FabZ that causes a leucine 85 to proline mutation. It is hypothesized that this FabZ point mutation elevates dehydrase activity thereby compensating for the higher cellular levels of LpxC (5 to 10-fold accumulation of LpxC as a result of losing FtsH) and suppressing lethality when FtsH is defective

(Ogura et al, 1999). To elucidate clues for LpxC regulation, it will be interesting to characterize the *ftsH* null strain *tolZ21* by looking at the relative amounts of LpxC and FabZ protein levels as well as sensitivity to LpxC inhibitors. If LpxC levels are no longer regulated (as a response to FabZ or LpxA overexpression or exposure to LpxC inhibitor) in this FtsH null background, then we can show that LpxC regulation requires FtsH and regulation likely occurs by affecting LpxC protein turnover.

Furthermore, it is also unclear what signal(s) triggers this regulation. To probe this effect, we overexpressed each enzyme in lipid A biosynthesis (*lpxA*, *lpxD*, *lpxH*, *lpxK*, *lpxB*, *kdtA*, *lpxL*, *lpxM*) on a pBAD(33.1) plasmid and used Western blotting to detect if overexpression of these enzymes result in altered LpxC expression. Indeed, only overexpression of *lpxA* resulted in a decrease of LpxC protein amount (Figure 4.14) while LpxC expression levels remain unchanged for the other enzymes. Likewise, *in vitro* enzymatic assays also show a 10-fold decrease in LpxC activity in cells when *lpxA* is overexpressed on a plasmid. Furthermore, overexpression of *lpxA* confers ~ 4 to 8-fold resistance to CHIR-090.

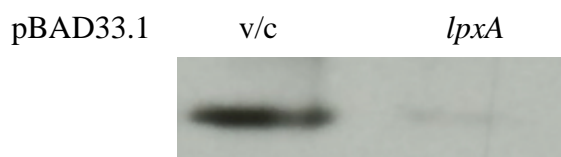


FIGURE 4.14: Western blot showing down-regulation of LpxC when *lpxA* is overexpressed on pBAD33.1 plasmid. Western blot was done using cell free extracts of *lpxA* over-expressing cells (right) compared to vector control (left) in the presence of 0.2% L-arabinose.

This suggests that the signaling molecule that causes LpxC regulation is likely an early substrate of lipid A biosynthesis, perhaps *R*-3-hydroxymyristoyl-ACP or the LpxC substrate (UDP-3-*O*-(*R*-3-hydroxymyristoyl)-GlcNAc). Indeed supplementing cells with *R*-3-hydroxymyristic acid in the growth media increases the MIC of CHIR-090 by ~ 4-fold; however, this result is not conclusive since this fatty acid was not soluble and precipitated out of solution. The resulting precipitation might have also decreased CHIR-090 solubility; hence the ~ 4-fold increased MIC could be due to a higher cellular concentration of *R*-3-hydroxymyristic acid or to the lowered solubility of CHIR-090 in the growth media (Figure 4.15).

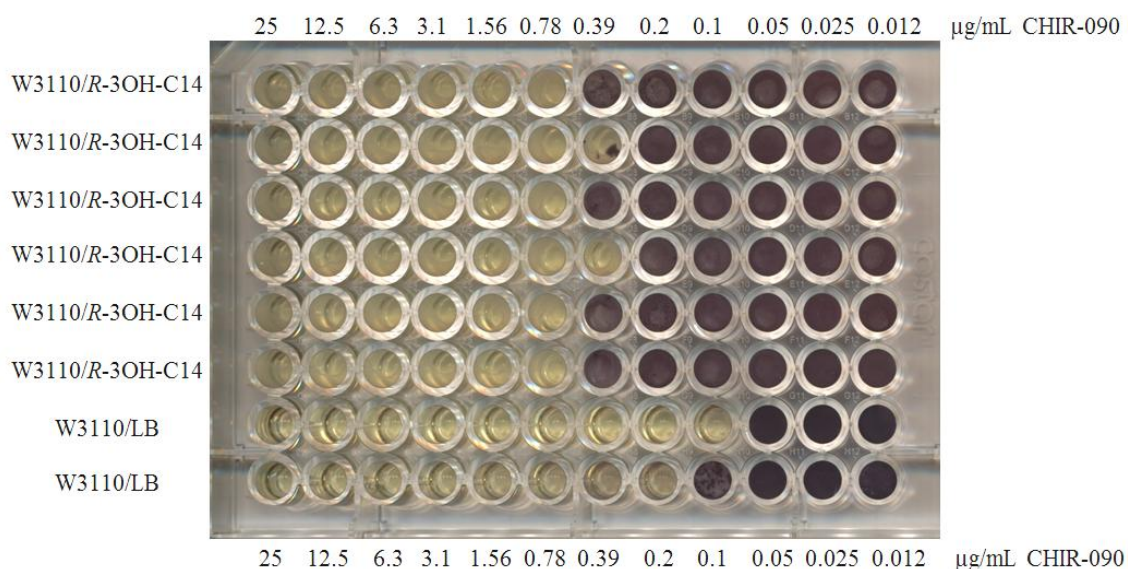


FIGURE 4.15: MIC of W3110 cells supplemented with 50 µg/mL of *R*-3-hydroxymyristic acid (*R*-3OH-C14). Though the MIC value increases by 4-fold, supplemental with *R*-3-hydroxymyristic acid clearly causes precipitation in solution (as seen by the increased turbidity of wells) and may decrease the solubility of CHIR-090. Decreasing the compound solubility of CHIR-090 would also cause an increase in the MIC value as it decreases the concentration of CHIR-090 in solution.

Further complicating this study, incorporation of exogenous fatty acids into fatty acid biosynthesis does not occur in *E. coli* as exogenous fatty acids are readily transported into the cell where they are converted to CoA thioesters and degraded to acetyl-CoA by the β -oxidation system (Clark, 2005). However, there is little to no elongation of the fatty acids, indicating they cannot enter the fatty acid synthetic pathway (Silbert et al, 1968); for example, radiolabeled 14-carbon fatty acids are detected only as glycerophospholipids with 14-carbon fatty acids, not as a 16- or 18-carbon fatty acid (Pluschke et al, 1978). Expression of *Vibrio harveyi* acyl-ACP synthetase (AasS), a soluble cytosolic enzyme that ligates fatty acids to ACP to form acyl-ACPs (Byers & Holmes, 1990), allowed exogenously supplemented fatty acids to become incorporated into the primary and secondary acyl chains of lipid A (Jiang et al, 2010). However, even in cells overexpressing *Vibrio harveyi* acyl-ACP synthetase, supplementation with *R*-3-hydroxymyristic acid did not increase the MIC value of CHIR-090 relative to vector control. This suggests that either increasing *R*-3-hydroxymyristoyl-ACP does not confer CHIR-090 resistance or the more likely explanation, *R*-3-hydroxymyristic acid is simply not soluble enough to enter the cells. Further studies need to be conducted to elucidate the signaling molecule for LpxC regulation and its role on resistance.

Though many questions remain to be answered, our results provide the essential clues for elucidating the regulatory mechanism(s) that is vital to expanding our knowledge of Gram-negative bacterial membrane homeostasis and will aid in the discovery of drugs targeting membrane biosynthesis.

Interestingly, though FabZ mutants are ~ 50-fold resistant to LpxC inhibitors, they appear to be ~ 4 to 8-fold hypersensitive to aminoglycosides including streptomycin, neomycin, tobramycin, and kanamycin (Table 4.3). Although the biochemical mechanisms for these observations remain to be characterized, this observation may have clinical relevance as it suggests that development of resistance via mutations in *fabZ* render these mutant hypersensitive to other antibiotics.

Table 4.3: MIC of FabZ mutants (CRM1 and CRM5) to aminoglycosides.

Strain	Streptomycin ($\mu\text{g}/\text{mL}$)	Neomycin ($\mu\text{g}/\text{mL}$)	Tobramycin ($\mu\text{g}/\text{mL}$)	Kanamycin ($\mu\text{g}/\text{mL}$)
W3110	22.1	12.5	4	9.9
CRM1	12.5	3.7	1.5	4.1
CRM5	10.2	3.4	1.0	4.9

Chapter 5
Characterization of ThrS Mutants

5.1: Introduction

Threonyl-tRNA synthetase (ThrS) is a member of the family of aminoacyl-tRNA synthetases, which covalently link amino acids to their specific tRNA molecules in a reaction driven by ATP hydrolysis (Figure 5.1) (Johnson et al, 1977). Unlike FabZ, there is no direct connection between ThrS and lipid A biosynthesis or even membrane biosynthesis. Hence how a point mutation in this gene can confer resistance to inhibitors of lipid A biosynthesis remains puzzling.



FIGURE 5.1: ThrS reaction scheme.

This chapter focuses on the characterization of our ThrS mutants. Biochemical characterization shows that the point mutation in ThrS impairs overall threonine-tRNA charging activity. Additionally, we observe that this mutation in *thrS* slows protein production and cellular growth, establishing that reduced protein biosynthesis can confer a suppressive effect on inhibition of membrane biosynthesis.

5.2: Materials and Methods

5.2.1: Construction of *pWSK29(thrS)*

Primers 5' GGCGCAGTCTAGATTAACCTTAAGAAGGAGATAT
ACATATGCCTGTTATAACTCTTCCTGATGGCA 3' and 5' GCAGAAGCTTTTA

TTCTCCAATTGTTTAAGACTGCGGCT 3' were used to amplify *thrS* from W3110 genomic DNA and cloning was done into a pWSK29 vector (Wang & Kushner, 1991) using restriction sites *Xba*I and *Hind*III. Cells were grown on LB agar containing 100 µg/mL ampicillin. Constructs were verified using primers 5' TAATACGACTCACTATAGGG 3' and 5' CTAGTTATTGCTCAGCGGTG 3', and transformed into chemically competent W3110, CRM1B *wtfabZ*, and CRM5B *wtfabZ* cells following previously described methods (Wang & Kushner, 1991). MICs were determined in LB media containing 100 µg/mL of ampicillin.

5.2.2: Preparation of *ThrS* constructs

Genomic DNA extracted from W3110 and CRM5B were used as the templates to amplify wild-type *thrS* and *thrS* T1549G respectively using primers 5' GGCGCAGTCTAGATTAACCTTTAAGAAGGAGATATACATATGCCTGTTATAA CTCTTCCTGATGGCA 3' and 5' GCAGAAGCTTTTCCTCCAATTGTTT AAGACTGCGGC 3' and restriction sites *Xba*I and *Hind*III. Cloning of these constructs was done as described above (FabZ assay).

Expression and purification of ThrS proteins was done as previously described (Bovee et al, 2003) with modifications. Briefly, one verified colony from each construct (wild-type ThrS and S517A ThrS) was chosen and grown in LB media supplemented with 100 µg/mL ampicillin to OD_{600nm} ~ 0.5 at 37 °C. Isopropyl-1-thio-D-galactopyranoside (Sigma, St. Louis, MO) was then added to a final concentration of 1 mM, and the cells were grown for an additional 3 hours. Cells were then harvested and

centrifuged at 8,000 rpm for 10 minutes at 4 °C. The supernatant was discarded and the cell pellets were washed with PBS and centrifuged again. The cell pellets were stored at -80 °C overnight.

The cell pellets were resuspended in 8 mL of 25 mM Tris pH 8 at 4 °C, 50 mM KCl, 5 mM MgCl₂, and 3 mM DTT. Cells were lysed using a French Pressure cell at 17000 psi and centrifuged at 45,000 rpm (~140,000 × g) in a Beckman type 70.1 Ti rotor for 1 hour at 4 °C to prepare membrane-free lysate. The supernatant, which contains the soluble proteins, was applied to a Ni-NTA column and washed with 20 column volumes of solution containing 20 mM imidazole, 25 mM Tris pH 8 at 4 °C, 50 mM KCl, 5 mM MgCl₂, and 3 mM DTT. His-tagged proteins were eluted using 20 column volumes of 150 mM imidazole in the same buffer. SDS-PAGE analysis was done on each fraction to determine protein purity. The purest fractions (~ 12mL) were collected, placed into a Slide-A-Lyzer Dialysis Cassettes, 10K MWCO (Thermo Scientific, Rockford, IL) and dialyzed into a 4 liter solution containing 20 mM Tris pH 7.5, 150 mM KCl, and 15 mM MgCl₂ overnight and concentrated to 20 mg/mL final concentration using Amicon Ultra Centrifugal Filters Regenerated Cellulose 30,000 MWCO (EMD Millipore, Billerica, MA). Final protein purity was > 90% homogeneous as determined by SDS-PAGE analysis (Figure 5.2). Final protein concentrations were determined using the Bradford Reagent (Sigma, St. Louis, MO) and previously described protocols (Bradford, 1976). Purified proteins were stored at -80 °C.

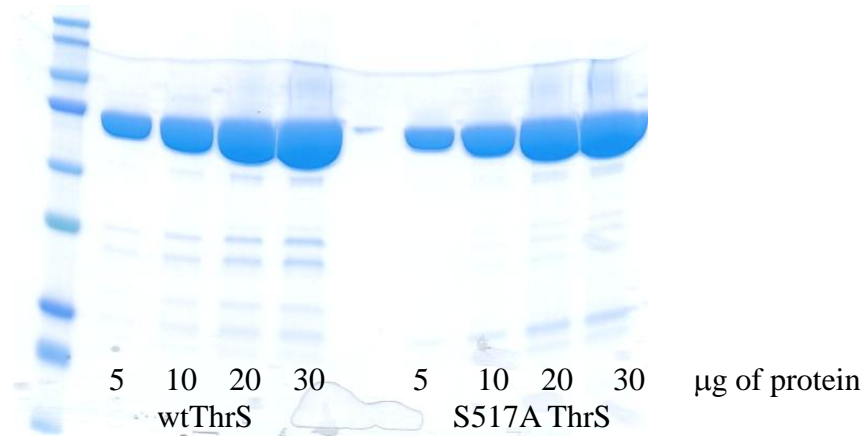


Figure 5.2: Final protein purity of ThrS judged by SDS-PAGE analysis

5.2.3: Preparation of RNA substrate

Primers 5' TAATACGACTCACTATAGGCTGATATAGCTCAGTTGGTAGA GCGCACCTTGGTAAGGGTGAGGTCGGCAGTTCGAATCTGCCTATCAGC 3', 5' TTTTGAATTCTAATACGACTCACTATAGGCTGATATAGCTCAGTTGGTAG AGCG 3', and 5' GGTGCTGATAGGCAGATTCGAACTGCCG 3' were used to create the DNA template for *in vitro* transcription of tRNA(GGU) lacking the 3' terminal adenosine for synthesis of radiolabeled substrate. Primers 5' TAATACGACTCACTATAGGCTGATATAGCTCAGTTGGTAGAGCGCACCTTG GTAAGGGTGAGGTCGGCAGTTCGAATCTGCCTATCAGC 3', 5' TTTTGAATTC TAATACGACTCACTATAGGCTGATATAGCTCAGTTGGTAGAGCG 3', and 5' TGGTGCTGATAGGCAGATTCGAACTGCCG 3' were used to create fully formed tRNA(GGU) for the synthesis of cold carrier substrate. The amplified DNA fragments were run on 2% agarose gel and purified as described before (Construction of

pBAD33.1(*fabZ*)). RNA transcription reactions and isopropanol purifications were done using MEGAscript Kit High Yield Transcription Kit (Applied Biosystems, Carlsbad, CA). The resulting RNA constructs were > 90% homogeneous as visualized by 8% PAGE gel/7M Urea chromatography and Ethidium Bromide (Sigma-Aldrich, St. Louis, MO) staining (Figure 5.3 A-B).

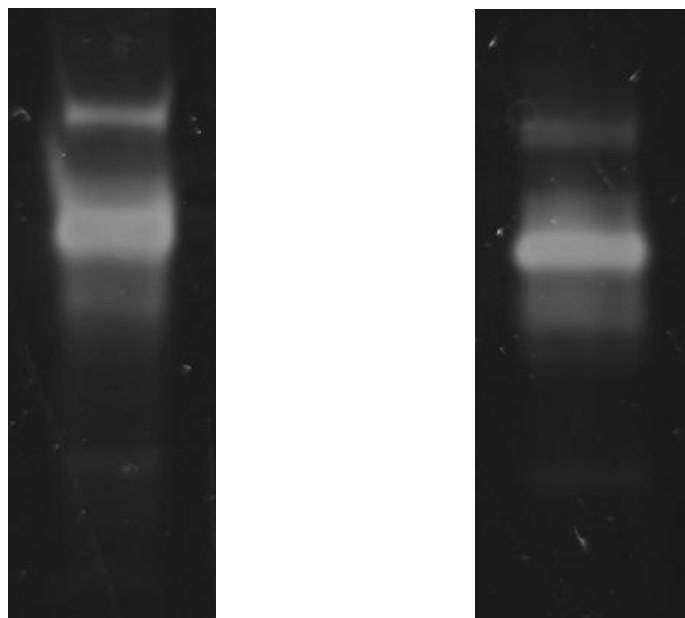


FIGURE 5.3: Purity analysis of transcribed RNA constructs on 8% PAGE gel/7M Urea chromatography. (A) Analysis of cold carrier fully formed tRNA(GGU) RNA. (B) Analysis of tRNA(GGU) transcript lacking the 3' terminal adenosine for radiolabeling substrate.

For preparation of radiolabeled substrate, *E. coli* tRNA nucleotidyltransferase enzyme was cloned from W3110 genomic DNA using primers 5' GGCGCAGCATATGGTGAAGATTTATCTGGTCGGTGGTGC 3' and 5' GGCGCAGGGATCCTCATT CAGGCTTTGGGCAACGTT 3' and restriction sites

NdeI and *BamHI* in a pET16b vector (EMD Biosciences, San Diego, CA) as described before (4.2.1: *Construction of pBAD33.1(fabZ)*). The construct was expressed and purified as previously described (Silbert et al, 1968) with modifications. Specifically, one verified colony containing the correct construct was chosen and grown in LB media supplemented with 100 µg/mL ampicillin to OD_{600nm} ~ 0.5 at 37 °C. Isopropyl-1-thio-D-galactopyranoside was then added to a final concentration of 1 mM, and the cells were grown for an additional 3 hours. Cells were then harvested and centrifuged at 8,000 rpm for 10 minutes at 4 °C. The supernatant was discarded and the cell pellets were washed with PBS and centrifuged again. The cell pellets were stored at -80 °C overnight.

The cell pellets were resuspended in 8 mL of 50 mM Tris pH 7.8, 300 mM KCl, 1 mM MgCl₂, and 1 mM beta-mercaptoethanol. Cells were lysed using a French Pressure cell at 17000 psi and centrifuged at 45,000 rpm (~140,000 × *g*) in a Beckman type 70.1 Ti rotor for 1 hour at 4 °C to prepare membrane-free lysate. The supernatant, which contains the soluble proteins, was applied to a Ni-NTA column and washed with 20 column volumes of solution containing 20 mM imidazole, 50 mM Tris pH 7.8, 300 mM KCl, 1 mM MgCl₂, and 1 mM beta-mercaptoethanol. His-tagged proteins were eluted using 20 column volumes of 200 mM imidazole in the same buffer. SDS-PAGE analysis was done on each fraction to determine protein purity. The purest fractions (~12mL) were collected, placed into a Slide-A-Lyzer Dialysis Cassettes, 10K MWCO (Thermo Scientific, Rockford, IL) and dialyzed into a 4 liter solution containing 50 mM Tris pH 7.8, 300 mM KCl, 1 mM MgCl₂, and 1 mM beta-mercaptoethanol overnight

and concentrated to 10 mg/mL final concentration using Amicon Ultra Centrifugal Filters Regenerated Cellulose 10,000 MWCO (EMD Millipore, Billerica, MA). Final protein purity was > 90% homogeneous as determined by SDS-PAGE analysis (Figure 5.4). Final protein concentrations were determined using the Bradford Reagent (Sigma, St. Louis, MO) and previously described protocols (Bradford, 1976). Purified proteins were stored at -80 °C.



FIGURE 5.4: Final protein purity of *E. coli* tRNA nucleotidyltransferase enzyme judged by SDS-PAGE analysis.

Radiolabeling of 3' adenosine was done as previously described (Ledoux & Uhlenbeck, 2008) with modifications. Briefly, a 50 μ L reaction mixture containing 2 μ M tRNA(GGU) lacking 3' adenosine, 50 μ M sodium pyrophosphatase (Sigma, St. Louis, MO), 3 μ M ATP (Applied Biosystems, Carlsbad, CA), 250 μ Ci [α - 32 P]-ATP (9.25 MBq) (Perkin-Elmer, Waltham, MA), 10 mM MgCl₂, and 50 mM glycine pH = 9.0 was reacted with 0.2 μ M of tRNA nucleotidyltransferase. The reaction mixture was incubated at 37 °C for 7 minutes, at which time the reaction mixture underwent

phenol/chloroform extraction, and the aqueous layer was put through two consecutive Micro Bio-spin P-6 columns (Bio-Rad, Hercules, CA). 1 μ L aliquots, taken before addition of enzyme, after 7 minutes of reaction, and after column purification, were spotted on a TLC PEI Cellulose-F plate (Merck, Darmstadt, Germany) and ran in a solvent system consisting of saturated ammonium sulfate to check conversion and purity of the final tRNA(GGU) substrate (Figure 5.5 and Figure 5.6). All tRNA substrates were stored at -20 °C in RNase-free water (Applied Biosystems, Carlsbad, CA).

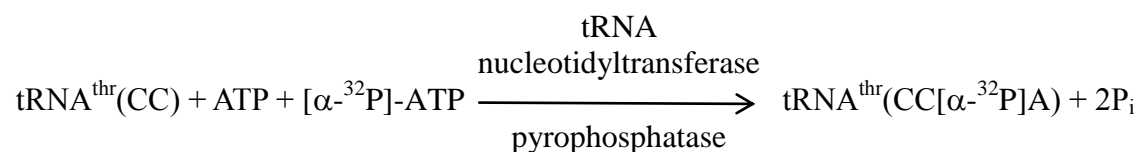


FIGURE 5.5: $[\alpha\text{-}^{32}\text{P}]\text{-tRNA}^{\text{thr}}$ labeling reaction.

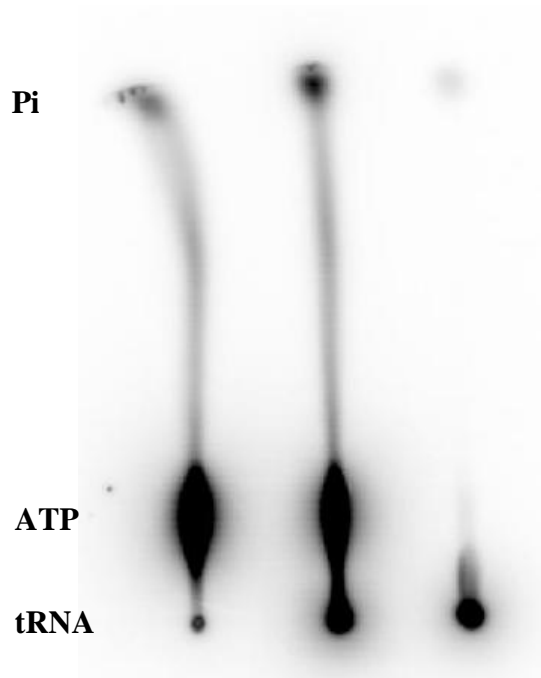


FIGURE 5.6: tRNA labeling reaction. PEI cellulose TLC plate showing [α - 32 P] ATP before (left), after (middle) incorporation into tRNA, and after column purification (right).

5.2.4: *ThrS* assay setup

Immediately before use in assay, tRNA substrates were refolded by heating to 95 °C for 3 minutes and then slowly cooled to 37 °C over the course of 30 minutes using a thermocycler. Each reaction mixture contained 50 mM Tris pH = 8, 20 mM KCl, 10 mM MgCl₂, 5 mM DTT, 100 μM ATP, 50 μM L-threonine, 10 μM of cold carrier tRNA(GGU), and 10,000 cpm/reaction of [α - 32 P]-tRNA(GGU) at 37 °C. Reactions were started with the addition of 5-10 nM of wild-type ThrS or 5-100nM of mutant ThrS. Time points were taken over the course of 10 minutes, and reactions were quenched in 4x volume of S1 Nuclease (10U total diluted in 1x reaction buffer)

(Fermentas, Glen Burnie, MD) at room temperature for 10 minutes. 1 μ L of each sample was spotted on a PEI Cellulose-F plate and run in a solvent system consisting of 5:10:85 volume ratio of glacial acetic acid/1M ammonium chloride/water respectively. Product formation was visualized using a Phosphor Image Screen and product conversion was calculated using ImageQuant TL (Amersham Biosciences, Piscataway, NJ). Product conversion was linear with respect to both time and enzyme concentrations used.

5.2.5: Construction of W3110 *muthrS*

Primers 5' GGCGCAGAAGCTTACTGCAAATAAGGATATAAAATGC CTGTTATAACTCTTCCT 3' and 5' GGCGCAGTCTAGATTATTCCTCCAATTG TTTAAGACTGCGGCT 3' were used to amplify *thrS* T1549G using genomic DNA extracted from CRM5B and ligated into a pMAK705 plasmid (Brown et al, 2012) using restriction enzymes *HindIII* and *XbaI*. Cloning was done as described above (Construction of pBAD33.1(*fabZ*)) and the verified construct was transformed into W3110 competent cells. Cells were grown on LB agar containing 25 μ g/mL chloramphenicol at 42 °C. In these conditions, the pMAK705 plasmid replicon cannot replicate (Brown et al, 2012) and surviving cells must have incorporated the plasmid into the chromosome through homologous recombination with the chromosomal copy of wild-type *thrS*. Purified colonies were then grown at 30 °C in same medium. At this permissive temperature, the pMAK705 plasmid replicon can replicate and surviving cells must have excised the plasmid leaving either the original chromosomal wild-type

copy of *thrS* or the plasmid-borne copy of *thrS* T1549G remaining on the chromosome. Single cells were then purified three times at 42 °C in the absence of antibiotic to dilute out the plasmid. Complete loss of the plasmid was confirmed by resulting cells' inability to grow on LB agar containing 25 µg/mL chloramphenicol at 30 °C (Figure 5.7). PCR analysis and DNA sequencing were employed to confirm the genotypes using primers 5' AACCTTTCAGACGCACCGTGATG 3', 5' ACGGAATTTAATTTCCTAACCTGGATAACTTTTTGC 3', 5' GTCTGGAGATCATTTCGTCACTCCTGT 3', and 5' ATTTCTCAAGTCTGCTTTAACACGAATGCC 3'. A construct with wild-type *thrS* remaining on the chromosome was designated "W3110 *wthrS*," while a construct with *thrS* T1549G on the chromosome was designated "W3110 *muthrS*".

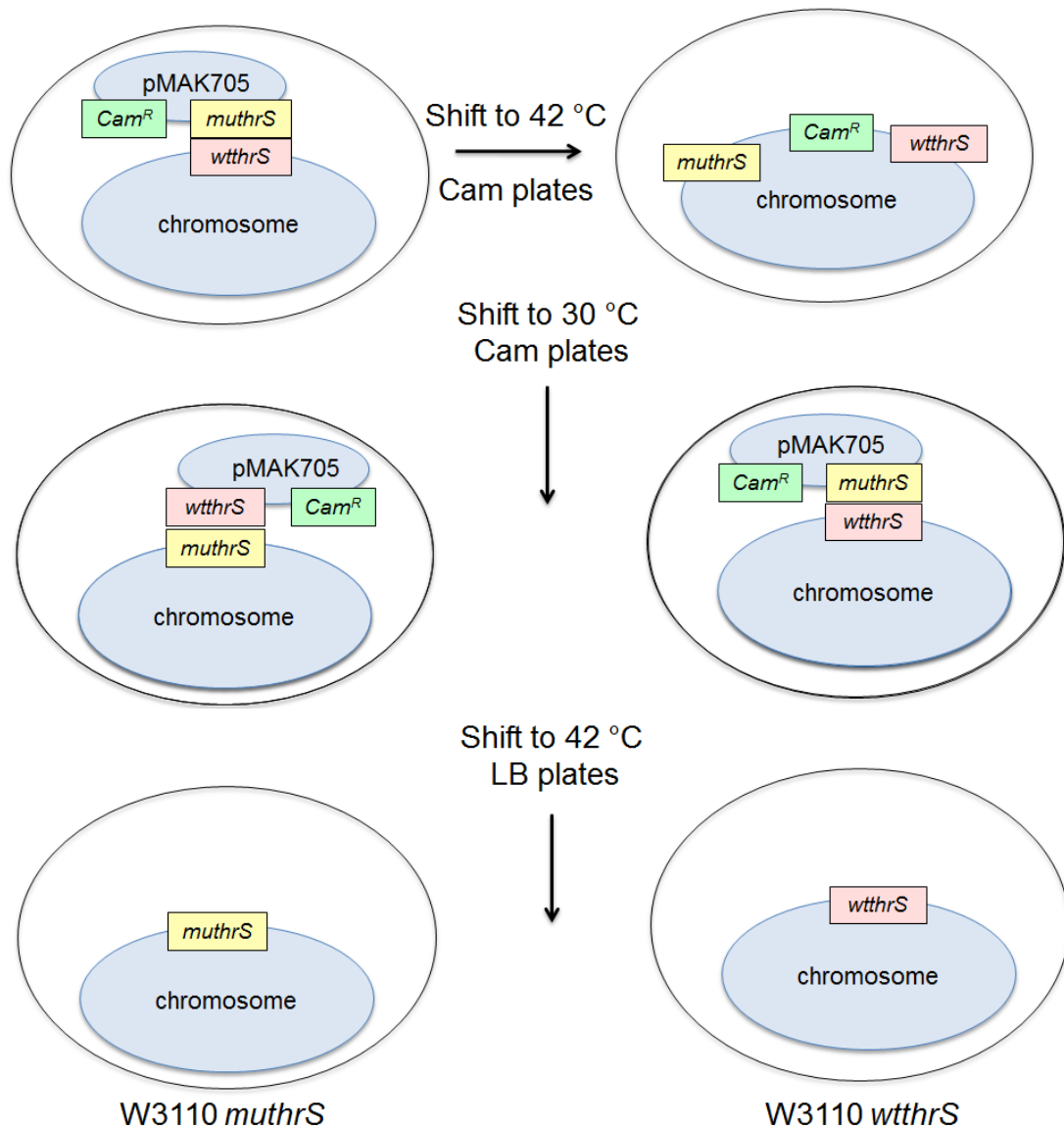


FIGURE 5.7: Generation of W3110 *muthrS*. *thrS* T1549G (*muthrS*) was cloned into a pMAK705 plasmid that has a temperature sensitive replicon disabling plasmid replication at 42 °C. This construct was transformed into W3110 cells at 30 °C. Cells were temperature shifted to 42 °C and grown in the presence of chloramphenicol (Cam) Surviving cells must have incorporated the plasmid into the chromosome through homologous recombination. Purified colonies were then grown at 30 °C in the same medium. At this permissive temperature, the pMAK705 plasmid replicon can replicate and surviving cells must have excised the plasmid, leaving cells that have wild-type *thrS* (*wthrS*) and cells that have *thrS* T1549G (*muthrS*) remaining on the chromosome. These cells were then purified three times at 42 °C in the absence of antibiotic to dilute out the plasmid.

5.2.6: Protein labeling experiments

Strains W3110, W3110 *wthrS*, and W3110 *muthrS* were grown in M9 media supplemented with 0.2% glucose, 1 mM MgCl₂, 100 μM CaCl₂, 3 mM iron chloride, 10 μg/mL thiamine until OD₆₀₀ ~ 0.2, at which time 5 μCi of [¹⁴C]-L-amino acids (1.85Mbpq) (Perkin-Elmer, Waltham, MA) was added to the growth culture. One mL samples were collected at 0.5, 2, 4, and 8 minutes by quenching with 200 μg/mL chloramphenicol and placed on ice. Samples were centrifuged to pellet the cells, the supernatant was decanted, and the remaining cell pellet was resuspended with Laemmli buffer using the ratio of 10⁹ cells/100 μL. Samples were heated to > 95 °C for 10 min, and 10 μL of each sample was loaded on 12% Tris-HCl gels (Bio-Rad, Hercules, CA) and ran in 1x Tris-Glycine Buffer (Bio-Rad, Hercules, CA) at 200V for 40 min. Incorporation of [¹⁴C] L-amino acids into proteins was visualized by a PhosphoImager and counts were quantified using ImageQuant TL (Amersham Biosciences, Piscataway, NJ). Counts for each time point (for W3110 *wthrS* and W3110 *muthrS*) were normalized to the counts detected in W3110 to measure a relative ratio of protein biosynthesis.

5.2.7: Growth curves

Bacterial cultures were diluted 1:100 from overnight cultures and grown till log phase (OD₆₀₀ ~ 0.5). At which point, cells were diluted 10-fold into unused LB media and OD₆₀₀ was measured over the course of ~ 12 generations. To ensure continuous log phase growth, once bacterial cultures reached OD₆₀₀ ~ 0.5, cells were continuously

diluted 10-fold into unused media. Doubling time for each strain was calculated using Kaleidagraph (Synergy Software, Reading, PA) by exponentially fitting the plot of log OD₆₀₀ versus minutes using the equation:

$$y = m1 * 2^{(x/m2)}$$

where y is log(OD₆₀₀), x is time (minutes), m1 is OD₆₀₀ of initial cells, and m2 is doubling time (minutes).

5.2.8: Isolation and characterization of other resistant mutants

Other spontaneously resistant mutants were generated in a similar manner as previously described (3.2.1: Isolation of CHIR-090 resistant mutants) except an intermediate step of exposure to 3 µg/mL CHIR-090 plates was added before exposure to 10 µg/mL CHIR-090 plates.

Resistant mutants (1h-15, 2h-6, 2h-10, 2h-12) were also generated using chemical mutagenesis. Briefly, a wild-type strain of *E. coli*, W3110A (Byers & Holmes, 1990), was exposed to the chemical mutagen ethyl methane sulfonate (EMS) following previously described protocols (Miller, 1992). The ethyl group of EMS reacts with guanine in DNA forming the abnormal base O-6-ethylguanine which base pairs with thymine. Following subsequent rounds of replication, the original G: C base pair becomes an A: T pair. EMS typically produces only point mutations and can induce mutations at a rate of 5×10^{-4} to 5×10^{-2} per gene without substantial killing. After 1 to 3 hours exposure to EMS, cells were washed, allowed to outgrow for several generations, and plated (10^9 cells) on 10 µg/mL CHIR-090 plates. Colonies that consistently grew on

10 µg/mL CHIR-090 plates were isolated at a frequency of ~ 1 in 10⁹ cells (Boon Hinckley unpublished data).

From these trials, we have isolated and characterized a combined total of 16 designated strains that are at least 50-fold more resistant to CHIR-090 relative to their parental strains. PCR amplification and DNA sequencing of the *thrS* gene using primers 5' AACCTTTCAGACGCACCGTGATG 3', 5' ACGGAATTTAATTCCTT AACCTGGATAACTTTTTGC 3', 5' GTCTGGAGATCATTTCGTCACCTCCTGT 3', and 5' ATTTCTCAAGTCTGCTTTAACACGAATGCC 3'. Of these 16 strains, only CRM1B and CRM5B have a point mutation in *thrS*, all the other mutants have wild-type *thrS* (Table 5.1).

Table 5.1: Table of CHIR-090 mutants.

Strain name	Chromosomal protein mutations that confer resistance	CHIR-090 (µg/mL)
CRM1B	FabZ = Leu(17) to Gln ThrS = Ser(517) to Ala	56.3
CRM1C	FabZ = Leu(17) to Gln Unknown point mutation (none in ThrS)	> 10
CRM1E	FabZ = Leu(17) to Gln RpsA: His(219) to Arg	25.6
CRM2B	FabZ = Leu(17) to Gln Unknown point mutation (none in ThrS)	> 10
CRM3C	FabZ = Leu(17) to Gln Unknown point mutation (none in ThrS)	> 10
CRM5B	FabZ = Ala(71) to Val ThrS = Ser(517) to Ala	56.3
3A-4C/A	FabZ = Arg(100) to Cys LpxC = Ile(2) to Asn Unknown point mutation (none in ThrS)	50
3A-1A/B	FabZ = Arg(100) to Cys LpxC = Val(37) to Cys Unknown point mutation (none in ThrS)	200
3A-1B/B	FabZ = Arg(100) to Cys LpxC = Val(37) to Cys Unknown point mutation (none in ThrS)	100
3A-1D/B	FabZ = Arg(100) to Cys LpxC = Val(37) to Cys Unknown point mutation (none in ThrS)	200
7B-4A/2	FabZ = Arg(100) to Cys LpxC = Leu(18) to Val Val(37) to Gly	50
3A-1C/B	FabZ = Arg(100) to Cys LpxC = Val(37) to Cys Unknown point mutation (none in ThrS)	50
1h-15	FabZ = Pro(62) to Ser 84 point mutation(s) (none in ThrS)	25
2h-6	FabZ = UTR LpxC = UTR 183 point mutation(s) (none in ThrS)	50
2h-10	FabZ = UTR 212 point mutation(s) (none in ThrS)	25
2h-12	FabZ = Arg(100) to Cys 190 point mutation(s) (none in ThrS)	50

UTR: untranslated region

Slow cellular growth phenotype was observed since mutant colonies on LB agar plates required > 24 hours of growth at 37 °C to become visible whereas, colonies of the wild-type strains W3110 and W3110A only required ~ 14 hours of growth.

5.2.9: Slowing cellular growth experiments

To decrease cellular growth, MIC assays were done at 30 °C in LB media as well as minimal M9 media (Miller, 1992) supplemented with 0.2% glucose as the carbon source, 1 mM magnesium chloride, 100 µM calcium chloride, 3 mM iron chloride, and 10 µg/mL thiamine and grown at 30 °C.

To decrease protein synthesis, cells were grown in the presence of sublethal doses of erythromycin (75 µg/mL) and tetracycline (0.78 – 1.56 µg/mL). Under these conditions, cells also grew > 3-fold slower relative to cells grown in the absence of antibiotic.

5.3: Results

5.3.1: Point mutation in thrS slows down protein synthesis

ThrS is the threonine-tRNA ligase (Johnson et al, 1977), and our data show that this mutation results in ~ 4 to 8-fold resistance to inhibition of lipid A biosynthesis by CHIR-090. Since ThrS plays no direct role in membrane biosynthesis, it is intriguing that a point mutation in this gene would confer resistance to LpxC inhibitors. To verify that this point mutation indeed confers resistance, we complemented the *thrS* mutants (CRM1B *wfabZ* and CRM5B *wfabZ*) with the wild-type *thrS* gene on a plasmid. The

resulting mutants completely lost resistance (Table 5.2) to CHIR-090, confirming that the point mutation in *thrS* is the *bona fide* resistance factor.

Table 5.2: MIC assay show *thrS* point mutations are recessive.

Mutant (pWSK29)	CHIR-090 ($\mu\text{g/mL}$)
W3110 (v/c)	0.2
W3110 (<i>thrS</i>)	0.2
CRM1B <i>wtfabZ</i> (v/c)	1.25
CRM1B <i>wtfabZ</i> (<i>thrS</i>)	0.2
CRM5B <i>wtfabZ</i> (v/c)	1.25
CRM5B <i>wtfabZ</i> (<i>thrS</i>)	0.2

v/c: vector control

The identified T1569G mutation in *thrS* causes a replacement of Ser517 by Ala. In the crystal structure of *E. coli* ThrS (PDB ID: 1QF6) (Sankaranarayanan et al, 1999), this residue is located in the ATP binding pocket, and its hydroxyl group lies within hydrogen bonding distance (2.8 Å) away from the N3 position of the adenine ring (Figure 5.8). Hence the Ser517Ala mutation likely results in the loss of a hydrogen bond which is expected to negatively impact overall catalytic activity.

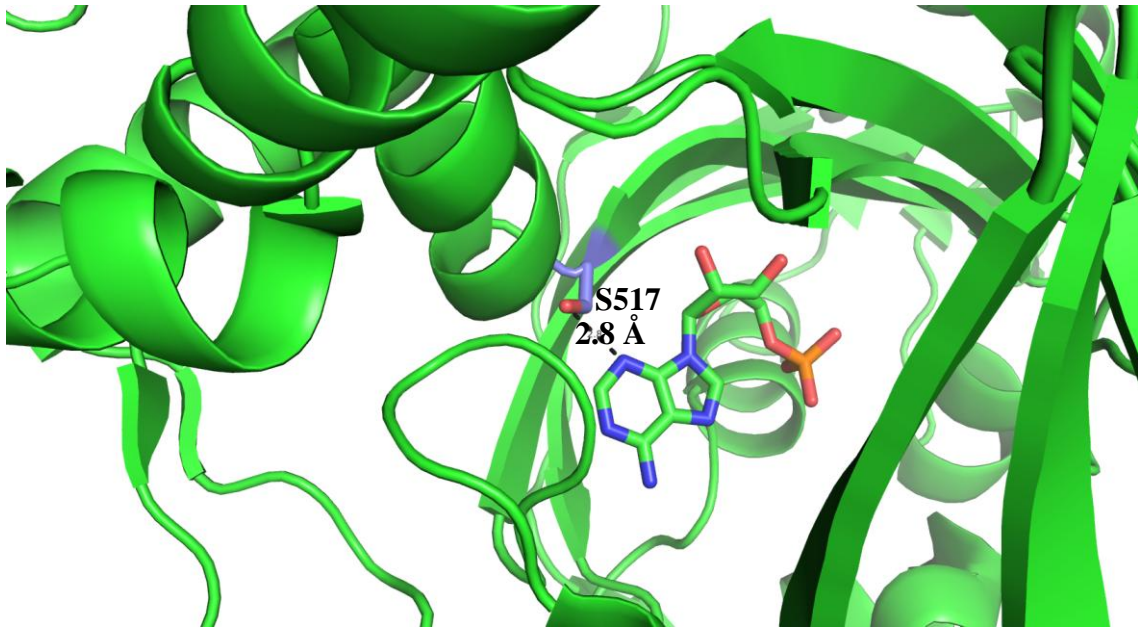


FIGURE 5.8: X-ray structure of *E. coli* ThrS (PDB ID: 1QF6). The hydroxyl group of serine 517 is located in the ATP binding pocket and is hydrogen bonding distance (2.8 Å) away from the N3 position of the adenine ring.

To measure ThrS enzymatic activity *in vitro*, we purified wild-type and mutant ThrS enzymes to homogeneity and [³²P] radiolabeled the alpha phosphate on the 3' terminal adenosine in tRNA^{Thr} to directly monitor Thr-tRNA charging activity. In this assay, ATP, L-Thr, and [³²P]tRNA^{Thr} were incubated with purified wild-type or mutant enzyme. Reaction samples were then digested with S1 nuclease, which cleaves off the radiolabeled 3' terminal adenosine to form [³²P]-AMP or [³²P]-AMP-Thr. These two species were separated using thin layer chromatography (TLC). Under the conditions of our assay, Ser517Ala ThrS has a ~ 20-fold decrease in Thr-tRNA^{Thr} charging activity compared to wild-type ThrS (Figure 5.9, Table 5.3).

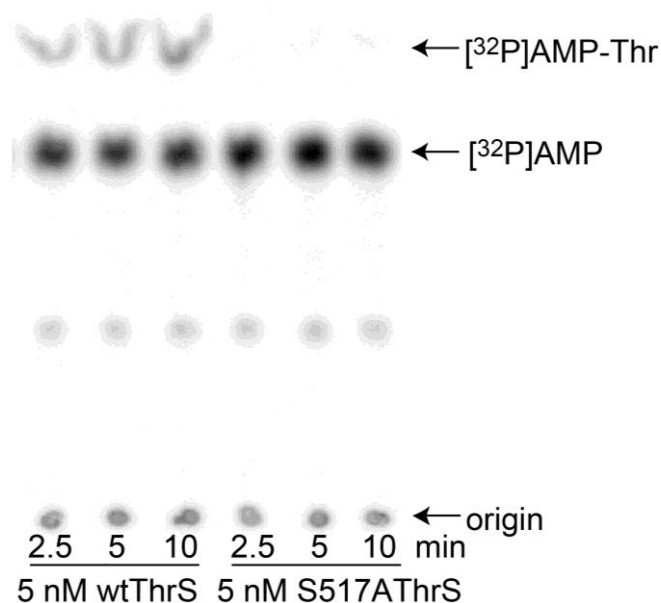


Figure 5.9: PEI-Cellulose plate shows Ser517Ala ThrS has significantly reduced Thr-tRNA charging activity compared to the wild-type enzyme (wtThrS).

Table 5.3: Ser517Ala ThrS has ~ 20-fold less Thr-tRNA charging activity compared to the wild-type enzyme.

ThrS protein	Specific Activity (nmol/min/mg)
Wild-type	344 ± 69
Ala71Val	15.7 ± 2.9

Since ThrS binds threonine and CHIR-090 has a threonyl scaffold, we wondered if either the wild-type ThrS or its mutant could be a secondary target of CHIR-090. We used the same radiometric assay to probe for any inhibitory effects of ThrS in the

presence of CHIR-090. Our results showed there was no change in specific activity when wild-type and mutant enzymes were incubated with up to 200 μ M CHIR-090, suggesting that neither the wild-type nor the mutant ThrS is a secondary target of CHIR-090.

To probe the functional consequence of the Ser517Ala ThrS point mutation *in vivo*, we moved the mutant *thrS* gene into a clean W3110 genetic background without any selective markers or scar sequences left on the chromosome. Using this mutant (W3110 *muthrS*), any phenotypes observed will be directly and solely caused by the point mutation in *thrS*. As a control, we also included a strain that went through the same construction process as W3110 *muthrS*; however, this cell (W3110 *wthtrS*) does not have any point mutations in *thrS* on the chromosome and should be genetically identical to W3110.

Since Thr-tRNA^{Thr} is an essential component of the protein synthetic machinery, we reasoned that a significant decrease in ThrS activity could lead to a reduction of the overall rate of protein synthesis. Indeed, when we pulse labeled whole cells with [¹⁴C]-L-amino acids, we found that the total counts of [¹⁴C]-L-amino acids incorporated into proteins visualized on a SDS gel in W3110 *muthrS* is ~ 2-fold less relative to wild-type strains W3110 and W3110 *wthtrS* (Figure 5.10).

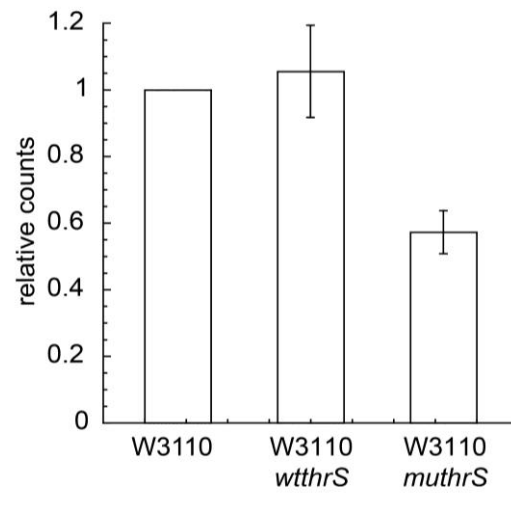


Figure 5.10: Point mutation in *thrS* reduces protein synthesis. Incorporation of [^{14}C]-L-amino acids into proteins in cell extracts was significantly lower for W3110 *muthrS* compared to wild-type strains W3110 and W3110 *wtthrS*. The counts for each strain are normalized to the counts detected for W3110. Values plotted are the average values taken at time points 0.5, 2, 4, and 8 minutes. Error bars represent the standard deviation.

Further supporting the observation of reduced protein synthesis, W3110 *muthrS* also grows ~ 2-fold slower compared W3110 and W3110 *wtthrS* (Figure 5.11) suggesting that the point mutation in *thrS* reduces cellular growth. Interestingly, in addition to being resistant to inhibitors of lipid A biosynthesis, this mutant has ~ 2-fold resistance to ciprofloxacin and nalidixic acid (Table 5.4), suggesting that this point mutation also confers slight resistance to inhibitors of DNA synthesis.

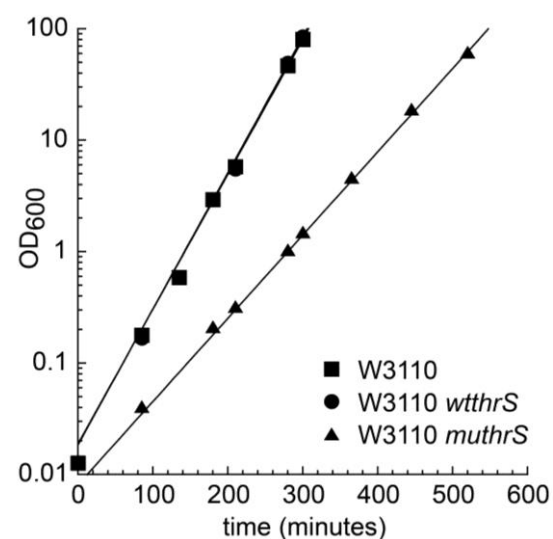


Figure 5.11: Point mutation in *thrS* reduces cellular growth. Growth curves show W3110 *muthrS* grows significantly slower compared to the wild-type strains W3110 and W3110 *wtthrS*. Each plot was exponentially fitted to calculate doubling times: 24.9 ± 0.39 min for W3110, 24.7 ± 0.57 min for W3110 *wtthrS*, and 40.3 ± 1.2 min for W3110 *muthrS*.

Table 5.4: MICs show W3110 *muthrS* is ~ 2-fold resistant to the fluoroquinolones ciprofloxacin and nalidixic acid relative to the wild-type strains W3110 and W3110 *wtthrS*.

Strain	Chromosomal mutations	Protein	CHIR-090 ($\mu\text{g/mL}$)	Ciprofloxacin ($\mu\text{g/mL}$)	Nalidixic Acid ($\mu\text{g/mL}$)
W3110	None	None	0.2	0.032 ± 0.01	6.25 ± 0
W3110 <i>wtthrS</i>	None	None	0.2	0.030 ± 0.01	6.25 ± 0
W3110 <i>muthrS</i>	<i>thrS</i> : T(1549) to G	ThrS: Ser(517) to Ala	1.25	0.069 ± 0.02	13.75 ± 3.95

wtfabZ: wild-type *fabZ*, *wtthrS*: wild-type *thrS*, and *muthrS*: mutant *thrS*

5.4: Discussion

5.4.1: Reduction of protein synthesis suppresses inhibition of lipid A biosynthesis

Initially, we were surprised that a point mutation in a tRNA synthetase conferred resistance to inhibitors of lipid A biosynthesis. Our data show that the point mutation in ThrS decreases enzymatic activity and protein synthesis, which in turn slows down cellular growth. In this state of hypo-metabolic activity, bacterial cells are more tolerant to inhibition of lipid A biosynthesis as well as DNA biosynthesis. Furthermore, the observation that a point mutation in the threonine tRNA ligase decreases cellular growth so significantly is consistent with previous studies implicating the importance of threonine in rapidly growing cells (Almaas et al, 2004; Wang et al, 2011).

Though defects in protein synthesis have previously been shown to suppress inhibition of DNA synthesis (Bollenbach et al, 2009), the same have not been observed for membrane biosynthesis. Here, our results show a point mutation that reduces protein biosynthesis can confer significant levels of resistance to inhibitors of membrane biosynthesis as well as DNA biosynthesis. This implies that there are regulatory interactions among all three major cellular processes in *E. coli*: membrane biosynthesis, protein biosynthesis, and DNA biosynthesis (Figure 5.12).

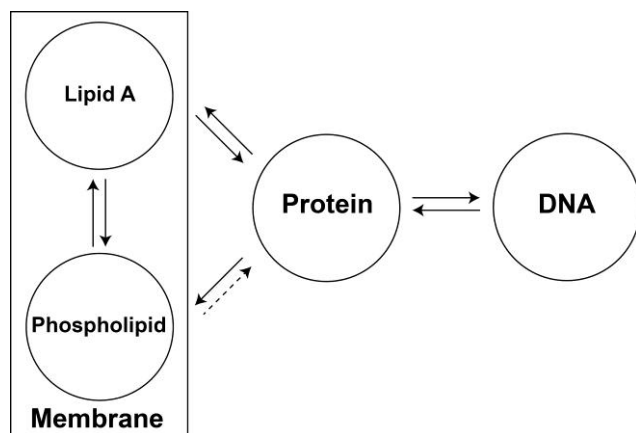


FIGURE 5.12: Schematic illustration showing homeostatic responses between lipid A, phospholipid, protein, and DNA biosyntheses to generate resistance to LpxC inhibitors.

5.4.2: Point mutation in thrS is not the only mechanism for resistance

In the course of our study, we have also isolated and generated other mutants that have > 200-fold resistance to CHIR-090. One of these mutants is CRM1E, which arose from the parental strain CRM1. Like CRM1B, CRM1E has a point mutation in FabZ resulting in a Leu17 to Gln replacement; however, CRM1E has no point mutations in ThrS. Instead, this mutant has a point mutation in RpsA, the 30S ribosomal protein S1 that is required for translation of most mRNAs (Sorensen et al, 1998). In addition, other similarly resistant mutants also do not have point mutations in ThrS (Table 5.1). The specific nucleotide changes in these mutants remain to be identified by whole genome sequencing; however, the absence of point mutations in ThrS suggests that resistance can be acquired through mutations in other genes.

We do note that all of the highly resistant mutants we have generated grow significantly slower (> 2-fold doubling time) than wild-type. However, slow growth

appears to be a side effect correlated with resistance but does not necessarily directly cause resistance as slowing down cellular growth in wild-type cells, via lower temperatures or nutrient deprived media, does not increase the MIC value of CHIR-090. Furthermore, we have also slowed down protein biosynthesis and cellular growth in wild-type cells by using sublethal doses of erythromycin and tetracycline, inhibitors of protein synthesis. Under pretreatment with erythromycin, we only observed a very modest increase (~ 1.5-fold) in the MIC of CHIR-090. We did not observe any differences in CHIR-090 MIC when cells were pretreated in sublethal doses of tetracycline. These data suggest that resistance may be generated by more specific mechanisms in protein metabolism than a general overall growth defect.

5.4.3: Significance of our study

The development of antibiotics requires a sound understanding of potential resistance mechanisms in order to continue their development to clinical usage. Our results reveal the presence of multiple resistance factors that collectively suppress the effect of LpxC-targeting antibiotics, suggesting the best strategy to counter the development of high-level resistance is to avoid gradual bacterial exposure to these compounds. Most interestingly, our studies highlight the existence of a regulatory mechanism for fatty acid and lipid A biosynthesis to maintain balance between phospholipids and LPS. Additionally, we present experimental evidence that alteration of protein biosynthesis suppresses the inhibitory effect of membrane biosynthesis. Both of these resistance mechanisms fall outside of the well-established paradigm of bacterial

resistance involving enhanced efflux of compound, modification of compound or target protein, and they highlight the amazing compensatory ability of the bacterial cell as well as the importance of understanding cellular homeostasis in drug development.

References

- Aderem A, Ulevitch RJ (2000) Toll-like receptors in the induction of the innate immune response. *Nature* **406**: 782-787
- Almaas E, Kovacs B, Vicsek T, Oltvai ZN, Barabasi AL (2004) Global organization of metabolic fluxes in the bacterium *Escherichia coli*. *Nature* **427**: 839-843
- Anderson MS, Bull HG, Galloway SM, Kelly TM, Mohan S, Radika K, Raetz CRH (1993) UDP-*N*-Acetylglucosamine Acyltransferase of *Escherichia coli* - the 1st Step of Endotoxin Biosynthesis Is Thermodynamically Unfavorable. *J Biol Chem* **268**: 19858-19865
- Anderson NHB, J.; Erwin, A.; Harwood, E.; Kline, T.; Mdluli, K.; Pfister, K. B.; Shawar, R.; Wagman, A.; Yabannavar, A. (2004) International Patent WO 2004/062601 issued to Chiron and the University of Washington
- Baba T, Ara T, Hasegawa M, Takai Y, Okumura Y, Baba M, Datsenko KA, Tomita M, Wanner BL, Mori H (2006) Construction of *Escherichia coli* K-12 in-frame, single-gene knockout mutants: the Keio collection. *Mol Syst Biol* **2**: 2006 0008
- Barb AW, Jiang L, Raetz CRH, Zhou P (2007a) Structure of the deacetylase LpxC bound to the antibiotic CHIR-090: Time-dependent inhibition and specificity in ligand binding. *Proc Natl Acad Sci U S A* **104**: 18433-18438
- Barb AW, McClerren AL, Snehelatha K, Reynolds CM, Zhou P, Raetz CRH (2007b) Inhibition of lipid A biosynthesis as the primary mechanism of CHIR-090 antibiotic activity in *Escherichia coli*. *Biochemistry* **46**: 3793-3802
- Barb AW, Zhou P (2008) Mechanism and inhibition of LpxC: an essential zinc-dependent deacetylase of bacterial lipid A synthesis. *Curr Pharm Biotechnol* **9**: 9-15
- Bligh EG, Dyer WJ (1959) A rapid method of total lipid extraction and purification. *Can J Biochem Physiol* **37**: 911-917
- Bodewits K, Raetz CR, Govan JR, Campopiano DJ (2010) Antimicrobial activity of CHIR-090, an inhibitor of lipopolysaccharide biosynthesis, against the *Burkholderia cepacia* complex. *Antimicrob Agents Chemother* **54**: 3531-3533
- Bollenbach T, Quan S, Chait R, Kishony R (2009) Nonoptimal microbial response to antibiotics underlies suppressive drug interactions. *Cell* **139**: 707-718

- Boucher HW, Talbot GH, Bradley JS, Edwards JE, Gilbert D, Rice LB, Scheld M, Spellberg B, Bartlett J (2009) Bad bugs, no drugs: no ESKAPE! An update from the Infectious Diseases Society of America. *Clin Infect Dis* **48**: 1-12
- Bovee ML, Pierce MA, Francklyn CS (2003) Induced fit and kinetic mechanism of adenylation catalyzed by *Escherichia coli* threonyl-tRNA synthetase. *Biochemistry* **42**: 15102-15113
- Bradford MM (1976) A rapid and sensitive method for the quantitation of microgram quantities of protein utilizing the principle of protein-dye binding. *Analytical biochemistry* **72**: 248-254
- Bradford PA (2001) Extended-spectrum beta-lactamases in the 21st century: characterization, epidemiology, and detection of this important resistance threat. *Clinical microbiology reviews* **14**: 933-951, table of contents
- Brown MF, Reilly U, Abramite JA, Arcari JT, Oliver R, Barham RA, Che Y, Chen JM, Collantes EM, Chung SW, Desbonnet C, Doty J, Doroski M, Engrakul JJ, Harris TM, Huband M, Knafels JD, Leach KL, Liu S, Marfat A, Marra A, McElroy E, Melnick M, Menard CA, Montgomery JI, Mullins L, Noe MC, O'Donnell J, Penzien J, Plummer MS, Price LM, Shanmugasundaram V, Thoma C, Uccello DP, Warmus JS, Wishka DG (2012) Potent inhibitors of LpxC for the treatment of Gram-negative infections. *Journal of medicinal chemistry* **55**: 914-923
- Byers DM, Holmes CG (1990) A soluble fatty acyl-acyl carrier protein synthetase from the bioluminescent bacterium *Vibrio harveyi*. *Biochemistry and cell biology = Biochimie et biologie cellulaire* **68**: 1045-1051
- Caughlan RE, Jones AK, Delucia AM, Woods AL, Xie L, Ma B, Barnes SW, Walker JR, Sprague ER, Yang X, Dean CR (2011) Mechanisms decreasing in vitro susceptibility to the LpxC inhibitor CHIR-090 in the Gram-negative pathogen *Pseudomonas aeruginosa*. *Antimicrob Agents Chemother*
- Chopra I, Schofield C, Everett M, O'Neill A, Miller K, Wilcox M, Frere JM, Dawson M, Czaplewski L, Urleb U, Courvalin P (2008) Treatment of health-care-associated infections caused by Gram-negative bacteria: a consensus statement. *The Lancet infectious diseases* **8**: 133-139
- Chung HS, Raetz CR (2010) Interchangeable domains in the Kdo transferases of *Escherichia coli* and *Haemophilus influenzae*. *Biochemistry* **49**: 4126-4137

- Clark D, and Cronan, J. (2005) *Two-Carbon Compounds and Fatty Acids as Carbon Sources*. In *EcoSal: Escherichia coli and Salmonella: Cellular and molecular biology*, Washington, DC.: American Society of Microbiology Press.
- Clements JM, Coignard F, Johnson I, Chandler S, Palan S, Waller A, Wijkmans J, Hunter MG (2002) Antibacterial activities and characterization of novel inhibitors of LpxC. *Antimicrob Agents Chemother* **46**: 1793-1799
- Clementz T, Zhou Z, Raetz CR (1997) Function of the *Escherichia coli* msbB gene, a multicopy suppressor of htrB knockouts, in the acylation of lipid A. Acylation by MsbB follows laurate incorporation by HtrB. *J Biol Chem* **272**: 10353-10360
- Cole KE, Gattis SG, Angell HD, Fierke CA, Christianson DW (2010) Structure of the Metal-Dependent Deacetylase LpxC from *Yersinia enterocolitica* Complexed with the Potent Inhibitor CHIR-090. *Biochemistry*
- Copeland RA (2005) *Evaluation of enzyme inhibitors in drug discovery*, Hoboken, NJ: John Wiley & Sons, Inc.
- Datsenko KA, Wanner BL (2000) One-step inactivation of chromosomal genes in *Escherichia coli* K-12 using PCR products. *Proc Natl Acad Sci U S A* **97**: 6640-6645
- Doublet B, Douard G, Targant H, Meunier D, Madec JY, Cloeckaert A (2008) Antibiotic marker modifications of lambda Red and FLP helper plasmids, pKD46 and pCP20, for inactivation of chromosomal genes using PCR products in multidrug-resistant strains. *Journal of microbiological methods* **75**: 359-361
- Dowd JE, Riggs DS (1965) A Comparison of Estimates of Michaelis-Menten Kinetic Constants from Various Linear Transformations. *J Biol Chem* **240**: 863-869
- Dulbecco R, Vogt M (1954) Plaque formation and isolation of pure lines with poliomyelitis viruses. *The Journal of experimental medicine* **99**: 167-182
- Eggert US, Ruiz N, Falcone BV, Branstrom AA, Goldman RC, Silhavy TJ, Kahne D (2001) Genetic basis for activity differences between vancomycin and glycolipid derivatives of vancomycin. *Science* **294**: 361-364
- Falagas ME, Kasiakou SK (2005) Colistin: the revival of polymyxins for the management of multidrug-resistant Gram-negative bacterial infections. *Clin Infect Dis* **40**: 1333-1341
- Fuhrer F, Langklotz S, Narberhaus F (2006) The C-terminal end of LpxC is required for degradation by the FtsH protease. *Molecular Microbiology* **59**: 1025-1036

- Galloway SM, Raetz CRH (1990) A mutant of *Escherichia coli* defective in the first step of endotoxin biosynthesis. *J Biol Chem* **265**: 6394-6402
- Guan Z, Eichler J (2011) Liquid chromatography/tandem mass spectrometry of dolichols and polyprenols, lipid sugar carriers across evolution. *Biochim Biophys Acta* **1811**: 800-806
- Heath RJ, Rock CO (1996) Roles of the FabA and FabZ beta-hydroxyacyl-acyl carrier protein dehydratases in *Escherichia coli* fatty acid biosynthesis. *J Biol Chem* **271**: 27795-27801
- Heron M (2007) Deaths: leading causes for 2004. *Natl Vital Stat Rep* **56**: 1-95
- Inoue H, Nojima H, Okayama H (1990) High efficiency transformation of *Escherichia coli* with plasmids. *Gene* **96**: 23-28
- Jackman JE, Fierke CA, Tumey LN, Pirrung M, Uchiyama T, Tahir SH, Hindsgaul O, Raetz CRH (2000) Antibacterial agents that target lipid A biosynthesis in Gram-negative bacteria - Inhibition of diverse UDP-3-O-(R-3-hydroxymyristoyl)-N-acetylglucosamine deacetylases by substrate analogs containing zinc binding motifs. *Journal of Biological Chemistry* **275**: 11002-11009
- Jackman JE, Raetz CR, Fierke CA (1999) UDP-3-O-(R-3-hydroxymyristoyl)-N-acetylglucosamine deacetylase of *Escherichia coli* is a zinc metalloenzyme. *Biochemistry* **38**: 1902-1911
- Jiang Y, Morgan-Kiss RM, Campbell JW, Chan CH, Cronan JE (2010) Expression of *Vibrio harveyi* acyl-ACP synthetase allows efficient entry of exogenous fatty acids into the *Escherichia coli* fatty acid and lipid A synthetic pathways. *Biochemistry* **49**: 718-726
- Johnson EJ, Cohen GN, Saint-Girons I (1977) Threonyl-transfer ribonucleic acid synthetase and the regulation of the threonine operon in *Escherichia coli*. *Journal of Bacteriology* **129**: 66-70
- Kimber MS, Martin F, Lu Y, Houston S, Vedadi M, Dharamsi A, Fiebig KM, Schmid M, Rock CO (2004) The structure of (3R)-hydroxyacyl-acyl carrier protein dehydratase (FabZ) from *Pseudomonas aeruginosa*. *J Biol Chem* **279**: 52593-52602
- Ledoux S, Uhlenbeck OC (2008) [3'-32P]-labeling tRNA with nucleotidyltransferase for assaying aminoacylation and peptide bond formation. *Methods* **44**: 74-80

- Lee CJ, Liang X, Chen X, Zeng D, Joo SH, Chung HS, Barb AW, Swanson SM, Nicholas RA, Li Y, Toone EJ, Raetz CR, Zhou P (2011) Species-specific and inhibitor-dependent conformations of LpxC: implications for antibiotic design. *Chem Biol* **18**: 38-47
- Liang X, Lee CJ, Chen X, Chung HS, Zeng D, Raetz CR, Li Y, Zhou P, Toone EJ (2011) Syntheses, structures and antibiotic activities of LpxC inhibitors based on the diacetylene scaffold. *Bioorg Med Chem* **19**: 852-860
- Livermore DM (2012) Fourteen years in resistance. *Int J Antimicrob Agents* **39**: 283-294
- Lu YH, Guan Z, Zhao J, Raetz CR (2011) Three phosphatidylglycerol-phosphate phosphatases in the inner membrane of *Escherichia coli*. *J Biol Chem* **286**: 5506-5518
- Magnuson K, Jackowski S, Rock CO, Cronan JE, Jr. (1993) Regulation of fatty acid biosynthesis in *Escherichia coli*. *Microbiological reviews* **57**: 522-542
- McClerren AL, Endsley S, Bowman JL, Andersen NH, Guan Z, Rudolph J, Raetz CR (2005) A slow, tight-binding inhibitor of the zinc-dependent deacetylase LpxC of lipid A biosynthesis with antibiotic activity comparable to ciprofloxacin. *Biochemistry* **44**: 16574-16583
- Miller JH (1992) *A short course in bacterial genetics : a laboratory manual and handbook for Escherichia coli and related bacteria*, Plainview, N.Y.: Cold Spring Harbor Laboratory Press.
- Miller SI, Ernst RK, Bader MW (2005) LPS, TLR4 and infectious disease diversity. *Nat Rev Microbiol* **3**: 36-46
- Miroux B, Walker JE (1996) Over-production of proteins in *Escherichia coli*: mutant hosts that allow synthesis of some membrane proteins and globular proteins at high levels. *J Mol Biol* **260**: 289-298
- Moffatt JH, Harper M, Harrison P, Hale JD, Vinogradov E, Seemann T, Henry R, Crane B, St Michael F, Cox AD, Adler B, Nation RL, Li J, Boyce JD (2010) Colistin resistance in *Acinetobacter baumannii* is mediated by complete loss of lipopolysaccharide. *Antimicrob Agents Chemother*
- Mohan S, Kelly TM, Eveland SS, Raetz CRH, Anderson MS (1994) An *Escherichia coli* gene (FabZ) encoding (3R)-hydroxymyristoyl acyl carrier protein dehydrase. Relation to *fabA* and suppression of mutations in lipid A biosynthesis. *J Biol Chem* **269**: 32896-32903

- NCCLS (1997) *Methods for Dilution Antimicrobial Susceptibility Tests for Bacteria that Grow Aerobically-Fourth Edition: Approved Standard M7-A4*, Wayne, PA: National Committee for Clinical Laboratory Standards.
- Nguyen BD, Cunningham D, Liang X, Chen X, Toone EJ, Raetz CR, Zhou P, Valdivia RH (2011) Lipooligosaccharide is required for the generation of infectious elementary bodies in *Chlamydia trachomatis*. *Proc Natl Acad Sci U S A* **108**: 10284-10289
- Normark S, Boman HG, Matsson E (1969) Mutant of *Escherichia Coli* with Anomalous Cell Division and Ability to Decrease Episomally and Chromosomally Mediated Resistance to Ampicillin and Several Other Antibiotics. *J Bacteriol* **97**: 1334-&
- Ogura T, Inoue K, Tatsuta T, Suzaki T, Karata K, Young K, Su LH, Fierke CA, Jackman JE, Raetz CRH, Coleman J, Tomoyasu T, Matsuzawa H (1999) Balanced biosynthesis of major membrane components through regulated degradation of the committed enzyme of lipid A biosynthesis by the AAA protease FtsH (HflB) in *Escherichia coli*. *Mol Microbiol* **31**: 833-844
- Ohnishi M, Golparian D, Shimuta K, Saika T, Hoshina S, Iwasaku K, Nakayama S, Kitawaki J, Unemo M (2011) Is *Neisseria gonorrhoeae* initiating a future era of untreatable *gonorrhea*? detailed characterization of the first strain with high-level resistance to ceftriaxone. *Antimicrob Agents Chemother* **55**: 3538-3545
- Onishi HR, Pelak BA, Gerckens LS, Silver LL, Kahan FM, Chen MH, Patchett AA, Galloway SM, Hyland SA, Anderson MS, Raetz CRH (1996) Antibacterial agents that inhibit lipid A biosynthesis. *Science* **274**: 980-982
- Peng DX, Hong WZ, Choudhury BP, Carlson RW, Gu XX (2005) *Moraxella catarrhalis* bacterium without endotoxin, a potential vaccine candidate. *Infect Immun* **73**: 7569-7577
- Pluschke G, Hirota Y, Overath P (1978) Function of phospholipids in *Escherichia coli*. Characterization of a mutant deficient in cardiolipin synthesis. *J Biol Chem* **253**: 5048-5055
- Projan SJ, Youngman PJ (2002) Antimicrobials: new solutions badly needed. *Curr Opin Microbiol* **5**: 463-465
- Raetz CR, Reynolds CM, Trent MS, Bishop RE (2007a) Lipid A modification systems in Gram-negative bacteria. *Annu Rev Biochem* **76**: 295-329

- Raetz CRH, Reynolds CM, Trent MS, Bishop RE (2007b) Lipid A Modification Systems in Gram-negative Bacteria. *Annu Rev Biochem*: in press
- Raetz CRH, Whitfield C (2002) Lipopolysaccharide endotoxins. *Annu Rev Biochem* **71**: 635-700
- Sankaranarayanan R, Dock-Bregeon AC, Romby P, Caillet J, Springer M, Rees B, Ehresmann C, Ehresmann B, Moras D (1999) The structure of threonyl-tRNA synthetase-tRNA(Thr) complex enlightens its repressor activity and reveals an essential zinc ion in the active site. *Cell* **97**: 371-381
- Silbert DF, Ruch F, Vagelos PR (1968) Fatty acid replacements in a fatty acid auxotroph of *Escherichia coli*. *J Bacteriol* **95**: 1658-1665
- Smith AM, Klugman KP (1998) Alterations in PBP 1A essential-for high-level penicillin resistance in *Streptococcus pneumoniae*. *Antimicrob Agents Chemother* **42**: 1329-1333
- Sorensen MA, Fricke J, Pedersen S (1998) Ribosomal protein S1 is required for translation of most, if not all, natural mRNAs in *Escherichia coli* in vivo. *Journal of molecular biology* **280**: 561-569
- Sorensen PG, Lutkenhaus J, Young K, Eveland SS, Anderson MS, Raetz CRH (1996) Regulation of UDP-3-O-[R-3-hydroxymyristoyl]-N-acetylglucosamine deacetylase in *Escherichia coli*. The second enzymatic step of lipid A biosynthesis. *J Biol Chem* **271**: 25898-25905
- Spellberg B, Guidos R, Gilbert D, Bradley J, Boucher HW, Scheld WM, Bartlett JG, Edwards J, Jr. (2008) The epidemic of antibiotic-resistant infections: a call to action for the medical community from the Infectious Diseases Society of America. *Clin Infect Dis* **46**: 155-164
- Steeghs L, den Hartog R, den Boer A, Zomer B, Roholl P, van der Ley P (1998) *Meningitis bacterium* is viable without endotoxin. *Nature* **392**: 449-450
- Tran AX, Lester ME, Stead CM, Raetz CR, Maskell DJ, McGrath SC, Cotter RJ, Trent MS (2005) Resistance to the antimicrobial peptide polymyxin requires myristoylation of *Escherichia coli* and *Salmonella typhimurium* lipid A. *J Biol Chem* **280**: 28186-28194
- Vaara M, Nurminen M (1999) Outer membrane permeability barrier in *Escherichia coli* mutants that are defective in the late acyltransferases of lipid A biosynthesis. *Antimicrob Agents Chemother* **43**: 1459-1462

- Vorachek-Warren MK, Ramirez S, Cotter RJ, Raetz CR (2002) A triple mutant of *Escherichia coli* lacking secondary acyl chains on lipid A. *J Biol Chem* **277**: 14194-14205
- Walsh C (2000) Molecular mechanisms that confer antibacterial drug resistance. *Nature* **406**: 775-781
- Wang J, Alexander P, McKnight SL (2011) Metabolic Specialization of Mouse Embryonic Stem Cells. *Cold Spring Harbor symposia on quantitative biology*
- Wang RF, Kushner SR (1991) Construction of versatile low-copy-number vectors for cloning, sequencing and gene expression in *Escherichia coli*. *Gene* **100**: 195-199
- Wyckoff TJO, Raetz CRH, Jackman JE (1998) Antibacterial and anti-inflammatory agents that target endotoxin. *Trends Microbiol* **6**: 154-159
- Yu D, Ellis HM, Lee EC, Jenkins NA, Copeland NG, Court DL (2000) An efficient recombination system for chromosome engineering in *Escherichia coli*. *Proc Natl Acad Sci U S A* **97**: 5978-5983

Biography

Daina Zeng was born on April 6th, 1987 in Hunan, China. She came to the United States when she was five years old. She attended the University of Michigan and graduated with a Bachelors of Science in Biochemistry in 2008. While there, her research in Dr. Carol Fierke's laboratory focused on developing a fluorescence energy resonance transfer (FRET) high-throughput assay for ribonuclease P by labeling synthetic substrates with a combination of two fluorescent labels to monitor product turnover and inhibition on a well-plate format for use in the screening of potential inhibitors. In September of 2008, she matriculated in the Biochemistry Program at Duke University. She joined the laboratories of Dr. Christian R.H. Raetz and Dr. Pei Zhou as a joint student in March of 2005. After the passing of Dr. Raetz in August of 2011, her co-advisor Dr. Pei Zhou became her primary doctoral advisor.

Following the completion of her Ph.D. studies, Daina will continue her research on developing therapeutics against multidrug-resistant bacteria by working as a scientist at Agile Sciences.

Her works during graduate school include:

Liang X, Lee CJ, Chen X, Chung HS, **Zeng D**, Raetz CRH, Li Y, Zhou P, Toone EJ. Syntheses, structures and antibiotic activities of LpxC inhibitors based on the diacetylene scaffold. *Bioorganic & Medicinal Chemistry* 19: 852-60 (2011).

Lee CJ, Liang X, Chen X, **Zeng D**, Joo SH, Chung HS, Barb AW, Swanson SM, Nicholas RA, Li Y, Toone EJ, Raetz CRH, Zhou P. Species-specific and inhibitor-dependent conformations of LpxC - Implications for antibiotic design. *Chemistry and Biology* 18: 1-10 (2011).

Zeng D, Zhao J., Chung HS, Guan Z, Raetz CRH, Zhou P. Mutants resistant to LpxC inhibitors by rebalancing cellular homeostasis. (submitted).